JSCSEN 64(5–6)317-394(1999)

UDC 54:66

YU-ISSN 0352-5139

DOCUMENTA CHEMICA YUGOSLAVICA

Journal of Serbian Chemistry Society

VOLUME 64

NO 5–6

BELGRADE 1999

Editor's Note

Due to the present war activities in Yugoslavia the Editorial Board regrets that because of the financial and teshnical problems has to reduce the number of the printed copies of the Journal to that which corresponds just to the number of paid subscriptions for 1999 and those needed for the exsisting Excange Program. Also, 10 free of charge reprints of the articles will be supplied to the corresponding author. Simultaneously, complete text of the forthcoming issues of the Journal will be available at the Journal's web site (http://www.shd.org.yu).

YU-ISSN 0352-5139
J. Serb. Chem. Soc. Vol. 64, No. 5– 6(1999)

CONTENTS

Published by the Serbian Chemical Society, Karnegijeva 4/III,
P. O. Box 35-08, YU-11001 Belgrade, Yugoslavia
Printed by the Faculty of Technology and Metallurgy, Karnegijeva 4,
P. O. Box 35-03, YU-11001 Belgrade, Yugoslavia

J. Serb. Chem. Soc. 64(5– 6)317-340(1999)
JSCS-2673

UDC 66.022.03:543.251:621. 793
Review paper

REVIEW

Mass transfer during electrodeposition of metals at a periodically changing rate

MIODRAG D. MAKSIMOVIĆ and KONSTANTIN I. POPOV

Faculty of Technology and Metallurgy, University of Belgrade, P.O.Box 3503, YU–11120 Belgrade, Yugoslavia

(Received 2 February 1999)

Key words: mass-transfer, electrodeposition, reversing current, pulsating current, alternating current superimposed on direct current, pulsating overpotential.

1. INTRODUCTION

It has been known for a relatively long time that the application of a periodically changing current in plating practice leads to improvements in the quality of electrodeposits. Three types of current variation have been found useful: a reversing current (RC); a pulsating current (PC); and a sinusoidal, alternating current superimposed on a direct current (AC).[1–15] In recent years, the beneficial effects of pulsating overpotential (PO) have also been discussed.[4] Even though this kind of electrodeposition at a periodically changing rate (EPCR) is important from a theoretical point of view and offers a variety of experimental possibilities, it is not as yet, frequently used in plating practice.

The mass transfer during metal electrodeposition at a periodically changing rate is not widely known but it will be treated in details in this paper. It is very

important, because the mass transfer conditions determine the morphology of metal deposits just as in the case of deposition at a constant rate.

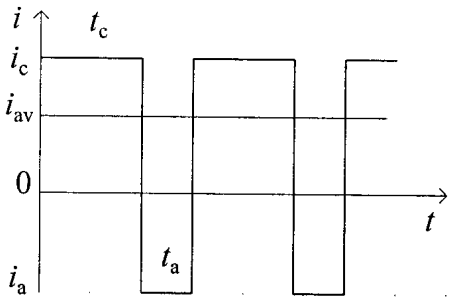

Fig. 1. Waveform of the reversing current.

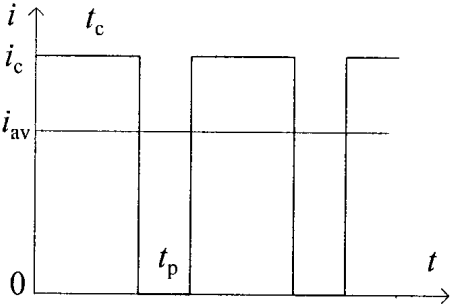

Fig. 2. Pulsatung current.

Reversing current is represented schematically in Fig. 1. It is characterized by the cathodic current density, i_c, and the anodic current density, i_a, as well as by the duration of flow of the current in the cathodic and the anodic direction, t_c and t_a, respectively. Naturally,

$$t_c + t_a = T \tag{1}$$

where T is the full period of the RC wave. The average current density is then given by

$$i_{av} = \frac{i_c t_c - i_a t_a}{t_c + t_a} \tag{2}$$

and for $i_c = i_a = i_A$

$$i_{av} = i_A \frac{1 - r}{1 + r} \tag{3}$$

where

$$r = \frac{t_a}{t_c} \tag{4}$$

RC is used in the second and millisecond range.

Pulsating current consists of a periodic repetition of square pulses. It is similar in shape to RC except for the absence of the anodic component, as is shown in Fig. 2. PC is characterized by the amplitude of the cathodic current, i_c, the cathodic deposition time, t_c (on period), and the time interval t_p in which the system relaxes (off period). The full period, T, is given by

$$t_c + t_p = T \tag{5}$$

and the average current density by

$$i_{av} = \frac{i_c t_c}{t_c + t_p} \tag{6}$$

or

$$i_{av} = \frac{i_c}{1 + p} \tag{7}$$

if

$$p = \frac{t_p}{t_c} \tag{8}$$

Note that rectified sinusoidal AC, especially half-rectified sinusoidal AC, often termed pulsating current in the literature, shows similar effects to those of PC.

Sinusoidal AC superimposed on direct current is represented in Fig. 3. It is characterized by i_{dc}, i_p, and the frequency, which is usually 50 or 60 Hz. The resultant is termed an asymmetric sinusoidal current. The average current is equal to i_{dc}. At given anodic DC values, three different types of current can be obtained, which can be denoted as follows: $i_p < i_{dc}$ "rippling current"; $i_p = i_{dc}$,"pulsating curren"; $i_p > i_{dc}$, "current with an anodic component". The last type is mainly used in plating practice.

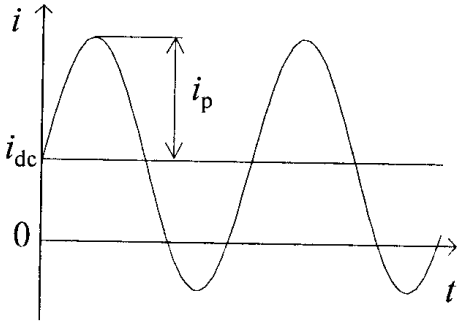

Fig. 3. The shape of the sinusoidal alternating current superimposed on the direct current.

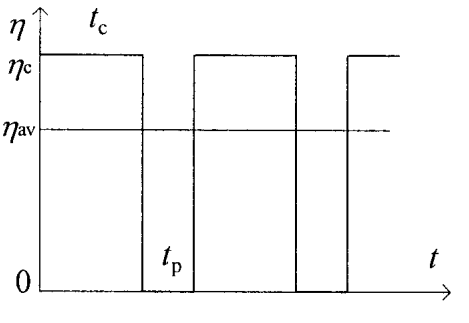

Fig. 4. Square-wave pulsating overpotential waveform.

Pulsating overpotential consists of a periodic repetition of overpotential pulses of different shapes. Square-wave PO is defined in the same way as PC except that the overpotential pulsates between the amplitude value η_A and zero instead of the current density (Fig. 4). Non-rectangular pulsating overpotential is defined by the amplitude of the overpotential, η_A, frequency, and the overpotential waveform.

There are a number of different current and overpotential waveforms used in EPCR,[16–18] the most important of which have been mentioned above.

2. MASS TRANSFER IN THE STEADY STATE PERIODIC CONDITION

Electrodeposition at a periodically changing rate can be described in terms of time and distance-dependent concentrations:

$$\frac{\partial c}{\partial t} = D\frac{\partial^2 c}{\partial x^2} \tag{9}$$

$$c(0,x) = c_0 \tag{10}$$

$$c(t,\delta) = c_0 \tag{11}$$

$$\left|\frac{\partial c}{\partial x}\right|_{x=0} = \frac{i(t)}{zFD} \tag{12}$$

Equations (9) to (12) are solved for different $i(t)$ and the solutions applied to different types of problems.[16–41]

2.1. Reversing current

For the periodic reverse current the current density $i(t)$ is a periodic function of time given by[36]

$$i(t) = \begin{cases} i_c, & \text{for } mT < t \le [m + 1/(r+1)]T \\ -i_a & \text{for } [m + 1/(r+1)]T < t \le (m+1)T \end{cases} \tag{13}$$

$$m = 0, 1, 2, \ldots$$

Millisecond range. For $i(t)$ given by Eq. (13), the solution of Eqs. (9) to (12) is given by

$$c(x,t) = c_0 - \frac{2i_c}{zF\delta}\sum_{k=0}^{\infty}\cos\left[\frac{(2k+1)\pi x}{2\delta}\right]\left\{\int_0^{T/(r+1)}\exp[-\lambda_k(t-\tau)]\,d\tau + \int_T^{T+T/(r+1)}\exp[-\lambda_k(t-\tau)]\,d\tau + \ldots\right.$$
$$\left.\ldots + \int_{mT}^{mT+T/(r+1)}\exp[-\lambda_k(t-\tau)]\,d\tau\right\} + \frac{2i_a}{zF\delta}\sum_{k=0}^{\infty}\cos\left[\frac{(2k+1)\pi x}{2\delta}\right]\left\{\int_{T/(r+1)}^{T}\exp[-\lambda_k(t-\tau)]\,d\tau + \right.$$
$$\left. + \int_{T+T/(r+1)}^{2T}\exp[-\lambda_k(t-\tau)]\,d\tau + \ldots + \int_{mT+T/(r+1)}^{(m+1)T}\exp[-\lambda_k(t-\tau)]\,d\tau\right\} \tag{14}$$

where

$$\lambda_k = \frac{(2k+1)^2\pi^2 D}{4\delta^2} = \frac{(2k+1)^2}{4t_0} \tag{15}$$

and

$$t_0 = \frac{\delta^2}{\pi^2 D} \tag{16}$$

For $t = [m + 1/(r+1)]T$ and $m \to \infty$, *i.e.*, at the end of the cathodic pulses under steady state conditions, the concentration distribution of the depositing ions inside the diffusion layer is given by

$$c_c(x) = c_0 - \frac{8\delta}{\pi^2 zFD} \sum_{k=0}^{\infty} \frac{1}{(2k+1)^2} \cos\frac{(2k+1)\pi x}{2\delta}$$

$$\left\{ i_c \frac{1 - \exp[-\lambda_k T/(r+1)]}{1 - \exp(-\lambda_k T)} - i_a \frac{\exp[-\lambda_k T/(r+1)] - \exp(-\lambda_k T)}{1 - \exp(-\lambda_k T)} \right\} \quad (17)$$

The concentration distribution at the end of the anodic pulses under the same conditions, *i.e.* for $t = (m + 1)T$, $m \to \infty$, is given by

$$c_a(x) = c_0 - \frac{8\delta}{\pi^2 zFD} \sum_{k=0}^{\infty} \frac{1}{(2k+1)^2} \cos\frac{(2k+1)\pi x}{2\delta}$$

$$\left\{ i_c \frac{\exp[-\lambda_k rT/(r+1)] - \exp(-\lambda_k T)}{1 - \exp(-\lambda_k T)} - i_a \frac{1 - \exp[-\lambda_k rT/(r+1)]}{1 - \exp(-\lambda_k T)} \right\} \quad (18)$$

It is easy to show that, for a sufficiently long period T ($T > t_o$), the system behaves as under DC conditions. For $T \to \infty$ Eqs. (17) and (18) become

$$\lim_{T\to\infty} c_c(x) = c_0 - \frac{i_c}{zFD}(\delta - x) \quad (19)$$

and

$$\lim_{T\to\infty} c_a(x) = c_0 - \frac{i_a}{zFD}(\delta - x) \quad (20)$$

On the other hand, for $T \to 0$ ($T << t_0$)

$$\lim_{T\to 0} c_c(x) = \lim_{T\to 0} c_a(x) = c(x) = c_0 - \frac{\delta - x}{zFD} \frac{i_c - r\, i_a}{r+1} = c_0 - \frac{\delta - x}{zFD} i_{av} \quad (21)$$

for $0 \le x \le \delta$

The concentration distribution inside the diffusion layer at the end of cathodic and anodic pulses under steady state conditions, calculated using Eqs. (17) and (18) and the following set of parameters $\delta = 10^{-2}$ cm, $D = 10^{-5}$ cm^2 s^{-1} and $t_0 = 1$ s, is given in Figs. 5 – 9 for different reversing regimes. At sufficiently large x/δ, the concentration distribution does not depend on time.[42] At x/δ close to the electrode, it is time dependent and the upper and lower parts of the curves correspond to the end of the anodic and the cathodic times, respectively.

It can be seen from Fig. 5 that, at lower periods of the RC wave, the concentration distribution is closer to one described by Eq. (21) for $T \to 0$. It can also be seen from Fig. 6 and Fig. 7 that, with other parameters, the same the distribution is closer to that given by Eq. (21) at lower r and i_{av} values.

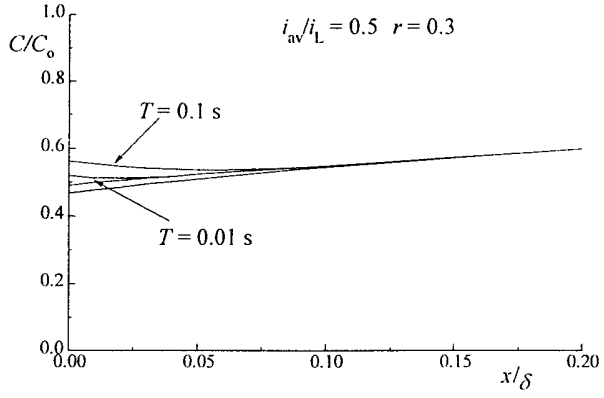

Fig. 5. The effect of the period of the RC wave on the concentration distribution inside the diffusion layer (From Maksimović and Popov[42]).

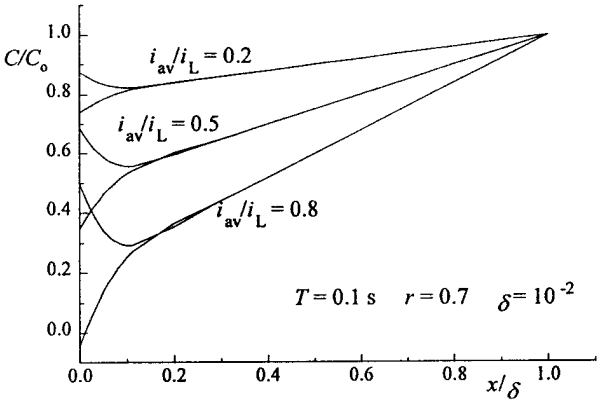

Fig. 6. The effect of the average current density on the concentration distribution inside the diffusion layer. (From Maksimović and Popov[42]).

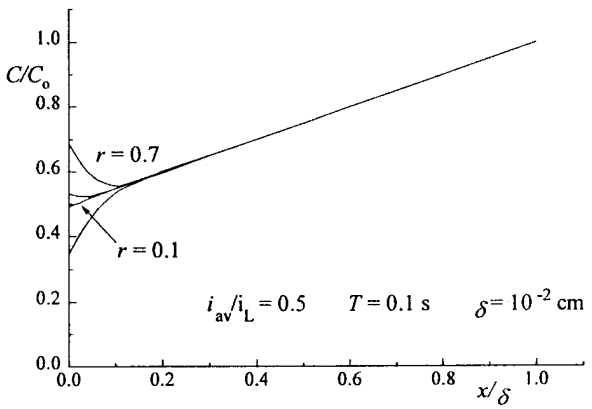

Fig. 7. The effect of the anodic to cathodic time ratio on the concentration distribution inside the diffusion layer. (From Maksimović and Popov[42]).

At $i_{av} = 0$, concentration polarization practically does not exists up to $i_A \approx i_L$, as is illustrated by Fig. 8.

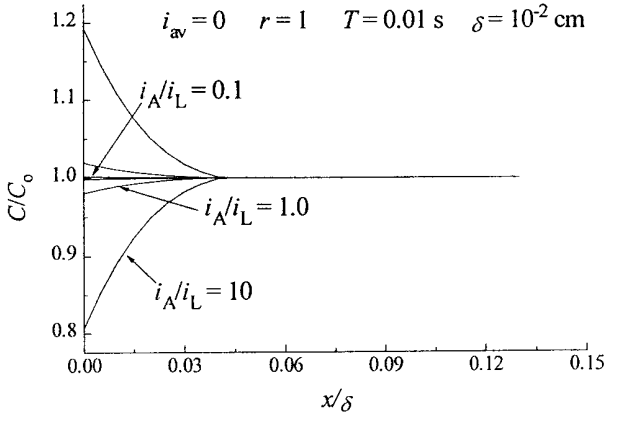

Fig. 8. The effect of the current amplitude on the concentration distribution inside the diffusion layer. (From Maksimović and Popov[42]).

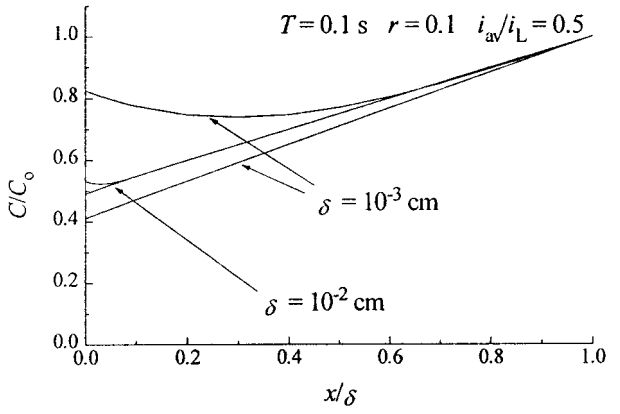

Fig. 9. The effect of the diffusion layer thickness on the concentration distribution inside the diffusion layer. (From Maksimović and Popov[42]).

Finally, the effect of the diffusion layer thickness is shown in Fig. 9. It follows from Eqs. (15) – (18) that the frequency of pulsation and diffusion layer thickness are related by the equation

$$\frac{T}{\delta^2} = \text{const.} \tag{22}$$

to produce the same effect on the concentration distribution inside the diffusion layer.

For $x = 0$, Eqs. (17) and (18) can be rewritten in the form

$$c_c = c_0 - \frac{8\delta}{\pi^2 zFD} \sum_{k=0}^{\infty} \frac{1}{(2k+1)^2} \left\{ i_c \frac{1 - \exp[-\lambda_k T/(r+1)]}{1 - \exp(-\lambda_k T)} - i_a \frac{\exp[-\lambda_k T/(r+1)] - \exp(-\lambda_k T)}{1 - \exp(-\lambda_k T)} \right\} \tag{23}$$

and (24)

$$c_a = c_0 - \frac{8\delta}{\pi^2 zFD}\sum_{k=0}^{\infty}\frac{1}{(2k+1)^2}\left\{i_c\frac{\exp[-\lambda_k rT/(r+1)] - \exp(-\lambda_k t)}{1-\exp(-\lambda_k T)} - i_a\frac{\exp[-\lambda_k T/(r+1)]}{1-\exp(-\lambda_k T)}\right\}$$

and Eqs. (19)–(21) in the form

$$\lim_{T\to\infty} c_c = c_0 - \frac{\delta i_c}{zFD} \tag{25}$$

$$\lim_{T\to\infty} c_a = c_0 - \frac{\delta i_a}{zFD} \tag{26}$$

and

$$\lim_{T\to 0} c_c = \lim_{T\to 0} c_a = c_s = c_0 - \frac{\delta}{zFD}\frac{i_c - r\,i_a}{r+1} = c_0 - \frac{\delta}{zFD} i_{av} \tag{27}$$

Second range. For T close to t_0, the behaviour of the system under RC conditions has to be analyzed using Eq. (24). In this case, the distribution of the concentration inside the diffusion layer at the end of the anodic pulse is close to that given by Eq. (10). It follows from Eq. (24) that this will happen at[36,43]

$$c_a = c_0 \tag{28}$$

or

$$\sum_{k=0}^{\infty}\frac{1}{(2k+1)^2}\left\{i_c\frac{\exp[-\lambda_k rT/(r+1)] - \exp(-\lambda_k T)}{1-\exp(-\lambda_k T)} - i_a\frac{1-\exp[-\lambda_k rT/(r+1)]}{1-\exp(-\lambda_k T)}\right\} = 0 \tag{29}$$

Obviously, r can be obtained by computer calculation from Eq. (29).

On the other hand, it is known[36,52] that for $rT/(r+1) \geq 1.5t_0$, the series in Eq. (29) can be approximated using only the first term ($k = 0$). Hence, for $i_c = i_a$,

$$\exp\left(-\frac{r}{r+1}\frac{T}{4t_0}\right) - \exp\left(-\frac{T}{4t_0}\right) = 1 - \exp\left(-\frac{r}{r+1}\frac{T}{4t_0}\right) \tag{30}$$

or

$$r = \frac{\dfrac{4t_0}{T}\ln\dfrac{2}{1+\exp(-T/4t_0)}}{1 - \dfrac{4t_0}{T}\ln\dfrac{2}{1+\exp(-T/4t_0)}} \tag{31}$$

It is easy to show that for $T = 3t_0$, $r = 0.7$ and for $T = 16t_0$, $r = 0.2$ by assuming that for $T > 3t_0$, Eq. (30) is valid and that at $T > 16t_0$, the system behaves as under DC conditions. The optimum ratio t_c/t_a is given by

$$1.5 \leq t_c/t_a \leq 5 \tag{32}$$

for periods T such that

$$3t_0 \leq T \leq 16t_0 \tag{33}$$

and the optimum t_c and t_a for a given T, calculated using Eq. (31), are shown in Fig. 10.

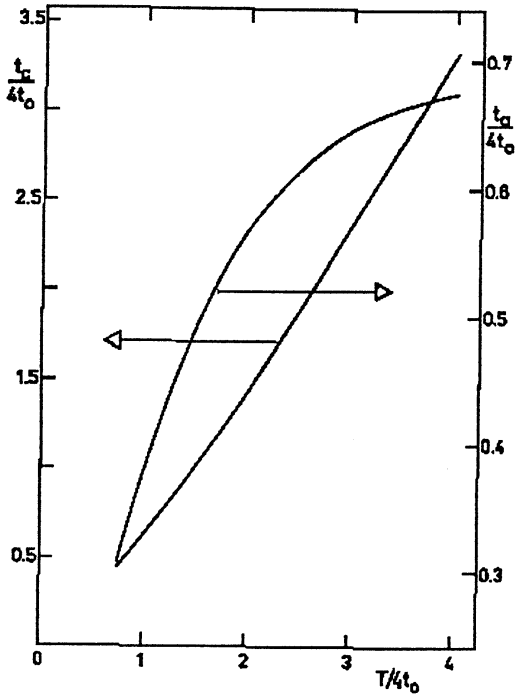

Fig. 10. $t_c/4t_0$ and $t_a/4t_0$ as a function of $T/4t_0$. (From Popov and Maksimović[43]).

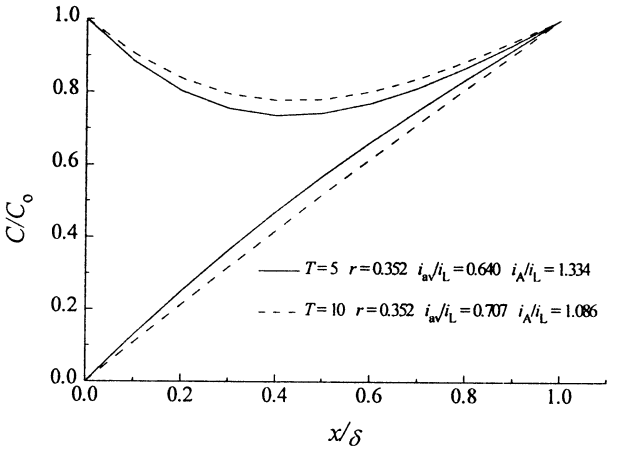

Fig. 11. The concentration distribution inside the diffusion layer at the end of the anodic (upper) and the cathodic (lower) times. Calculated by computer using Eqs. (17) and (29).

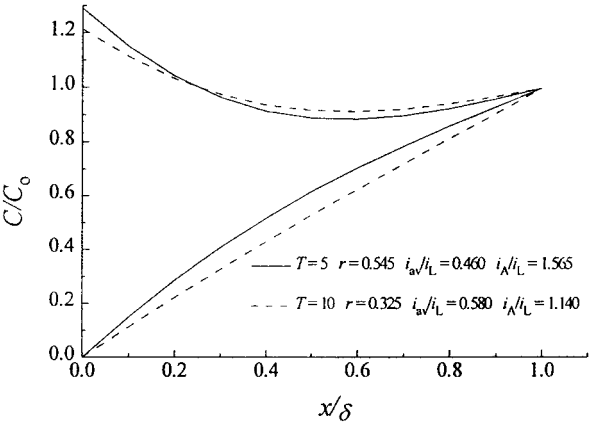

Fig. 12. The concentration distribution inside the diffusion layer at the end of the anodic (upper) and the cathodic (lower) times. Calculated by computer using Eqs. (17) and (31).

In Fig. 11. and Fig. 12, the concentration distribution at the end of the cathodic and anodic pulses for optimum current wave shapes are shown, calculated by computer (Fig. 10.) and by using Eq. (33) if $t_0 = 1$ s for $\delta = 10^{-2}$ cm and $D = 10^{-5}$ cm^2 s^{-1} (Fig. 11.). It is seen that the approximation used is satisfactory. A good agreement between the shape and the frequency of the RC calculated in this way and literature data is obtained, because in practically all cases

$$1 \text{ s} \leq T \leq 30 \text{ s} \tag{34}$$

according to Bakhvalov.[3]

For periods T:

$$3\ t_0 \leq \mathrm{T} \leq 16\ t_0 \tag{35}$$

It is obvious that, because of Eq. (35) and the dependence of t_0 on the diffusion layer thickness, in strongly stirred solutions the period T must be considerably smaller.

2.2. Pulsating current

For $i(t)$ given by

$$i(t) = \begin{cases} i_c, & \text{for } mT < t \leq [m + 1/(p+1)]T \\ 0, & \text{for } [m + 1/(p+1)]T < t \leq (m+1)T \end{cases} \tag{36}$$

i.e. for pulsating current,' solution of Eqs. (9) to (12) is given by

$$c(x,t) = c_0 - \frac{2i_c}{zF\delta} \sum_{k=0}^{\infty} \cos\left[\frac{(2k+1)\pi x}{2\delta}\right]$$

$$\left\{ \int_0^{T/(p+1)} \exp\left[-\lambda_k (t-\tau)\right] d\tau + \int_T^{T+T/(p+1)} \exp\left[-\lambda_k (t-\tau)\right] d\tau + \ldots + \int_{mT}^{mT+T/(p+1)} \exp[-\lambda_k (t-\tau)]\, d\tau \right\} \tag{37}$$

For $t = [m + 1/(p+1)]T$, *i.e.*, at the end of pulses, Eq. (37) can be rewritten as

$$c\left\{x, \left(m + \frac{1}{p+1}\right)T\right\} = c_0 - \frac{8\delta\, i_c}{\pi^2\, zFD} \sum_{k=0}^{\infty} \frac{1}{(2k+1)^2} \cos\frac{(2k+1)\pi x}{2\delta}$$
$$\left\{\exp(-\lambda_k T) - \exp\left[-\lambda_k\left(T + \frac{T}{p+1}\right)\right] + ... + 1 - \exp\left(-\frac{\lambda_k T}{p+1}\right)\right\} \tag{38}$$

In steady state conditions

$$c_{on}(x) = \lim_{m\to\infty} c\left\{x, \left(m + \frac{1}{p+1}\right)T\right\} =$$

$$= c_0 - \frac{8\delta\, i_c}{\pi^2\, zFD} \sum_{k=0}^{\infty} \frac{1}{(2k+1)^2} \cos\frac{(2k+1)\pi x}{2\delta} \frac{1 - \exp[-\lambda_k T/(p+1)]}{1 - \exp(-\lambda_k t)} \tag{39}$$

For $t = (m+1)T$, *i.e.*, at the end of pauses, Eq. (37) can be rewritten in the form

$$c[x, (m+1)T] = c_0 - \frac{8\delta i_c}{\pi^2\, zFD} \sum_{k=0}^{\infty} \frac{1}{(2k+1)^2} \cos\frac{(2k+1)\pi x}{2\delta} \cdot \left\{\exp\left[-\lambda_k\left((m+1)T + \frac{T}{p+1}\right)\right] - \right.$$
$$\left. - \exp[-\lambda_k (m+1)T] + \ldots + \exp\left[-\lambda_k\left(T - \frac{T}{p+1}\right)\right] - \exp(-\lambda_k T)\right\} \tag{40}$$

In steady state conditions

$$c_{off}(x) = \lim_{m\to\infty} c[x, (m+1)T] =$$

$$= c_0 - \frac{8\delta\, i_c}{\pi^2 zFD} \sum_{k=0}^{\infty} \frac{1}{(2k+1)^2} \cos\frac{(2k+1)\pi x}{2\delta} \frac{\exp\{-\lambda_k[T - T/(p+1)]\} - \exp(-\lambda_k T)}{1 - \exp(-\lambda_k T)} \tag{41}$$

For $T \to \infty$ Eqs. (39) and (41) becomes

$$\lim_{T\to\infty} c_{on}(x) = c_0 - \frac{i_c}{zFD}(\delta - x) \tag{42}$$

and

$$\lim_{T\to\infty} c_{off}(x) = c_0 \tag{43}$$

while for $T \to 0$

$$\lim_{T\to 0} c_{on}(x) = \lim_{T\to 0} c_{off}(x) = c(x) = c_0 - \frac{\delta - x}{zFD} \frac{i_c}{p+1} \tag{44}$$

At the same time for $x = 0$, Eqs. (39) and (41) becomes

$$c_{on} = c_0 - \frac{8\delta i_c}{\pi^2 zFD} \sum_{k=0}^{\infty} \frac{1}{(2k+1)^2} \frac{1 - \exp[-\lambda_k T/(p+1)]}{1 - \exp(-\lambda_k T)} \tag{45}$$

and

$$c_{off} = c_0 - \frac{8\delta i_c}{\pi^2 zFD} \sum_{k=0}^{\infty} \frac{1}{(2k+1)^2} \frac{\exp[-\lambda_k pT/(p+1)] - \exp(-\lambda_k T)}{1 - \exp(-\lambda_k T)} \tag{46}$$

As in the previous case for $T >> t_0$, the system behaves as under DC conditions where

$$\lim_{T\to\infty} c_{on} = c_0 - \frac{\delta i_c}{zFD} \tag{47}$$

and

$$\lim_{T\to\infty} c_{off} = c_0 \tag{48}$$

For $T << t_0$, it follows from Eqs. (45) and (46) that

$$\lim_{T\to 0} c_{on} = \lim_{T\to 0} c_{off} = c_s = c_0 - \frac{\delta i_c}{zFD} \frac{1}{p+1} \tag{49}$$

It is obvious from Eqs. (2), (4), (7) and (8) and Eqs. (27) and (49) that, in both cases,

$$c_s = c_0 - \frac{\delta i_{av}}{zFD} \tag{50}$$

The concentration distribution inside the diffusion layer at the end of the cathodic pulses and during the pauses in the steady state conditions, calculated using Eqs. (39) and (41) and the already used set of parameters, are given in Figs. 13–16.[45]

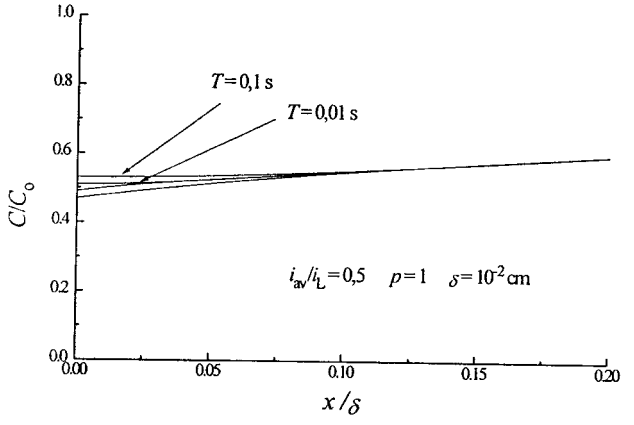

Fig. 13. The effect of the period of the PC wave on the concentration distribution inside the diffusion layer. (From Maksimović and Popov[45]).

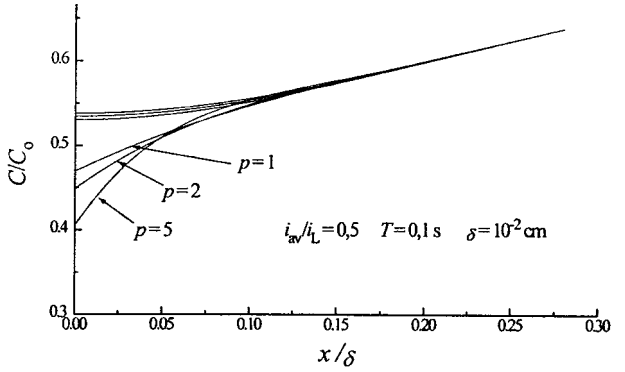

Fig. 14. The effect of the pause to pulse ratio on the concentration distribution inside the diffusion layer. (From Maksimović and Popov[45]).

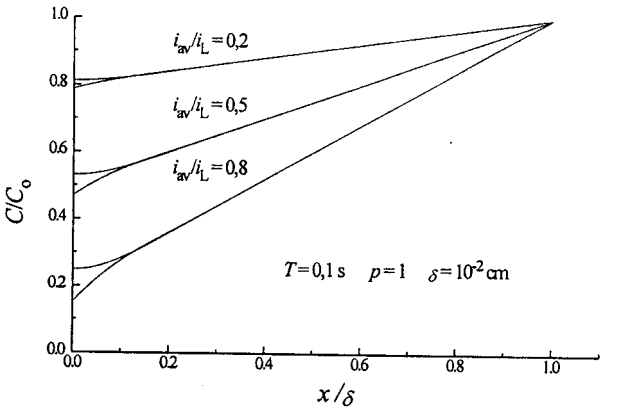

Fig. 15. The effect of the average current density on the concentration distribution inside the diffusion layer. (From Maksimović and Popov[45]).

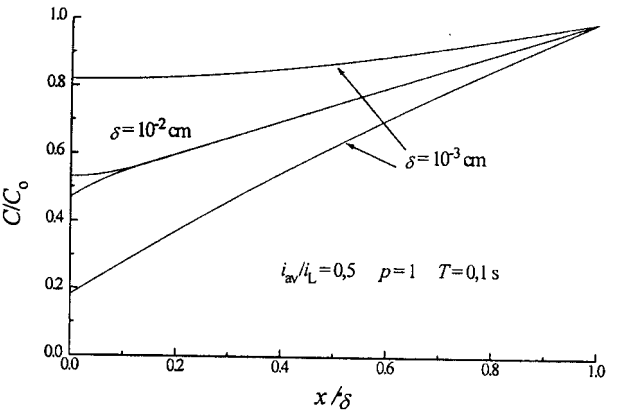

Fig. 16. The effect of the diffusion layer thickness on the concentration distribution inside the diffusion layer. (From Maksimović and Popov[45]).

It can be seen from Fig. 13, that at the lower period of the PC wave, the concentration distribution is closer to that described by Eq. (50) for $T \rightarrow 0$. It can

also be seen from Fig. 14. and Fig. 15, that with other parameters, the same distribution is closer to that given by Eq. (50) at lower p and i_{av} values. Finally, the effect of the diffusion layer thickness is shown in Fig. 16, being the same as in the RC case (see Eq. (22)).

2.3. Alternating current superimposed on direct current

For $i(t)$ given by

$$i(t) = i_{dc} + i_p \sin(\omega t) \tag{51}$$

i.e., for alternating current superimposed on direct current, the solution of the problem is obtained in the form[35,37]

$$c(x,t) = c_0 - \frac{2}{zF\delta}\sum_{k=0}^{\infty}\cos\left[\frac{(2k+1)\pi x}{2\delta}\right]\int_0^t (i_{dc} + i_p \sin(\omega\tau))\exp[-\lambda_k (t-\tau)]\,d\tau \tag{52}$$

and

$$c(x,t) = c_0 - \frac{2}{zF\delta}\sum_{k=0}^{\infty}\cos\left[\frac{(2k+1)\pi x}{2\delta}\right]$$

$$\left\{\frac{i_{dc}}{\lambda_k}[1-\exp(-\lambda_k t)] + \frac{i_p}{\lambda_k^2+\omega^2}\left[\lambda_k \sin(\omega t) - \omega\cos(\omega t) + \omega\exp(-\lambda_k t)\right]\right\} \tag{53}$$

Under steady state conditions, Eq. (53) becomes

$$c(x) = c_0 - \frac{2}{zF\delta}\sum_{k=0}^{\infty}\cos\left[\frac{(2k+1)\pi x}{2\delta}\right]\left\{\frac{i_{dc}}{\lambda_k} + \frac{i_p}{\lambda_k^2+\omega^2}\left[\lambda_k \sin(\omega t) - \omega\cos(\omega t)\right]\right\} \tag{54}$$

and the surface concentration ($x = 0$) is

$$c_s = c_0 - \frac{2}{zF\delta}\sum_{k=0}^{\infty}\left\{\frac{i_{dc}}{\lambda_k} + \frac{i_p}{\lambda_k^2+\omega^2}\left[\lambda_k \sin(\omega t) - \omega\cos(\omega t)\right]\right\} \tag{55}$$

Equation (55) can be transformed into a more convenient form:[37]

$$c_s = c_0\left(1 - \frac{i_{dc}}{i_L}\right) - \frac{i_p}{zF(D\omega)^{1/2}}\sin(\omega t - \pi/4) \tag{56}$$

The solution obtained is of the same form as in the case of an unstirred electrolyte,[20,46] *i.e.,* if the condition are given by Eq. (11) it can be written in the form

$$c(t,\infty) = c_0 \tag{57}$$

The maximum difference between the surface concentration and the surface concentration in DC steady state conditions, *i.e.*,

$$c_s = c_0\left(1 - \frac{i_{dc}}{i_L}\right) = c_0 - \frac{\delta\, i_{av}}{zFD} \tag{58}$$

corresponds to the values $\sin(\omega t - \pi/4) = \pm 1$. For $z = 2$, $F = 10^5$ C mol^{-1}, $c_0 = 10^{-4}$ mol cm^{-3} and $\nu = 50$ Hz the term $\dfrac{i_p}{zF(D\omega)^{1/2}}$ can be neglected in Eq. (56) relative to $c_0\left(1 - \dfrac{i_{dc}}{i_L}\right)$, except for the cases of high i_p and $i_{dc} = i_L$.[37]

Hence, at sufficiently small T and not extremely high i_p, c_s in AC will also be given by Eq. (50), implying that at sufficiently high frequencies, the surface concentration is determined by the average current density, regardless of the shape of the current wave.

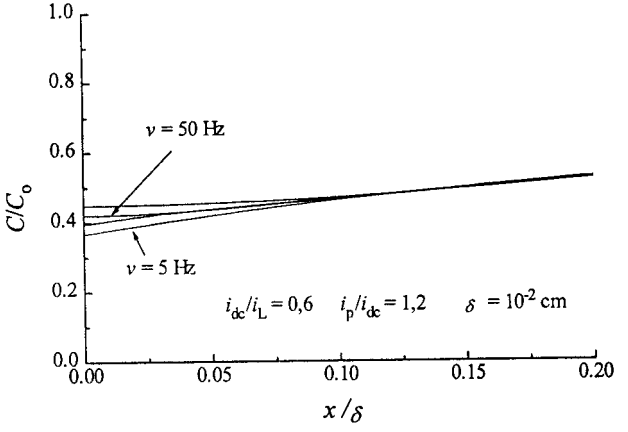

Fig. 17. The effect of the AC frequency on the concentration distribution inside the diffusion layer. (From Maksimović and Popov[47]).

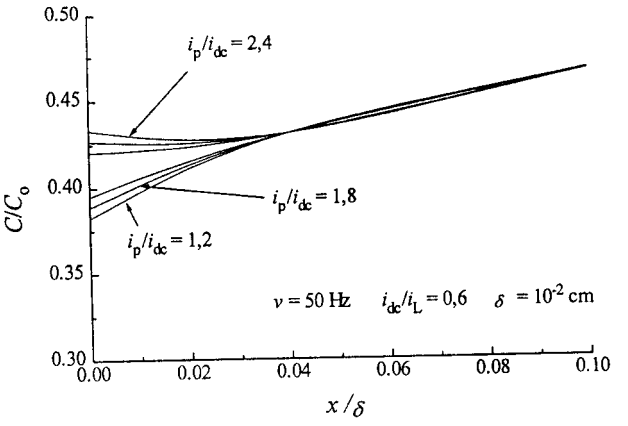

Fig. 18. The effect of the AC amplitude on the concentration distribution inside the diffusion layer. (From Maksimović and Popov[47]).

The concentration distribution inside the diffusion layer, using Eq. (54) and the already used set of parameters ($\delta = 10^{-2}$ cm, $D = 10^{-5}$ cm^2 s^{-1} and $t_0 = 1$ s), is given in Figs. 17–20 for different AC regimes and $\cos(\omega t - \pi/4) = 0$.[47]

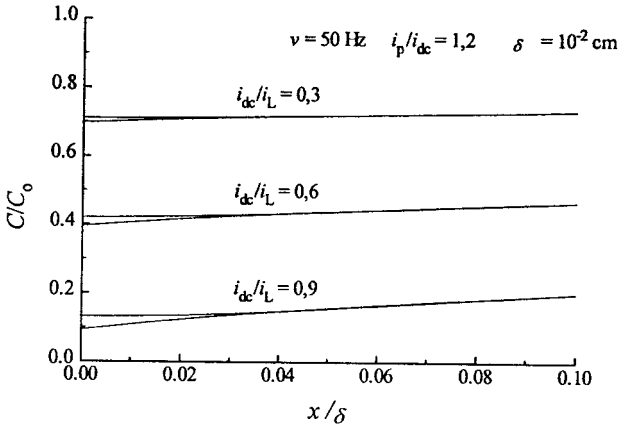

Fig. 19. The effect of the average current density on the concentration distribution inside the diffusion layer. (From Maksimović and Popov[47]).

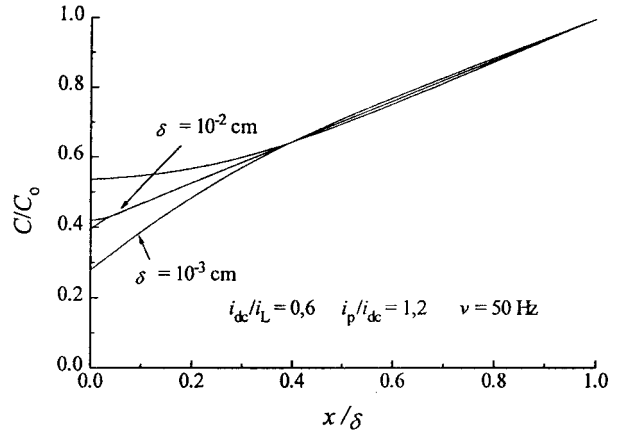

Fig. 20. The effect of the diffusion layer thickness on the concentration distribution inside the diffusion layer. (From Maksimović and Popov[47]).

It can be seen that the effects of frequency, current density and i_p/i_{dc} ratios are practically negligible; the effect of the diffusion layer thickness is more pronounced, being still lower than in the other cases of periodic currents.

3. THE INFLUENCE OF THE CHARGE AND DISCHARGE OF THE ELECTRICAL DOUBLE LAYER

The useful range of frequencies in electrodeposition at a periodically changing rate is known to be limited by mass-transfer effects at low frequencies. At high frequencies, the useful range is limited by the effect of the capacitance of the electrical double layer.[44,48] Details are given in a previous review.[49]

4. THE VALIDITY OF THE MATHEMATICAL MODEL

4.1. Reversing current in the millisecond range

The fact that in the millisecond range, the surface concentration under periodic conditions practically does not vary with time has been experimentally verified. For example, it follows from Eq. (27) that for $i_c = i_a$ and $r = 1$ during RC deposition

$$c_s = c_0 \tag{59}$$

The shape of the RC used and a typical overpotential *versus* time response are shown in Fig. 21 for copper deposition from 0.075 M $CuSO_4$ in 0.5 M H_2SO_4.[50] The current densities and overpotential from these oscillographs, corrected for the ohmic drop, are plotted in Fig. 22. The Tafel lines obtained in this way are similar to those obtained by Mattsson and Bockris[51] in the galvanostatic single-pulse regime for the same system. This is because, at 100 Hz, condition (27) is satisfied and a concentration overpotential does not appear.

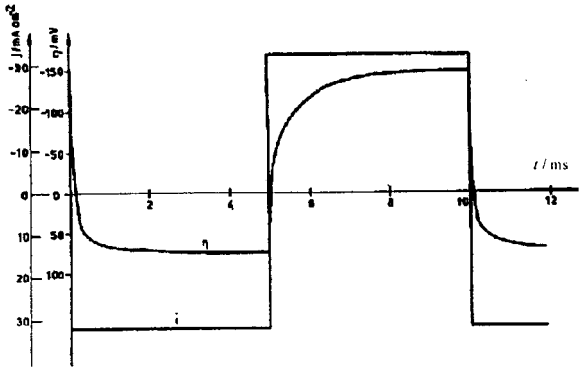

Fig. 21. The shape of the square-wave alternating current and the typical overpotential *versus* time response. Copper electrodeposition from 0.075 M $CuSO_4$ in 0.5 M H_2SO_4. (From Popov *et al.*[50]).

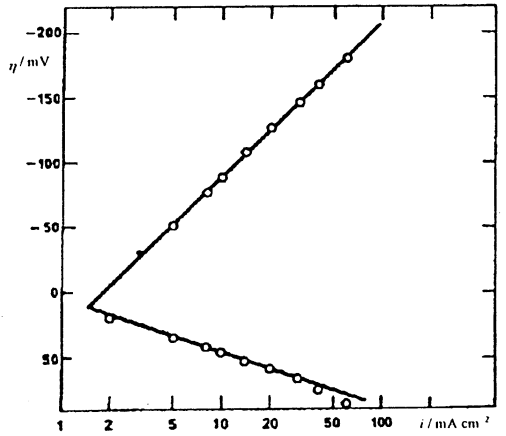

Fig. 22. The cathodic and anodic Tafel lines (obtained from graphs similar to those in Fig. 21) for the $Cu^{2+}|Cu$ system from 0.075 M $CuSO_4$ in 0.5 M H_2SO_4. (From Popov et al. [50]).

4.2. Reversing current in the second range

The mathematical model of RC in the second range can be easily tested for $i_c > i_L$. The solution of Eqs. (9) to (12) for

$$i(t) = i_c \tag{60}$$

is given by[43,52]

$$c_s = c_0 - \frac{i_c \delta}{zFD}\left\{1 - \frac{8}{\pi^2}\sum_{k=0}^{\infty}\frac{1}{(2k+1)^2}\exp\left[-\frac{(2k+1)^2 t}{4t_0}\right]\right\} \tag{61}$$

and the surface concentration of depositing ions for $t \geq t_0$ is given by[43]

$$c_s = c_0 - \frac{i_c \delta}{ZFD}\left\{1 - \frac{8}{\pi^2}\exp\left(-\frac{t}{4t_0}\right)\right\} \tag{62}$$

The maximum amplitude of the current density variation, i_A, corresponding $c_s = 0$ after a deposition time t_c is given by

$$i_A = \frac{i_L}{1 - \frac{8}{\pi^2}\exp\left(-\frac{t_c}{4t_0}\right)} \tag{63}$$

or taking into account $t_c = T/(r+1)$ by

$$i_A = \frac{i_L}{1 - \frac{8}{\pi^2}\exp\left(-\frac{T}{4(r+1)\,t_0}\right)} \tag{64}$$

Substitution of r from Eq. (31) in Eq. (64) and further rearranging gives[53]

$$T = \frac{4\delta^2}{\pi^2 D}\ln\frac{1 - \frac{\pi^2}{16} + \frac{i_L}{i_A}}{\frac{\pi^2}{16}\left(1 - \frac{i_L}{i_A}\right)} \tag{65}$$

In this way the period T of the RC wave and the amplitude current density i_A, which makes the surface concentration at the end of the cathodic pulse zero, are related if the final surface concentration (the end of the anodic pulse) is equal to the initial surface concentration (the beginning of the cathodic pulse) and $i_A \geq i_L$.

Dependencies of overpotential on time were obtained upon application of different RC input waves. The results for the unstirred solution are shown in Figs. 23a – 23c. It can be seen from Fig. 23a that the shape of the overpotential wave does not vary with time after about the first 3 periods, meaning that a steady state periodic response was established. With anodic pulses of shorter duration (Fig. 23b), the overpotential at the end of the cathodic pulses increases, indicating a decrease in the surface concentration. The opposite effect takes place with longer anodic pulse duration (Fig. 23c).

The results for stirred solution are presented at Fig. 23d. Following the same procedure as in the previous case, the RC wave which leads to a steady state periodic response was determined. The shape of the RC wave from Fig. 23d is the same as for the case of unstirred solution, but, due to different hydrodynamic conditions, the period T is quite different.

The T *versus* δ^2 plot shown in Fig. 24. proves that Eq. (65) is valid and that, for metal deposition by RC in the second range, the condition $T/\delta^2 = \text{const.}$ must be fulfilled in order to obtain the same effect on the mass transfer under hydrodynamic conditions, for the same i_A/i_L.

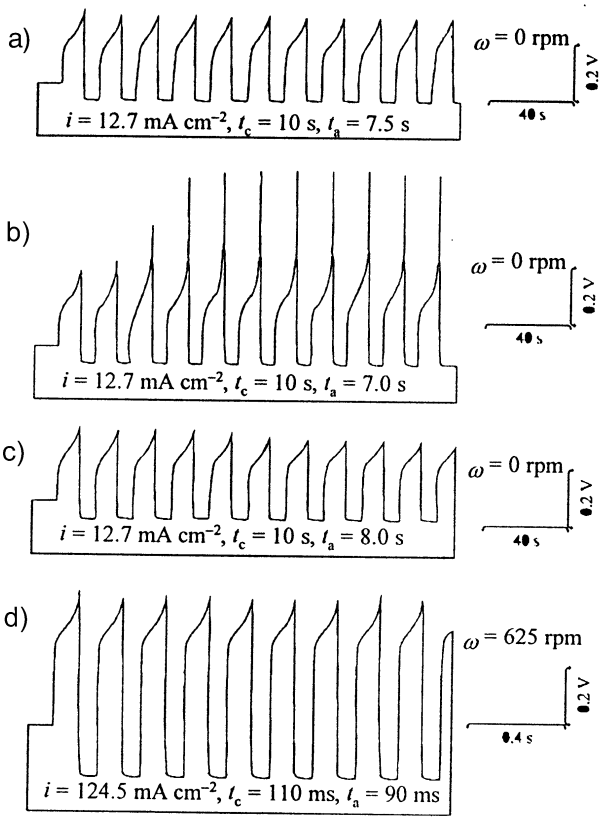

Fig. 23. The dependencies of the overpotential on time, obtained upon application of different RC wave inputs in 0.1 M $CuSO_4$ in 0.5 M H_2SO_4. (From Maksimović *et al.*[54]).

Finally, the current wave with the same i_A and t_c/t_a ratio, but in the millisecond range leads to a potential response characteristic for the dominance of activation control (Fig. 25). The above fact is a continuation of all earlier theoretical predictions.

4.3. Pulsating current

During the pause, under non-current conditions, at frequency values below those of double layer effects, which may, therefore, be neglected, but for which Eq. (44) is valid, the measured potential is equal to the Nernst concentration potential

$$\varphi = \frac{RT}{zF} \ln \frac{c_0}{c_s} \tag{66}$$

Taking into account that

$$c_s = c_0 \left(1 - \frac{i_{av}}{i_L}\right) \tag{67}$$

Eq. (66) can be rewritten in the form

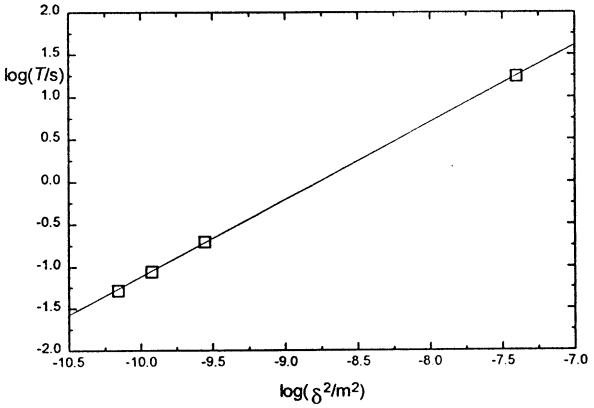

Fig. 24. The dependence of the period of pulsation, T, on the square of the diffusion layer thickness, δ^2 for copper electrodeposition from 0.1 M $CuSO_4$ in 0.5 M H_2SO_4. (From Maksimović *et al.*[54]).

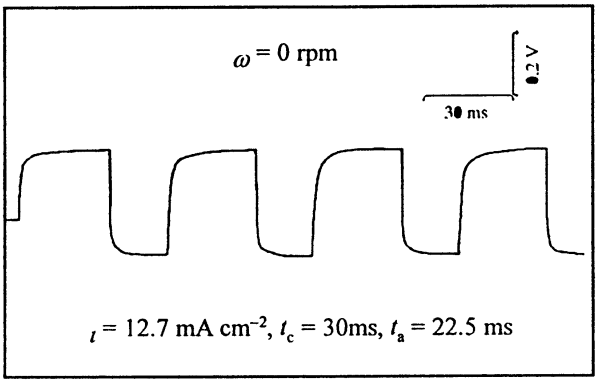

Fig. 25. The potential response to the RC in the millisecond range with the same i_A and t_c/t_a as in Fig 23a. Copper electrodeposition from 0.1 M $CuSO_4$ in 0.5 M H_2SO_4. (From Maksimović *et al.* [54]).

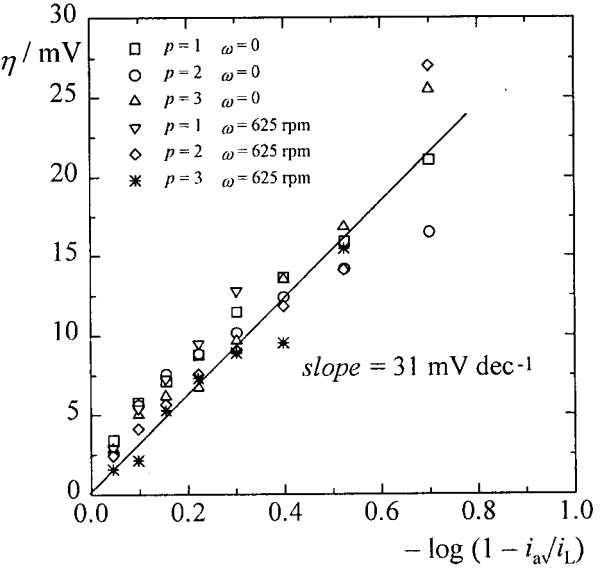

Fig. 26. The Nernst concentration potential at the end of the pause *vs.* log $(1 - i_{av}/i_L)$ in stirred and unstirred solutions (0.1 M $CuSO_4$ and 0.5 M H_2SO_4) for a pulse duration of 50 ms and different pause to pulse ratio. (From Maksimović *et al.* [54]).

$$\varphi = -\frac{RT}{zF}\ln\left(1-\frac{i_{av}}{i_L}\right) \tag{68}$$

The validity of Eq. (68) was tested by determining the concentration in an unstirred and stirred solution as a function of the i_{av}/i_L value. A PC with on period duration of 50 ms and p values of 1,2 and 3 was used. Fig. 26 shows that, in all cases, a straight line with a slope of 31 mV dec^{-1} was obtained. The slope value is very close to 29.5 mV dec^{-1} which is predicted by the Eq. (68), meaning that the mathematical model of PC is operative. This was also proven by considering the overpotentials during the current pulses.[55]

4.4. Pulsating overpotential

In the case of a rectangular pulsating overpotential, $\eta(t)$ as a function of time is given by [56]

$$\eta(t) = \begin{cases} \eta_A, & \text{for } mT < t \le [m + 1/(p+1)]T \\ 0, & \text{for } [m + 1/(p+1)]T < t \le (m+1)T \end{cases} \tag{69}$$

Assuming that the surface concentration is determined by the average current density, the current response to the input overpotential is given by

$$i(t) = i_0\left[\left(1-\frac{i_{av}}{i_L}\right)\exp\left(\frac{\eta(t)}{\eta_{oc}}\right) - \exp\left(\frac{-\eta(t)}{\eta_{oa}}\right)\right] \tag{70}$$

For a sufficiently high η_A, Eq. (70) reduces during the on periods to

$$i_{on} = i_0\left(1-\frac{i_{av}}{i_L}\right)\exp\left(\frac{\eta_A}{\eta_{oc}}\right) \tag{71}$$

and during the off periods to

$$i_{off} = -i_0\frac{i_{av}}{i_L} \tag{72}$$

The average current in PO deposition can easily be determined by

$$i_{av} = \frac{i_0}{p+1}\left[\left(1-\frac{i_{av}}{i_L}\right)\exp\left(\frac{\eta_A}{\eta_{oc}}\right) - p\frac{i_{av}}{i_L}\right] \tag{73}$$

The average overpotential is then given by

$$\eta_{av} = \frac{\eta_{dc}}{p+1} + \frac{\eta_{oc}}{p+1}\ln\left(p+1+p\frac{i_0}{i_L}\right) \tag{74}$$

where

$$\eta_{dc} = \eta_{oc}\ln\frac{i_{av}}{i_0} - \eta_{oc}\ln\left(1-\frac{i_{av}}{i_L}\right) \tag{75}$$

and

$$\eta_{av} = \frac{\eta_A}{p+1} \tag{76}$$

Polarization curves for the average values for copper deposition have been successfully calculated from the stationary polarization curve using Eq. (74)[56] for $i_0 << i_L$, as shown in Fig. 27.

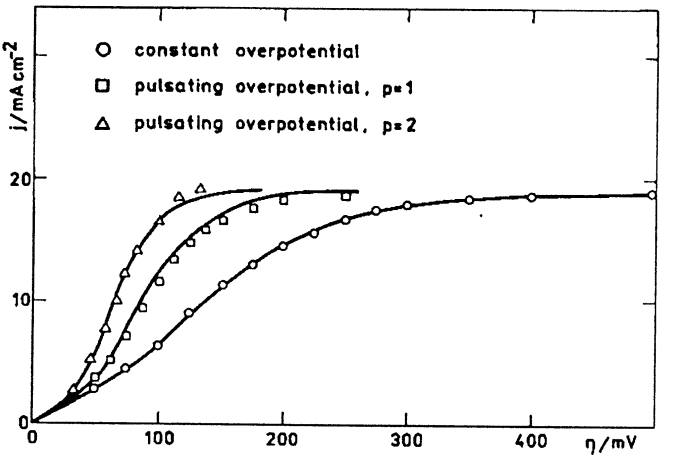

Fig. 27. The stationary polarization curve and the polarization curves of the average values for different pause-to-pulse ratios in a square-wave PO copper electrodeposition from 0.2 M $CuSO_4$ in 0.5 M H_2SO_4. Pulse duration 20 ms. The points represents measured values and the full lines are calculated using Eq. (76) and values from the constant polarization curve. (From Popov *et al.* [56]).

This is a good proof that in PO deposition, the average current density also determines the surface concentration of the depositing ion.

5. CONCLUSION

The mass-transfer conditions during metal electrodeposition at a periodically changing rate are very important because they determine the morphology of metal deposits just as in the case of electrodeposition at a constant rate. Electrodeposition at a periodically changing rate was described by a common mathematical model and the particular solutions for each type of waveform used are given in the form of time and distance-dependent concentrations inside electrode diffusion layer. It was shown that in all cases of deposition in the millisecond range the surface concentration of depositing ions is constant and determined by the average deposition current density at sufficiently large frequencies of pulsation. At lower frequencies the surface concentration oscillates around the value corresponding to the deposition by the average current density during the constant current deposition. In the case of reversing current deposition in a second range the concentration varies with time in a way that surface concentration at the end of the anodic pulse is close to initial one. All theoretical conclusion are verified by appropriate experiments. The above

solutions are important because they permit to correlate the morphology of deposits with depositing regime, as in the case of constant current deposition.

SUMMARY

The mass-transfer conditions during electrodeposition of metals at a periodically changing rate are considered. The concentration distribution inside the diffusion layer and the surface concentration of depositing ions for pulsating and reversing current and pulsating overpotential are discussed and illustrated by the appropriate experiments. On the basis of the above results, the maximum deposition rates and the effect on the morphology of metal deposits can be elucidated in all cases under consideration.

ИЗВОД

ПРЕНОС МАСЕ ТОКОМ ЕЛЕКТРОХЕМИЈСКОГ ТАЛОЖЕЊА МЕТАЛА ПЕРИОДИЧНО ПРОМЕНЉИВОМ БРЗИНОМ

МИОДРАГ Д. МАКСИМОВИЋ и КОНСТАНТИН И. ПОПОВ

Технолошко-металуршки факултет, Универзитет у Београду, п.пр. 3503, 11120 Београд

Размотрени су услови преноса масе током електрохемијског таложења метала периодично променљивом брзином. Расподела концентрације унутар дифузиног слоја и површинска концентрација јона који се таложе дискутоване су и илустроване одговарајућим експериментима за пулсирајућу и реверсну струју и пулсирајућу пренапетост. На основу изнетих резултата могуће је проценити максималну брзину таложења и утицаја на морфологију у свим размотреним случајевима.

(Примљено 2. фебруара 1999)

REFERENCES

1. N.N.Bibikov, *Electrodeposition of Metals by AC*, Mashgiz, Moscow, 1961 (in Russian)
2. J.W.Dini, *Met. Finish.* **61** (1963) 52
3. G.T.Bakhvalov, *New Technology of Electrodeposition of Metals*, Izd. Met., 1966 (in Russian)
4. A.R.Despić, K.I.Popov, *Modern Aspects of Electrochemistry*, No. 7, B.E.Conway and J.O'M.Bockris, Eds., Plenum Press, New York, 1972, p. 199
5. C.C.Wan, H.Y.Cheh, H.B.Linford, *Plating* **61** (1974) 559
6. R.B.Snider, H.Y.Cheh, *Plat. Surf. Finish.* **62** (1975) 786
7. J.Cl.Puippe, N.Ibl, *Oberfläche-Surface* **18** (1977) 205
8. G.Perger, P.M.Robinson, *Met. Finish.* **77** (12) (1979) 17
9. S.Venkatesh, D.T.Chin, *Isr. J. Chem.* **18** (1979) 56
10. N.Ibl, *Surface Technol.* **10** (1980) 81
11. E.Robert, *Oberfläche-Surface* **24** (1983) 413
12. D.Landolt, *Oberfläche-Surface* **25** (1984) 6
13. Yu.M.Polukarov, V.V.Grinina, *Itogi nauki i tehniki (Elektrokhimiya)*, No. 22, Viniti, Moscow, 1985, p. 8
14. A.M.Pesco, H.Y.Cheh, *Modern Aspects of Electrochemistry*, No. 19, B.E.Conway, J.O'M.Bockris and R.E.White, Eds., Plenum Press, New York, 1989, p. 251

15. K.I.Popov, M.D.Maksimović, *Modern Aspects of Electrochemistry*, No. 19, B.E.Conway, J.O'M.Bockris and R.E.White, Eds., Plenum Press, New York, 1989, p. 193
16. K.I.Popov, D.N.Keča, S.I.Vidojković, B.J.Lazarević, V.B.Milojković, *J. Appl. Electrochem.* **6** (1976) 365
17. K.Viswanathan, H.Y.Cheh, *J. Electrochem. Soc.* **126** (1979) 398
18. D.T.Chin, *J. Electrochem. Soc.* **130** (1983) 1657
19. E.Warburg, *Ann. Physik.* **67** (1899) 493
20. F.Krüger, *Z. Phys. Chem.* **45** (1903) 1
21. T.R.Rosebrugh, W.L.Miller, *J. Phys. Chem.* **14** (1910) 816
22. V.I.Chernenko, M.A.Loshkarev, Z.I.Levitin, *Zh. fiz. khim.* **37** (1963) 1015
23. V.I.Chernenko, K.I.Litovchenko, *Elektrokhimiya* **4** (1968) 1452
24. H.Y.Cheh, *J. Electrochem. Soc.* **118** (1971) 551
25. H.Y.Cheh, *J. Electrochem. Soc.* **118** (1971) 1133
26. A.R.Despić, K.I.Popov, *J. Appl. Electrochem.* **1** (1971) 275
27. V.I.Belokon, B.B.Chernov, N.Ya.Kovarskiy, *Elektrokhimiya* **11** (1975) 1655
28. K.Tokuda, H.Matsuda, *J. Electroanal. Chem.* **82** (1977) 157
29. K.Tokuda, H.Matsuda, *J. Electroanal. Chem.* **90** (1978) 147
30. N.N.Alekseenko, S.L.Goldsteyn, D.F.Rakipov, S.P.Raspopin, *Elektrokhimiya* **14** (1978) 676
31. K.Viswanathan, M.A.Farrell Epstein, H.Y.Cheh, *J. Electrochem. Soc.* **125** (1978) 1772
32. K.Viswanathan, H.Y.Cheh, *J. Appl. Electrochem.* **9** (1979) 537
33. K.I.Popov, M.D.Maksimović, B.M.Ocokoljić, B.J.Lazarevic, *Surface Technol.* **11** (1980) 99
34. P.C.Andricacos, H.Y.Cheh, *J. Electroanal. Chem.* **121** (1981) 133
35. S.Venkatesh, D.T.Chin, *J. Electrochem. Soc.* **128** (1981) 2588
36. K.I.Popov, M.D.Maksimović, M.S.Simić, *Surface Technol.* **16** (1982) 209
37. M.D.Maksimović, D.C.Totovski, A.P.Ivic, *Surface Technol.* **18** (1983) 233
38. R.Sethi, D.T.Chin, *J. Electroanal. Chem.* **160** (1984) 79
39. C.Y.Cheng, D.T.Chin, *Am. Inst. Chem. Eng. J.* **30** (1984) 757
40. C.Y.Cheng, D.T.Chin, *Am. Inst. Chem. Eng. J.* **30** (1984) 765
41. A.M.Pesco, H.Y.Cheh, *J. Electrochem. Soc.* **131** (1984) 2259
42. M.D.Maksimović, K.I.Popov, *Zaštita materijala*, **36** (1995) 91
43. K.I.Popov, M.D.Maksimović, *J. Serb. Chem. Soc.* **56** (1991) 25
44. K.I.Popov, M.D.Maksimović, D.C.Totovski, *J. Serb. Chem. Soc.* **50** (1985) 319
45. M.D.Maksimović, K.I.Popov, *Zaštita materijala*, **37** (1996) 45
46. Z.Kovač, *J. Electrochem. Soc.* **118** (1971) 51
47. M.D.Maksimović, K.I.Popov, *Zaštita materijala,* **38** (4) (1997) 8
48. J.Cl.Puippe, *Theory and Practice of Pulse Plating*, J. Cl. Puippe and F. Leaman, Eds., AESFS, Orlando, 1986. Chap. 1
49. M.D.Maksimović, *J. Serb. Chem. Soc.* **60** (1995) 119
50. K.I.Popov, M.D.Maksimović, V.M.Nakić, M.D.Spasojević, *Glasnik Hem. društva Beograd*, **47** (1982) 511
51. B.E.Mattsson, J.O'M.Bockris, *Trans. Farday Soc.* **55** (1959) 1586
52. K.J.Vetter, *Elektrokhimicheskaya Kinetika*, Khimiya, Moskva, 1967
53. J.Cl.Puippe, *Theory and Practice of Pulse Plating*, J.Cl.Puippe and F.Leaman, Eds., AESFS, Orlando, 1986. Chap. 4
54. M.D.Maksimović, S.Gojković, R.M.Stevanović, K.I.Popov, *Bull. Electrochem.* **13** (1997) 413
55. K.I.Popov, M.D.Maksimović, V.M.Nakić, M.D.Spasojević, *Surf. Technol.* **15** (1982) 161
56. K.I.Popov, M.D.Maksimović, S.K.Zečević, M.R.Stojić, *Surf. Technol.* **27** (1986) 117.

J. Serb. Chem. Soc. 64(5– 6)341-347(1999)
JSCS-2674

UDC 621.352:537.313/.314:543.251
Original scientific paper

The current distribution in an electrochemical cell. Part IV. The relation to the Haring-Blum method

KONSTANTIN I. POPOV, SLAVIŠA M. PEŠIĆ* and TANJA M. KOSTIĆ

*Faculty of Technology and Metallurgy, University of Belgrade, Karnegijeva 4, P. O. Box 3503, YU-11120 Belgrade, Yugoslavia, *Ei-Štampana kola d.d., Printed Circuit Board Factory, Bul. Cara Konstantina 80-84, YU-18000 Niš, Yugoslavia*

(Received 26 January, revised 25 February 1999)

It was shown that the current density-cell voltage curves recorded in a cell with parallel plate electrodes for different distances between the edges of the electrodes and side walls of the cell can be used to determine the current distribution in cells of the Haring-Blum type.

Key words: metal electrodeposition, electrochemical cell, current distribution.

It has been shown earlier[1] that the ohmic resistance of the electrolyte in a cell decreases as the distance between the edge of the electrode and the side wall of the cell increases,according to relation

$$R_{\text{eff}} = \frac{R_{\text{h}}}{2k} \ln (1 + 2k) \tag{1}$$

where R_{eff} is the electrolyte resistance in a cell in which the edges of the electrodes do not touch the side wall of the cell and R_{h} is the electrolyte resistance of the same cell but with the edges of the electrodes touching the side walls. The parameter k is given by

$$k = \frac{L}{A} \tag{2}$$

where L is the distance between the edge of the electrode and the side wall of the cell, and A is the electrode length.

It was found experimentaly, using the bridge method, that Eq. (1) is valid up to $k \approx 1$, when $R_{\text{eff}} \approx 0.5\, R_{\text{h}}$. The value of R_{eff} does not change as k increases further.

As a consequence of this, the current in a cell in which the edges of the electrodes do not touch the side wall will be considerably larger than in a cell in which the edges of the electrodes do touch the side walls[2-4] (at the same cell voltage and inter-electrode distance and if the activation overpotential is not very large). It

is easy to show that, for a distance l_{eff}, the ohmic resistance of the electrolyte in a cell in which the edges of the electrodes touch the side walls is equal to the ohmic resistance of the electrolyte in a cell in which the edge of the electrode is at a distance L from the side wall of the cell and at the inter-electrode distance l, providing

$$l_{\text{eff}} = \frac{lA}{2L} \ln\left(1 + \frac{2L}{A}\right) \tag{3}$$

Hence, from the current density-cell voltage dependences for different distances between the edge of the electrode and the side wall of the cell, the current distribution between cathodes at different distances from the anode can be obtained and used for the calculation of the current distribution indexes according to Haring and Blum,[5] Heatly,[6] Pan,[7] Field,[8] and Popov *et al.*[4] It is to note that the throwing power index, defined recently by Popov *et al.,* is very similar to that of Heatley[6] and Pan.[7] In all the above methods, the ratio of the primary current densities, P, and that of the actual metal distribution, M, are included in the corresponding formulas.

According to Haring and Blum,[5] the throwing power is given by

$$T = \frac{P-M}{P} \times 100\% \tag{4}$$

and according to Heatley[6] and Pan[7]

$$T = \frac{P-M}{P-1} \times 100\% \tag{5}$$

and Field[8]

$$T(\text{BSI}) = \frac{P-M}{P+M-2} \times 100\% \tag{6}$$

where $P = \frac{l_{\text{far}}}{l_{\text{near}}}$ and $M = \frac{\Delta m_{\text{near}}}{\Delta m_{\text{far}}}$, l_{far} and l_{near} are the far and near cathode-anode distance, respectively, and Δm_{far} and Δm_{near} the weight of deposit on the far and near electrode, respectively. It is obvious that $l_{\text{far}} = l$ and $l_{\text{near}} = l_{\text{eff}}$ in the region where Eq. (3) is valid, and that it is possible to obtain the P values as the ratio of corresponding ohmic resistances calculated from the slopes of ohmic controlled current density-cell voltage curves. The values of M are obtained from mixed controlled current density-cell voltage curves for the same geometry of the system, because, in the case of copper deposition from acid sulphate solution, M can be substituted by current density ratios.

It can be seen from Eqs. (4) and (5) that for no deposit on the far cathode T must be minus infinity and according to Eq. (6) – 100%. According to a more suitable definition, the throwing power index S can be viewed as the degree to which the secondary current density distribution cancels the bad effects of the primary current density distribution from 0 –100% or, for no deposit on the far cathode, from $\frac{-1/P}{1-1/P}$ up to 100%, as can be seen from Eq. (7).

$$S = \frac{\frac{1}{M} - \frac{1}{P}}{1 - \frac{1}{P}} \times 100\ \% \qquad (7)$$

Typical Haring-Blum throwing power cells have $P = 5$, *i.e.*, the far cathode is 5 times as far from the anode as the near cathode. Also, cells with $P = 2$ are used. These measured quantities depend on the scale of the experiment and so are not absolute values; but, in general, a solution exhibiting good throwing power in such a test will exhibit it in practise also.

RESULTS AND DISCUSSION

The different effects on the current distribution can be illustrated in a qualitative way by all the cited equations, however, Eq. (7) seems to be the best one.

The values of T calculated using Eqs. (4–6) and S using Eq. (7) for different situations as functions of the normalized deposition current density (to the limiting diffusion current for $L = 0$) are shown in Figs. 1–3. The primary current distributions for l = 50 mm and l = 150 mm were calculated from the slopes of the current density-cell voltage curves (complete ohmic control) for different electrode edges-side wall distances from Figs. 3 and 6 from Ref. 3, respectively, and the actual current density distribution from Figs. 5 and 7 from Ref. 2, and Figs. 1 and 2 from Ref. 3 (mixed controlled deposition).

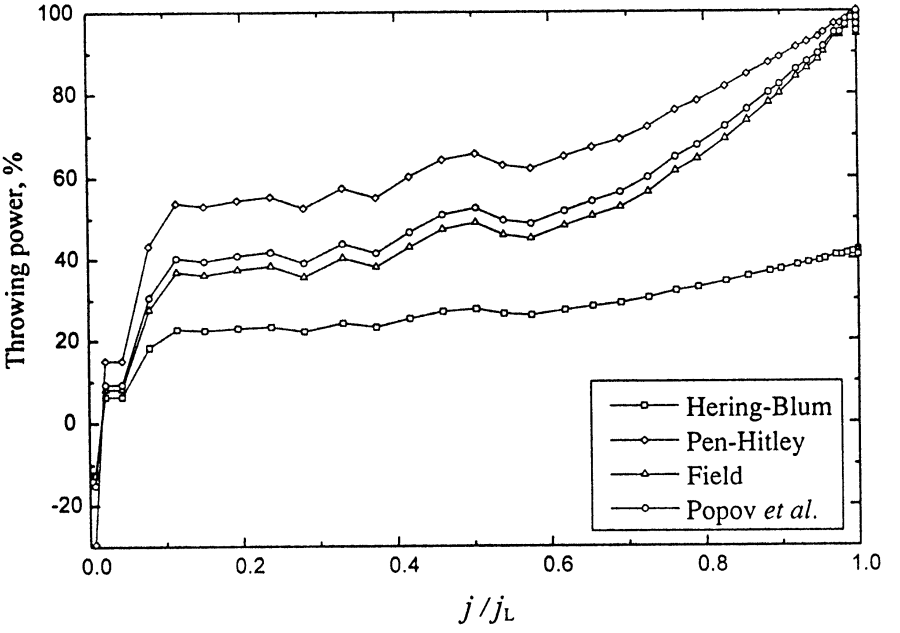

Fig. 1. The throwing power indexes for the system Cu|0.1 M $CuSO_4$, 0.1 M H_2SO_4|Cu with l = 50 mm and L = 25 mm as functions of the normalized current density. (Data from Fig. 5, Ref. 2 and Fig. 3, Ref. 3).

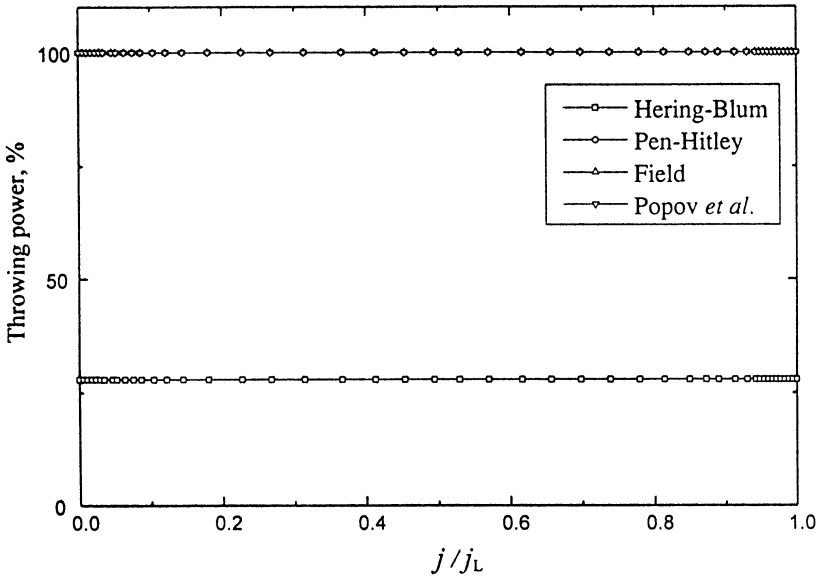

Fig. 2. The throwing power indexes for the system Cu|0.1 M $CuSO_4$, 0.5 M H_2SO_4|Cu with l = 50 mm and L = 25 mm as functions of the normalized current density. (Data from Fig. 1 and Fig. 3, Ref. 3).

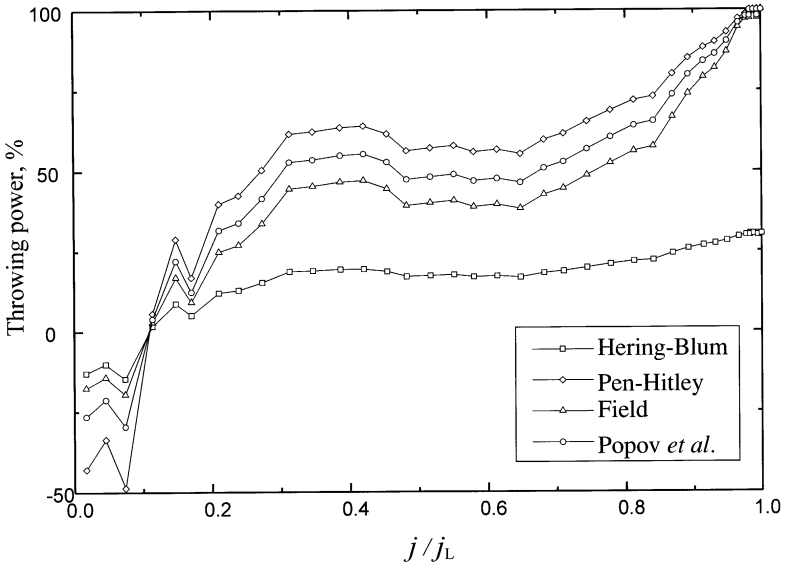

Fig. 3. The throwing power indexes for the system Cu|0.1 M $CuSO_4$, 0.5 M H_2SO_4|Cu with l = 150 mm and L =50 mm as functions of the normalized current density. (Data from Fig. 2 and Fig. 6, Ref. 3).

The effects of the inter-electrode distance and resistivity of the electrolyte are illustrated by Figs. 3–6. It can be seen that the current distribution is better with smaller

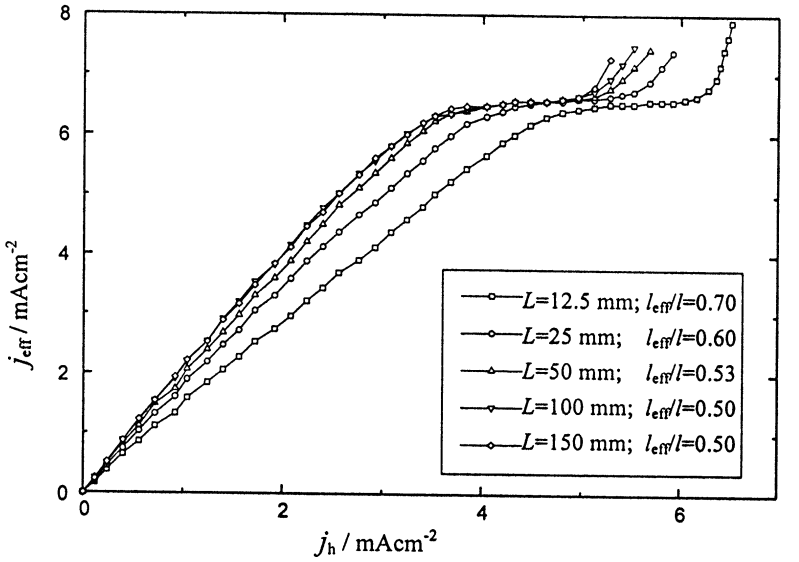

Fig. 4. Current density for different L and l_{eff} as a function of the current density in the cell with inter-electrode distance l and $L = 0$ for the system Cu|0.1 M $CuSO_4$, 0.1 M H_2SO_4|Cu. (Data from Fig. 7, Ref. 2).

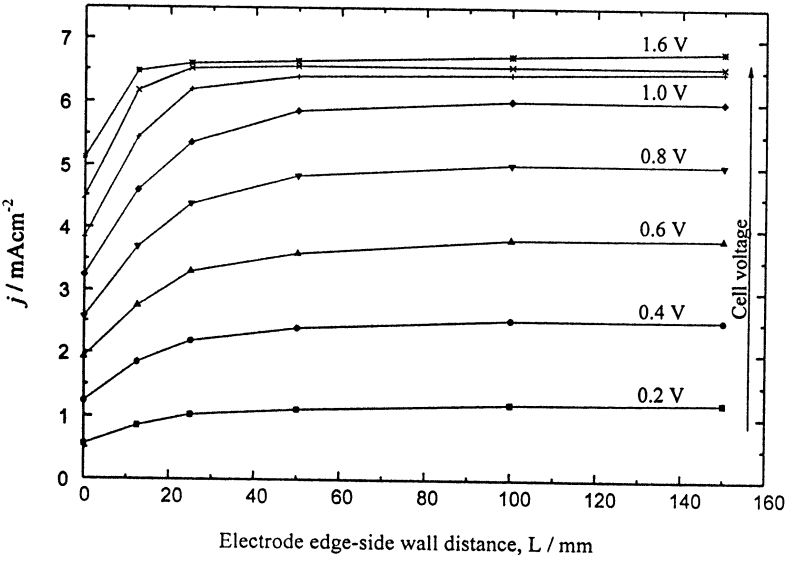

Fig. 5. Current density for different cell potentials as functions of L in a cell with an inter-electrode distance $l = 150$ mm for the system Cu|0.1 M $CuSO_4$, 0.1 M H_2SO_4|Cu. (Data from Fig. 7, Ref. 2).

inter-electrode distances and larger supporting electrolyte concentrations.[3] The ideal current distribution for an inter-electrode distance of 50 mm is obtained at 0.5 M H_2SO_4; for an inter-electrode distance of 150 mm with the same concentration of supporting electrolyte, the current distribution is similar to that from Fig. 1.

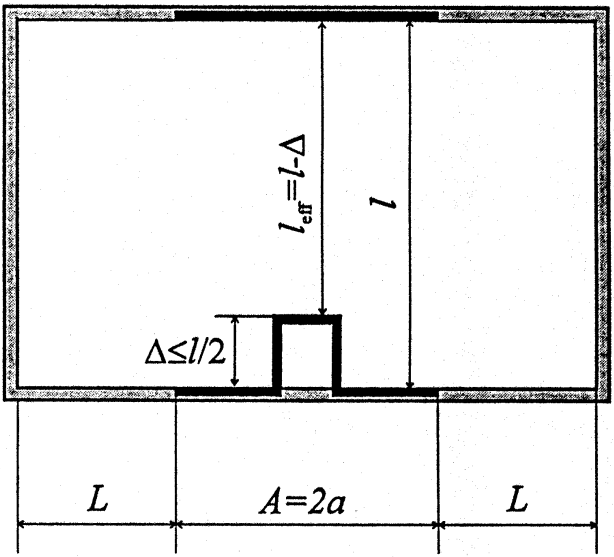

Fig. 6. The scheme of the electrochemical cell with plane-parallel electrodes and different inter-electrode distances.

On the other hand, the absolute values of current densities on the flat electrode surfaces at different distances from the anode can be obtained directly from the current density-cell voltage dependences from Ref. 2–4, making the calculation of the throwing power indexes unusefull. Besides, in this way, j_h/j_{eff} for different inter-electrode distances in the region $0 \leq l_{eff} \leq l/2$ can be easily determined from the polarization curves slopes up to $L = l/2$. The current density-cell voltage dependences from Ref. 2–4 can be reploted in the form permitting the correlation between the current in the cell for an inter-electrode distance l and $L = 0$ mm and the current in the same cell for $0 < L \leq l/2$, *i.e.,* with different l_{eff}, as seen from Fig. 4. They can also be reploted in the form shown in Fig. 5, permitting the determination of current in cell with different L at different cell potentials. It is also seen from Fig. 5 that the change of current with increasing L is practically finished at $L = A$, and is completely finished at $L = l/2$. Hence, for the determination of the current density distribution in the cell, schematically shown in Fig. 6, a method for the estimation of the current densities at the very edges of the electrodes is required. Such a method will be proposed in a future paper.

И З В О Д

РАСПОДЕЛА СТРУЈЕ У ЕЛЕКТРОХЕМИЈСКОЈ ЋЕЛИЈИ. ДЕО 4. ВЕЗА СА МЕТОДОМ ХАРИНГ-БЛУМА

КОНСТАНТИН И. ПОПОВ, СЛАВИША М. ПЕШИЋ* и ТАЊА М. КОСТИЋ

*Технолошко-металуршки факултет, Универзитет у Београду, Карнегијева 4, п.пр. 3503, 11120 Београд и *ЕИ-Штампана кола д.д., Бул. Цара Константина 80-84, 18000 Ниш*

Показано је да се криве густина струје-напон регистроване за ћелију са план-паралелним електродама различитих растојања између ивица електрода и бочних зидова ћелије могу искористити за одређивање расподеле струје у ћелијама типа Харинг-Блум.

(Примљено 26. јануара, ревидирано 25. фебруара 1999)

REFERENCES

1. K. I. Popov, M. D. Maksimović, D. Ć. Totovski, V. M. Nakić, *Surface Technology* **19** (1983) 173
2. K. I. Popov, S. K. Zečević, S. M. Pešić, *J. Serb. Chem. Soc.* **60** (1995) 307
3. K. I. Popov, S. K. Zečević, S. M. Pešić, *J. Serb. Chem. Soc.* **61** (1996) 583
4. K. I. Popov, S. K. Zečević, S. M. Pešić, *J. Serb. Chem. Soc.* **61** (1996) 1225
5. H. E. Haring, W. Blum, *Trans. Electrochem. Soc.* **44** (1923) 313
6. A. H. Hitley, *Trans, Electrochem. Soc.* **44** (1923) 283
7. L. C. Pan, *Trans. Electrochem. Soc.* **58** (1930) 423
8. S. Field, *Metal Ind.* (London) **44** (1934) 614*; J. Electrodepositors' Techn. Soc.* **9** (1934) 144.

J. Serb. Chem. Soc. 64(5– 6)349-358(1999)
JSCS-2675

UDC 547.979.732:546.56/.562
Original scientific paper

Cretaceous-Tertiary boundary layer at Stevns Klint (Denmark): copper and copper(II) porphyrins

PAVLE I. PREMOVIĆ, NIKOLA D. NIKOLIĆ, IVANA R. TONSA, DEJAN T. DULANOVIĆ and MIRJANA S. PAVLOVIĆ*

*Laboratory for Geochemistry and Cosmochemistry, Department of Chemistry, Faculty of Science, University of Niš, P.O.Box 91, YU-18000 Niš, Yugoslavia and * Vinča Institute of Nuclear Sciences, P.O. Box 522, YU-11001 Belgrade, Yugoslavia*

(Received 2 September 1998, revised 11 February 1999)

High concentrations (up to 4000 ppm) of copper(II) porphyrins have been detected in the kerogen of the Cretaceous/Tertiary (KT) boundary informal type sediment, the Fish Clay, at Stevns Klint, Denmark. These pigments have also been found in the Danish KT sediment at Nye Kløv, which is about 300 km away from Stevns Klint. However, copper(II) porphyrins cannot be detected in the Danich boundary rock of the Dania site, which is separated from Stevns Klint by about 200 km. It is proposed that the kerogen copper(II) porphyrins are derived from humic materials of terrestrial (peat/soil) sources already enriched with these compounds, which were redeposited in the Danish KT boundary Basin. In addition, our results show that the kerogen copper(II) porphyrins are present, for comparison, in the Permian Kupferschiefer shale from Poland. The amounts are comparable to those in the Fish Clay kerogen. To our opinion, the same processes responsible for the kerogen copper(II) porphyrin enrichment have occurred in the Stevns Klint KT boundary sediment and in the Kupferschiefer.

Key words: copper, porphyrins, kerogen, electron spin resonance.

The foundation of modern organic geochemistry is associated with Treibs' suggestion that sedimentary extractable (alkyl) metalloporphyrins are principally diagenetic end products of chlorophylls and bacterio-chlorophylls.[1] Nickel (Ni) and vanadyl (VO^{2+}) alkyl porphyrins are the two principal types of metalloporphyrins found in petroleums and carbonaceous sedimentary rocks, however, recent electron spin resonance (ESR) work in our laboratory have shown that the kerogens isolated from ancient carbonaceous sedimentary rocks of marine origin also contain significant amounts of VO^{2+} porphyrins incorporated into the kerogen structure.[2] It is generally agreed that the incorporation of the porphyrin nuclei into the kerogen matrix is essentially due to abiotic, diagenetic reactions and modifications of initial humic substances and associated chlorophylls.

We report here the wide occurrence of high concentrations of copper(II) porphyrins (named Cu^{2+}-P) (up to 4000 ppm) incorporated into the kerogen struc-

tures of the Cretaceous-Tertiary (KT) boundary layers from the Stevns Klint locality (Denmark). In addition, the Nye Kløv and Dania boundaries in the Jylland sequences near Stevns Klint were similarly investigated by ESR spectroscopy for the presence of Cu^{2+}-P in kerogen. These boundary layers are mineralogically identical to that at Stevns Klint.[3] For comparison, a study was conducted on Cu^{2+}-P of the kerogen of metalloferrous Permian Kupferschiefer (Poland) of comparable origin and geologic/geochemical history.

Cu^{2+}-P are found in acid-insoluble (humic acid) fractions in a wide variety of soil environments: recent soils[4-6] and paleosols.[7] These humic Cu^{2+}-P are largely derived from land plant chlorophylls under oxidizing conditions of the peat/soil formation. Although the widespread occurrence of VO^{2+}-P and nickel porphyrins in ancient sediments from different depositional environments has been reported, they are few reports of porphyrins complexed to Cu^{2+}. The occurrence of extractable Cu^{2+}-P is perhaps best authenticated by Palmer and Baker[8] and Baker and Louda[9,10] who isolated such species in very low concentrations (<1 ppm TOC) from a number of immature sedimentary rocks, giving evidence based on accurate mass measurement.[8] Baker and Louda[9,10] proposed that these Cu^{2+}-P may derive from, and be markers for, oxidized terrestrial organic matter redeposited in a marine environment.

During the debate about Stevns Klint KT boundary deposition, several genetic models were discussed in order to explain the source and enrichment processes for the base metals present in the boundary layer. Christensen *et al.*[11] attributed the metal enrichment in the Stevns Klint KT boundary layer (that is the Fish Clay) to an accumulation of mainly terrigenous materials with minor amounts of clay minerals of diagenetic origin. These authors subdivided the Fish Clay into four layers from the bottom bed II to the top bed V. In a benchmark paper, Alvarez *et al.*[12] explained the anomalous iridium (Ir) concentrations in the KT boundary layer at Stevns Klint, to global fall-out of extraterrestrial materials. According to these authors, the Stevns Klint boundary was produced by the impact event and consists of a mixture of terrestrial ejecta and meteoric material. Kyte *et al.*[13] suggested that only beds III and IV of the Fish Clay (hereinafter referred to as III and IV) can be used to estimate the primary asteroidal fallout. However, geochemical analyses of the KT layers revealed that not only Ir (and other meteoric/partly meteoric metals), but also non-meteoric terrestrial trace metals, such as Cu and V, are substantially enriched in these materials.

Most authors have concluded that metals of terrestrial origin in the Fish Clay were derived from natural aqueous solutions, enriched with these elements, in contact with unconsolidated sediment. Premović *et al.*[14] suggested that the Danish KT boundaries represent weathered clay (mainly smectite) (along with some asteroid/local materials) that was redeposited at the Danish boundary sites after the KT event. These authors claimed that most of terrestrial metals associated with the smectite fraction are strictly detrial in character, *i.e.,* were transported to the Danish boundary sites already contained in clay. Elliot *et al.*[15] argued that the anomalous

metal enrichments of the Fish Clay are comparable with those of the Kupferschiefer shale. These authors suggested that metals in the Fish Clay are derived from the same kind of "non-impact" sources that contributed to the high metal contents in the Kupferschiefer rock. They postulated that the same processes were responsible for the metal enrichment in the Fish Clay as in the Kupferschiefer rock.

The average Cu concentration in the Earth's crust ranges from 24–55 ppm and in soils from 20–30 ppm. Cu is usually associated in sediments with organic matter, the Fe/Mn oxides, sedimentary clays and other minerals.[16] In the Fish Clay, the Cu content ranges from 50 – 80 ppm[11,13] and is thus, of the same order of magnitude as in other ancient shaly type sedimentary rocks of marine origin.[17]

EXPERIMENTAL

Emission spectrometry

A PGS-2 plane grating spectrograph (Carl Zeiss, Jena) was used with an attachment for photoelectric detection, an arc plasma excitation source, and a Bausch and Lomb diffraction grating as the monochromator.[18]

Atomic absorption spectrometry (AAS)

A Perkin-Elmer model 4000 atomic absorption spectrometer was used with a Perkin-Elmer platinum hollow-cathode lamp and a nitrous oxide/acetylene burner head.[14]

Instrumental neutron activaiton analysis (INAA)

The kerogen samples and corresponding standards of $(NH_4)_3VO_4$ were irradiated simultaneously in the TRIGA MK II reactor at a neutron flux of 4×10^{12} n cm^{-2} s^{-1}. The γ-induced activity of Cu isotopes was measured on a germanium Ge(Li) detector connected to a 4000 channel analyser (Canberra).[19] The kerogen Cu contents were also determined by inductively coupled plasma-atomic emission spectroscopy (ICP-EAS).[20]

Electron microprobe

All analyses were obtained with a Jeol JSM-35 electron microscope equipped with a Tracor TN-2000 energy dispersive X-ray (EDX) spectrometer. Operating conditions for EDX analyses were at 25 keV accelerating voltage, 0.1 μA beam current, and a beam spot diameter of approximately 3 μm.[14]

Electron spin resonance (ESR)

ESR measurements were performed on the finely-ground powders of the samples which were trnsferred to an ESR quartz tube (4 mm o.d., 3 mm i.d.). Spectra were recorded on a Bruker ER-200 series ESR spectrometer with either a Bruker ER-044 X-band bridge or a Bruker ER-053 Q-band bridge, using standard 100 kHz field modulation. X-band measurements were made at 9.3 GHz utilizing a rectangular TE cavity, and those at 35 GHz Q-band using a cylindrical TE cavity. Further details of the ESR measurements are given in Ref. 21.

The *g*-values and hyperfine coupling constants were determined relative to a solution of potassium nitrosodisulfonate (Fremy's salt) for which $g = 2.0055 \pm 0.0001$ and the nitrogen hyperfine splitting, $a_N = 1.309 \pm 0.001$ mT.[22] A quartz sample tube was used for Fremy's solution (*ca.* 10^{-3} M) that was taped on the exterior of the sample tube.

RESULTS

To obtain an indication about the chemical nature of the Cu present in III, this boundary material was analysed by both AAS and emission spectrography for Cu determination at various stages of demineralization. The results are given in Table

Ia. It is obvious that the Cu occurs in various forms, including adsorbed on smectite (50%) and organically bound within the kerogen (30%). Schmitz *et al.*[23] presented data on the Stevns Klint boundary samples, in which the Cu content was as high as in our case. According to these authors, 30% of total Cu is associated with the III kerogen. The kerogen Cu contents were determined by both INAA and ICP-AES and the results are summarized in Table Ib. Finally, the ascorbic acid + H_2O_2 test[24] indicates that a very low concentration (<10 ppm) of Cu is resident in the sulfide fraction of III.

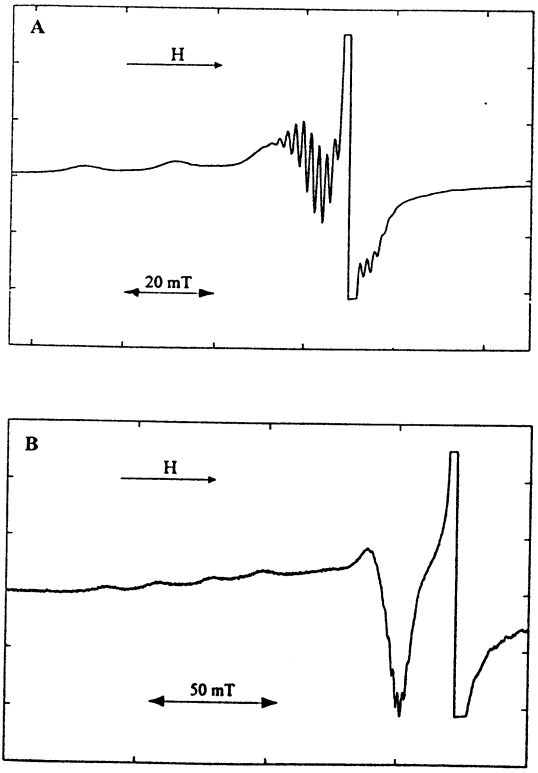

Fig. 1. First-derivative room-temperature anisotropic ESR spectra of Cu^{2+}-P in the III kerogen: a) X-band; b) Q-band[20] spectra. Anisotropic hyperfine Cu^{2+}-P parameters are: $A_{\|} = 19.9 \pm 0.1$ mT; $A_{\perp} = < 1.0$ mT; $g_{\|} = 2.189 \pm 0.002$; $g_{\perp} = 2.039 \pm 0.001$; $a^N = 1.45 \pm 0.10$ mT.

The III kerogen occurs typically as organic laminae when viewed perpendicular to the bedding. EDX spectra of areas which are substantially free of Si, Al, Ca and Fe always show S as the major component and sometimes with Cu as a minor component. Electron microprobe analyses of the III kerogen showed S (up to 3%) and Cu (up to 1000 ppm). These results are consistent with the previously known organic associations of Cu.[16] The association of Cu with kerogen in different sediment types is not a rare phenomenon and is discussed in a number of articles. For instance, Patterson *et al.*[25] showed that Cu in the Julia Creek bituminous shale (Australia) is closely associated with kerogen. According to these authors, the Cu

is associated mainly with sulfides (75% of the total Cu) and to a lesser extent with kerogen (12%) and clay (10%).

The X-band (Fig. 1a) and Q-band (Fig. 1b) ESR spectra of the III kerogen are typical of Cu^{2+}-P. The X-band spectrum resembles that Cu^{2+}-P associated with recent soils[4-6] and paleosols.[7] The Cu^{2+}-P in the III kerogen (Fig. 1a) consists of four lines which are almost equally spaced, but not of equal width. These lines are attributed to the Cu nucleus, which has a nuclear spin of 3/2. Superimposed on each Cu hyperfine absorption are nine absorptions due to the four N nuclei, each of spin 1 on the narrowest Cu hyperfine line. The spacing of the N hyperfine structure is 1.45 mT. The line widths of the Cu hyperfine lines increase with magnetic field from 8 mT (for the nuclear quantum number $m_I = -3/2$) up to 13 mT (for $m_I = 1/2$). The asymmetry of the Cu hyperfine structure is, partly, attributed to the contribution of the anisotropic nuclear hyperfine interactions to the linewidth.[26] Small-scale ESR experiments on the IV and Nye Kløv kerogens gave similar but not identical results. However, ESR analysis of the Dania kerogen shows no evidence for Cu^{2+}-P above the limit of detection of 20 ppm.

Simulated powder spectra were computed using a Fortran program for $s = 1/2$ systems, modified to include two different hyperfine interactions. The first- and second-order perturbation theories were used for the metal (Cu) and ligand (N) nuclear hyperfine interactions, respectively. The simulated spectra were compared with the experimental ones in order to estimate the anisotropic hyperfine parameters. The best fitted anisotropic hyperfine paramteres (which were adjusted to give best fit of the experimental spectrum) are shown in Fig. 1. We were unable to find evidence for the departure from axial symmetry in either the experimental or simulated spectra.

DISCUSSION

No analysis of the nature of the kerogen in the Fish Clay has been made so far, but it is likely that the kerogen mainly represents the remains of terrestrial (fresh water) algae (*botryococcus*) and to a lesser extent bacteria.[27] The observation that the Cu observed in III occurs in the inorganic fraction and is predominantly associated with the kerogen component of the rock suggests that the origin of the Cu is related to the origin of the III kerogen and its humic precursor(s). According to Premović *et al.*[14] terrestrial humic substances played an important role in terrestrial metal transport and fixation through the III boundary column. These authors also suggested that during the deposition of IV the input of terrestrial humic substances was considerably reduced or ceased to exist at all. The sudden and sharp drop in both the Cu and Cu^{2+}-P contents from III to IV (Table Ib) is in line with such a claim.

Geochemical data and observations provide strong evidence that the III layer was deposited either under anoxic conditions or soon after deposition the conditions became anoxic and H_2S was present in both the layer and the overlying seawater.[14]

In general, the kerogen of this rock type is thought to be derived from lipid-enriched humic substances.[28] One of the most important characteristics of these substances is their high sequestering ability for Cu^{2+}. Humic substances with suitable functional (including porphyrin) groups form coordination complexes with Cu^{2+}. However, under strong anoxic sedimentary conditions (such as those of the Julia Creek black shale) most of the Cu^{2+} is precipitated as sulfides and free Cu^{2+}-P is exceedingly labile;[29] though such conditions preserve porphyrins. On the other hand, in oxic sedimentary environments, Cu^{2+} is the predominant Cu species in aqueous solution which is capable of metallating humic porphyrin sites. If this is correct, we can only surmise that Cu^{2+} chelation by humic porphyrin sites must occur in oxygenated freshwaters prior to entering the III marine KT deposition milieu. The fact that < 2 % of total Cu in the III layer is present as sulfides support such a contention and indicates that Cu^{2+} incorporation into porphyrin site(s) of terrestrial humic materials just preceded the redeposion of these substances into the marine Stevns Klint KT Basin.

TABLE I. Geochemical data for the III and IV boundary layers

(a) The III layer

Fraction	Sediment [±5%]	Cu[a] [± 10 ppm]	Total Cu [%]
Carbonate	40	10	5
Sulfide	<2	<10	<1
Smectite	30	150	50
Silicate	25	50	15
Kerogen	3	800	30
Sediment	100	86[b] 100[c]	100

[a]The Cu content determined by AAS; [b]The Cu content obtained by summation of the fraction Cu concentrations, determined by AAS; [c]The Cu content determined by emission spectrography [14]

(b) The III/IV layers

Total sediment [± 0.5%]		Cu[± 50 ppm]	Cu^{2+}-P[±100ppm][a]
Kerogen III	3.0	700[b] 750[c]	4000
Kerogen IV	0.3	400[b] 450[c]	2000

[a]The Cu^{2+}-P content determined by ESR.[14] The Cu^{2+}-P content calculated from the Cu^{2+} concentration using 440 as the average porphyrin molecular weight; [8] [b]The Cu content determined by ICP-AES; [c]The Cu content determined by INAA

Relative abundance of VO^{2+} and the absence of kerogen VO^{2+}-P in the III layer,[14] as well as the high concentration of the III kerogen Cu^{2+}-P are indications that the kerogen Cu^{2+}-P within the III layer is strictly detrital in character, *i.e.*, was transported to the III deposition site already contained in humic materials (as the III kerogen precursor(s)). The general absence of Cu^{2+}-P in sediments from shallow marine depositioinal paleoenvironments with abundant VO^{2+}-P (*e.g.*, sedimentary

millieu of the Julia Creek rock) is consistent with such rationalization. The III kerogen has a surprisingly low atomic H/C ratio (0.9) and a high O/C ratio (>0.3), which indicate intensive (surface) oxidation. Kerogen typically has a relatively high H/C atomic ratio and a low O/C atomic ratio. The concentration of oxygen-containing molecules and the possible contribution of oxygen from surface oxidation and degradation could readily produce H/C < 1 and O/C > 0.3 in the III kerogen before its rapid burial in the Stevns Klint Basin during the KT event.

The kerogen concentrate of the Nye Kløv boundary sediment contains also a relatively high Cu^{2+}-P (< 1000 ppm). This rock was deposited in the same marine basin, although separated by about 300 km from the Stevns Klint location. This fact indicates that the redeposition of the kerogen Cu^{2+}-P came from a common source(s) at a considerable distance. However, in contrast to the III layer the Nye Kløv analogue was redeposited in aerated (oxic) seawater.[14] These facts are in accordance with the detrial hypothesis for the kerogen Cu^{2+}-P which was displaced from its original deposition site and ponded in the Danish KT Basin.

The Kupferschiefer shale is thought to have accumulated in anoxic bottom waters of a shallow, stratified epicontinental sea, the Zechstein Sea (Germany/Poland).[30] The high content of amorphous (laminated) organic matter is derived mainly from algae/cyanobacteria, and to lesser amount from green sulphur bacteria (*Chlorobiceae*).[31] The X-band/Q-band ESR spectra of the kerogen Cu^{2+}-P from the Kupferschiefer rock samples are similar to those of the Fish Clay samples, although the kerogen Cu^{2+}-P contents were lesser (< 2000 ppm). However, in contrast to the Fish Clay, the Kupferschiefer rock contains high concentrations of both VO^{2+}-P and Ni^{2+}-porphyrins (> 3000 ppm).

Organic/inorganic geochemical studies by Püttmann *et al.*[32,33] indicate that the Kupferschiefer Basin acted as a geochemical trap. Accordingly, Cu^{2+} was accumulated in the Kupferschiefer location from ascending oxidizing solutions (brines) which transported high amounts of the metal ion from L. Permian red beds into the Kupferschiefer Basin. Nevertheless, given the high concentrations of VO^{2+}-/Ni^{2+}-porphyrins, it seems more likely that the kerogen Cu^{2+}-P are detrital. In other words, we suggest that the kerogen Cu^{2+}-P in the Kupferschiefer originated, also, from an external humic source(s) that contributed to the high content of these species.

One of the biggest problems of the Danish KT boundary layers has been the many speculations on and search for the (ultimate) source rocks of terrestrial metals (such as red beds or metal-bearing volcanics) which are missing in the Danish KT Basin.[14] From available geochemical data, it appears that the Fish Clay and the Kupferschiefer shale exibit a striking resemblance in geochemical fine details. For instance, in both rocks the bulk of Ir (and other platinium metals) is associated with the kerogen fraction: a value of 600 ppm is reported by Kucha[34] in the Kupferschiefer kerogen and 590 ppm in the III kerogen.[23] Considering that the Fish Clay and Kupferschiefer rocks belong to the same Zechstein Basin and they are separated

from each other by only 400 km[34] then these geochemical similarities (including the ubiquitous presence of the kerogen Cu^{2+}-P) might not be after all a mere coincidence. In our opinion, the striking similarities between the Fish Clay and the Kupferschiefer shale show that these two rocks are somehow generically related.

Results, to date, lead us to propose that the enhanced erosion of near-by terrestrial Kupferschiefer accumulations during or immediately after extraterrestrial-caused KT event is the prime force in translocating terrestrial metals to marine KT boundary sediments of the Danish Basin. At the moment this suggestion remains an open question and we have to wait until more geochemical data on both the Danish KT boundary sedimentary rocks and the Kupferschiefer rock are available for a more substantiated interpretation.

CONCLUSIONS

(1) High concentrations of both Cu (up to 1000 ppm) and Cu^{2+}-P (up to 4000 ppm) have been found in the kerogen structures of the Danish KT boundary layers (the Fish Clay) at Stevns Klint and Nye Kløv.

(2) It is suggested that the kerogen Cu^{2+}-P are derived from the enhanced erosion of terrestrial humic accumulations (*e.g.,* peats/soils) during or after the extraterrestrial caused KT event.

(3) Similar the kerogen Cu^{2+}-P have been detected in near-by L. Permian Kupferschiefer shale from Poland.

(4) The striking similarities (in some fine geochemical details) between the Danish KT boundary rocks and the Kupferschiefer rock imply that these rocks are generically related.

Acknowledgments: We are thankful to both the ORSTOM Institution (France) and the Ministry of Science and Technology (Serbia) for support of this work. Funding support from le Ministére Francais de l'Education Nationale, de l'Enseignement Supérieur et de la Recherche, to P. I. P. for his stay at the Universite Pierre et Marie Curie (Paris) is gratefully acknowledged. We also grate fully acknowledge the donors of the samples, Dr. H. J. Hansen (the Fish Clay) and Z. Sawlowicz (the Kupferschiefer).

И З В О Д

КРЕДА-ТЕРЦИЈАР ГРАНИЧНИ СЛОЈ НА ЛОКАЛИТЕТУ STEVNS KLINT (ДАНСКА): БАКАР И БАКАР(II) ПОРФИРИНИ

ПАВЛЕ И. ПРЕМОВИЋ, НИКОЛА Д. НИКОЛИЋ, ИВАНА Р. ТОНСА, ДЕЈАН Т. ДУЛАНОВИЋ и МИРЈАНА С. ПАВЛОВИЋ*

*Лабораторија за геохемију и космохемију, Филозофски факултет, Универзитет у Нишу, п.пр. 91, 18000 Ниш, и *Институт за нуклеарне науке Винча, п.пр. 522, 11001 Београд*

Детектоване су високе концентрације бакар(II) порфирина (до 4000 ppm) у керогенима креда/терцијар (KT) граничног типа седимента, Рибља глина на локацији Stevns Klint, Данска. Ови пигменти су такође нађени у данском KT седименту на локацији Nye

Kløv koja je udaljena oko 300 km od Stevns Klint-a. Međutim, nismo uspeli da detektujemo bakar(II) porfirine u danskoj graničnoj stени iz Dania predela koji je udaljen oko 200 km od Stevns Klint-a. Predloženo je da kerogenski bakar(II) porfirini potiču od humičnih materijala iz kopnenih izvora (tresset/zemljište), već obogaćenih ovim jedinjenjima, deponovanih u danskom KT basenu. Naši rezultati pokazuju da su kerogenski bakar(II) porfirini prisutni u permskim Kupferschiefer škriljcima iz Poljske u količinama koje se mogu uporediti sa onima iz kerogena Ribље gline. Po našem mišljenju, procesi koji su kontrolisali obogaćenje kerogenskim bakar(II) porfirinima Stevns Klint graničnog sedimenta su odgovorni i za visok sadržaj ovih pigmenata u Kupferschiefer-u.

(Primljeno 2. septembra 1998, revidirano 11. februara 1999)

REFERENCES

1. A. Triebs, *Angew. Chem.* **49** (1936) 682
2. P. I. Premović, M. S. Pavlović, N. Z. Pavlović, *Geochim. Cosmochim. Acta* **50** (1986) 1923
3. M. R. Rampino, R. C. Reynolds, *Scence* **219** (1983) 495
4. B. A. Goodman, M. V. Cheshire, *J. Soil. Sci.* **27** (1976) 337
5. M. V. Cheshire, M. I. Berrow, B. A. Goodman, C. M. Mundie, *Geochim. Cosmochim. Acta* **41** (1977) 1131
6. A. L. Abdul-Halim, J. C. Evans, C. C. Rowlands, J. H. Thomas, *Geochim. Cosmochim. Acta* **45** (1981) 481
7. N. Senesi, G. Calderoni, *Org .Geochem.* **13** (1988) 1145
8. S. E. Palmer, E. W. Baker, *Science* **201** (1978) 49
9. E. W. Baker, J. W. Louda, in *Advances in Organic Geochemistry 1983*, P. A. Schenck, J. W. de Leeuw, G. W. M. Lijmbach, Eds., *Org. Geochem. 6*, Pergamon Press, Oxford, 1984, p. 183
10. E. W. Baker, J. W. Louda, *Org. Geochem.* **10** (1986) 905
11. L. Christensen, S. Fregerslev, A. Simonsen, J. Thiede, *Bull. Geol. Soc. Denmark* **22** (1973) 193
12. L. W. Alvarez, W. Alvarez, F. Asaro, H. V. Michel, *Science* **208** (1980) 1095
13. F. T. Kyte, Z. Zhou, J. T. Wasson, *Nature* **288** (1980) 651
14. P. I. Premović, N. Z. Pavlović, M. S. Pavlović, N. D. Nikolić, *Geochim. Cosmochim. Acta* **57** (1993) 1433
15. W. C. Elliott, J. L. Aronson, Jr. H. T. Millard, E. Gierlowski-Kordesch, *GSA Bull.* **101** (1989) 702
16. D. E. Baker, J. P. Senft, in *Heavy Metals in Soils,* B. J. Alloway, Ed., Blackie Academic & Professional, London, 1995, p. 179
17. M. J. Buchaeur, *Environ. Sci. Technol.* **7** (1973) 131
18. M. Marinković, T. Vickers, *Appl. Spectrosc.* **25** (1971) 319
19. A. R. Byrne, *Radiochem. Radioanal. Letters* **52** (1982) 99
20. J. P. Muller, A. Manceau, G. Calas, T. Allard, P. Ildefonse, J. L. Hazemann, *Am. J. Sci.* **295** (1995) 1115
21. N. D. Nikolić, *Ph. D. Thesis*, Faculty of Science, University of Niš, Niš, 1999
22. R. J. Faber, G. K. Fraenkel, *J. Chem. Phys.* **47** (1967) 2462
23. B. Schmitz, P. Anderson, J. Dahl, *Geochim. Cosmochim. Acta* **52** (1988) 229
24. J. J. Lynch, *Can. Inst. Min. Metall.* **11** (1971) 313
25. J. H. Patterson, A. R. Ramsden, L. S. Dale, J. J. Fardy, *Chem. Geol.* **55** (1986) 1
26. B. A. Goodman, J. B. Raynor, *Adv. Inorg. Chem. Radiochem.* **13** (1970) 135
27. H. J. Hansen, R. Gwozdz, K. L. Rasmussen, *Rev. Esp. Paleont.* (1988) 21
28. B. P. Tissot, D. H. Welte, *Petroleum Formation and Occurrence,* Springer Verlag, Berlin, 1984, p. 236
29. J. W. Buchler, in *Porphyrins and Metalloporphyrins*, K. M. Smith, Ed., Elsevier, Amsterdam, 1975, p. 157

30. J. Paul, *Z. dt. Geol. Ges.* **133** (1982) 571
31. K. Grice, P. Schaeffer, L. Schwark, J. R. Maxwell, *Org. Geochim.* **25** (1996) 131
32. W. Püttmann, H. W. Hagemann, C. Merz, S. Speczik, in *Advances in Organic Geochemistry 1987,* L. Mattavelli, L. Novelli, Eds., *Org. Geochem.* **14**, Pergamon Press, Oxford, 1988, p. 357
33. W. Püttmann, H. Heppenheimer, R. Diedel, *Org. Geochem.* **16** (1990) 1145
34. H. Kucha, *Tschermaks. Min. Pet. Mitt.* **28** (1981) 1.

J. Serb. Chem. Soc. 64(5– 6)359-364(1999) UDC 547.867:546.215:547.295.72/546.226
JSCS-2676 *Original scientific paper*

Influence of sodium dodecyl sulfate on the reaction between Nile Blue A and hydrogen peroxide

IVANA A. JANKOVIĆ,[1*] MIRA M. ČAKAR[2] and JOVAN M. NEDELJKOVIĆ[1]

[1*] *Vinča Institute of Nuclear Sciences, P.O.Box 522, YU-11001 Belgrade, and* [2] *Faculty of Pharmacy, University of Belgrade, YU-11000 Belgrade, Yugoslavia*

(Received 25 November 1998, revised 5 February 1999)

The influence of the anionic surfactant sodium dodecyl sulfate on the rate of the reaction between the cationic form of Nile Blue A and hydrogen peroxide was investigated in the pH range from 5 to 8.5. A retardation of the oxidation of Nile Blue A with hydrogen peroxide of three orders of magnitude was observed at pH 8.5 in the presence of anionic micelles compared to the kinetic data in water. The retardation effect was less pronounced at lower pH values. These effects were explained by the electrostatic interaction of the species involved in the reaction with the negatively charged micellar surface and their effective separation in the vicinity of the micellar surface.

Key words: Nile Blue A, hydrogen peroxide, sodium dodecyl sulfate, micelles.

It is well-established that, in many cases, the rates and pathways of all kinds of chemical reactions can be altered by performing the reactions in micellar media instead of pure bulk solvents.[1,2] Micellar effects on the rate of chemical and biochemical processes can be quite varied, ranging from inhibition to activation.[3] These kinetic effects are generally explained in terms of the partition of the substrate between the aqueous and the micellar phase. Surfactants affect reaction rates by incorporating one or both of the reactants into the micellar aggregates. Together with this concentration effect through hydrophobic and electrostatic interactions, micelles also exert a medium effect (microviscosity, polarity, *etc.*) that influence the reactivity.

Many results have been published in the literature showing the different catalytic or inhibitory effects of anionic, cationic and non-ionic surfactants.[4-15] Because of the structural similarities between micelles and globular proteins, these studies are important from biochemical aspects, as model systems for electron-transfer and ligand-exchange reactions on the surfaces of biomembranes or at the interfaces of globular proteins.

In the present paper, the influence of the anionic surfactant sodium dodecyl sulfate (SDS) on the rate of oxidation of the protonated form of the phenoxazine dye Nile Blue A persulfate ($NBA^+HSO_4^-$) with hydrogen peroxide (both reactants being hydrophilic)

* E-mail: ivanaj@rt270.vin.bg.ac.yu

was strudied. This reaction, whose characteristics in water are well understood, has been used for the analytical determination of traces of selenium.[16]

EXPERIMENTAL

Nile Blue A persulfate (Fluka), sodium dodecyl sulfate (Sigma) and hydrogen peroxide (Merck) were of analytical grade and used without further purification. Water purified by a Millipore Milli-Q system was used for the preparation of solutions. The pH of the solutions were adjusted with phosphate or borate buffer (0.5 mM). The hydrogen peroxide solutions were prepared from 30% H_2O_2 by dilution, and their concentrations were determined from the concentration of H_2TiO_4 formed in the reaction of hydrogen peroxide with Ti(IV).[17]

All spectrophotometric and kinetic measurements were performed on a Perkin Elmer Lambda 5 UV-vis spectrophotometer thermostated at 35 °C. When the reaction time (at least four half-lives) was less than 5 min, the universal rapid kinetic accessory HI-TECH model SFA12 was fitted to the spectrophotometer. The kinetic experiments were performed by mixing equal volumes of NBA^+ and hydrogen peroxide solutions, SDS being added in equal concentrations to both solutions prior to mixing. The reaction rates were determined from the decrease of the absorbance at the NBA^+ absorption maximum in the visible spectral range with time. Pseudo-first-order rate constants with respect to hydrogen peroxide (k_{obs}) were obtained from the slopes of ln A_t *versus* time. The quoted values of k_{obs} are the averages of at least ten runs under identical expeirmental conditions. All kientic measurements were reproducible within the limits of error of ±10%.

The critical micellization concentration (CMC) of SDS in the presence of hydrogen peroxide was determined by measuring the relative light scattering intensity using a Chromatix KMX-6 low-angle laser photometer operating at 633 nm.

RESULTS AND DISCUSSION

Absorption spectra and pK_a of NBA^+ in the presence of anionic micelles

Aqueous solutions of NBA^+ exhibit a characteristic absorption spectrum with absorption maxima at 279, 329 and 639 nm. The absorption maxima of its conjugated base, the neutral compound Nile Blue base (NBB), are shifted to lower wavelengths (265, 313 and 500 nm, respectively).

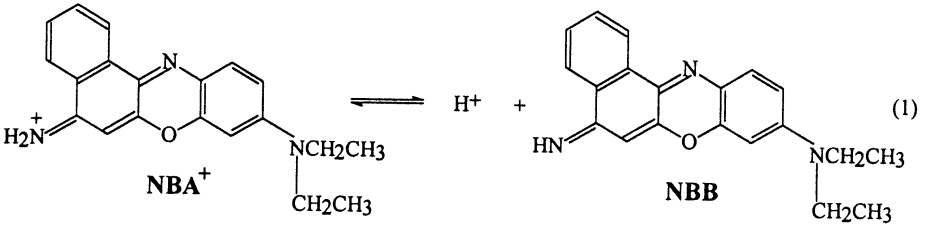

Scheme 1.

From the decrease of the absorbance at 639 nm on increasing the pH from 7 to 12, the protonation constant of NBA^+ in aqueous solution was estimated to be $pK_a = 9.25 \pm 0.05$. From the spectrophotometric pH titration of a Nile Blue solution containing 10 mM SDS in the pH range from 8.5 to 12.5, using both the decrease of the absorbance at 645 nm and the increase of the absorbance at 500 nm, the

protonation constant of NBA^+ localized at the negatively charged micellar surface was estimated to be $pK_a = 11.4 \pm 0.1$. The apparent increase of the pK_a of NBA^+ in micellar solutions of about two pH units can be explained by the higher concentration of hydrogen ions in the vicinity of the micellar surface compared to bulk solution.[18,19] It must be pointed out that the pH of the solution, measured using a glass electrode, refers to the bulk concentration of H^+ ions.

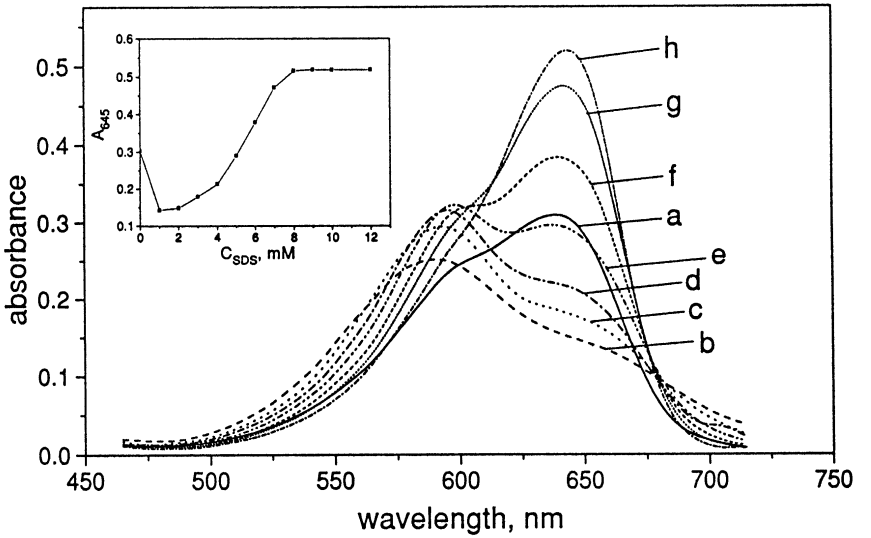

Fig. 1. The effect of the SDS concentration on the absorption spectrum of a 10 μM Nile Blue A persulfate solution at pH 8.5: a) without SDS; b) 2 mM SDS; c) 3 mM SDS; d) 4 mM SDS; e) 5 mM SDS; f) 6 mM SDS; g) 7 mM SDS; h) 8–12 mM SDS. Inset: Absorbance at 645 nm as a function of the concentration of SDS.

Significant changes of the intensity and slight changess in the position of the absorption maxima of NBA^+ were observed in the presence of SDS, the greatest effect being obtained in the visible spectral region (see Fig. 1). It is well known that changes in the optical properties of some molecules can be induced by the presence of surfactant molecules, providing an easy way for the estimation of the CMC of the surfactant.[20] The saturation of the absorbance of NBA^+ was observed at a SDS concentration of 8 mM (see inset in Fig. 1), which corresponds to the CMC value of SDS. The obtained CMC value in the presence of a low concentration of NBA^+ (10 μM) is in good agreement with the reported CMC value at zero ionic strength.[21]

The increase of the absorption coefficient of NBA^+ in the presence of anionic micelles of more than 50%, compared with an aqueous solution, indicates a diminution in the polarity in the immediate vicinity of the organic cation as a result of its localization at the negatively charged micellar surface. This was proved by recording the spectra of NBA^+ in media of variable dielectric constant (water/ethanol mixtures[22]). The absorbance at 640 nm increases with increasing ethanol content, *i.e.*, with decreasing medium polarity.

The kinetics of the oxidation of NBA^+ with hydrogen peroxide in the presence of SDS

The oxidation of NBA^+ in the presence of hydrogen peroxide results in the formation of a colorless product and, consequently, a decrease of the absorbance at 639 nm. It has been shown that the oxidation of NBA^+ with hydrogen peroxide is base catalyzed and a rate equation for the reaction in aqueous solutions was postulated ($-d[NBA^+]/dt = k_0 [NBA^+] [H_2O_2] [\text{buffer}] [H_3O^+]^{-0.5}$).[16] However, the significantly slower spontaneous decomposition of NBA^+ was not taken into account.

The kinetics of the oxidation of NBA^+ with hydrogen peroxide in the presence of the micelle forming surfactant SDS was followed in the pH range from 5 to 8.5. Under pseudo-first-order conditions ($[H_2O_2] >> [NBA^+]$), defined pH and constant buffer concentration (0.5 mM), the experimentally determined rate constant (k_{obs}) followed the simple rate expression:

$$k_{obs} = k_s + k [H_2O_2] \quad (2)$$

where k_s corresponds to the spontaneous decomposition of NBA^+ in the absence of hydrogen peroxide, while k is the pH dependent second-order rate constant.

The values of $k [H_2O_2] = k_{obs} - k_s$ at constant acidity both in the presence and absence of SDS (k_{SDS} and k_W, respectively) are presented in Table I. Over the entire investigated range of acidity, the values of k_s were $<10^{-6}$ s^{-1} and $(5.0 \pm 0.5) \times 10^{-5} s^{-1}$ in the case of micellar and aqueous solutions, respectively. The significant increase of the pseudo-first-order rate constant with decreasing acidity, both in the presence and in the absence of micelles, confirmed that the oxidation of NBA^+ with hydrogen peroxide is base catalyzed.

TABLE I. Pseudo-first-order rate constants $k [H_2O_2]=k_{obs} - k_s$ for the reaction of oxidation of NBA^+ (6 μM) with H_2O_2 (1 M) as a function of pH in water (k_w) and in the presence of 10 mM SDS (k_{SDS}), as well as the retardation factor ($RF = k_w/k_{SDS}$)

pH	5.0	5.9	7.0	8.0	8.5
k_w/s^{-1} [a]	$(4.2\pm0.4)\times10^{-4}$	$(1.1\pm0.1)\times10^{-3}$	$(8.5\pm0.6)\times10^{-3}$	$(5.8\pm0.4)\times10^{-2}$	$(4.3\pm0.2)\times10^{-1}$
k_{SDS}/s^{-1}	$(2.4\pm0.2)\times10^{-6}$	$(4.5\pm0.3)\times10^{-6}$	$(2.3\pm0.1)\times10^{-5}$	$(6.4\pm0.1)\times10^{-5}$	$(2.2\pm0.1)\times10^{-4}$
RF	175±35	244±45	370±45	900±80	1955±190

[a] Corrected for the spontaneous decay of NBA^+, $k_s = (5.0\pm0.5)\times10^{-5}$ s^{-1}

A significant retardation of the oxidation of NBA^+ with hydrogen peroxide was observed in the presence of micelles. At pH 8.5, the retardation factor (the ratio between the pseudo-first-order rate constants in the absence and in the presence of SDS) was around two thousand. Increasing the adicity led to a gradual decrease of the retardation factor up to a few hundreds. It should be pointed out that the effect of micelles on the oxidation of NBA^+ with hydrogen peroxide is more pronounced (three orders of magnitude) compared to the kinetic data obtained under similar experimental conditions for complex formation involving hydrophilic species (one order of magnitude).[9-11] Also, the observed micellar effect is comparable to the

kinetic data obtained for electron-transfer reactions involving reactants of opposite polarities.[5,6]

Retardation of the oxidation of NBA^+ with hydrogen peroxide in the pH range from 5 to 8.5 can be explained in terms of the effective separation of the species involved in the reaction in the presence of anionic micelles. Anionic micelles provide a dispersed negatively charged surface in the solution. As a consequence, the positively charged NBA^+ ions partition out of the bulk aqueous phase into the surface region of the micelles. Apart from the electrostatic interaction, the hydrophobic interaction cannot be neglected since, due to its aromatic structure, NBA^+ is very probably located in the interfacial "water-rich" region of the micelle where the polarity is lower than in water (effective dielectric constant of the micellar surface was estimated as 36[3]). The retardation of the oxidation of NBA^+ with hydrogen peroxide in the presence of SDS can be explained keeping in mind that the reaction is base catalyzed. Due to the electrostatic repulsion between the negatively charged micellar surface and the negatively charged hydroxyl ions, the OH^- ions are located solely in the bulk aqueous phase. Therefore, in the presence of anionic micelles, the species involved in the reaction are effectively separated and the oxidation process is slowed down.

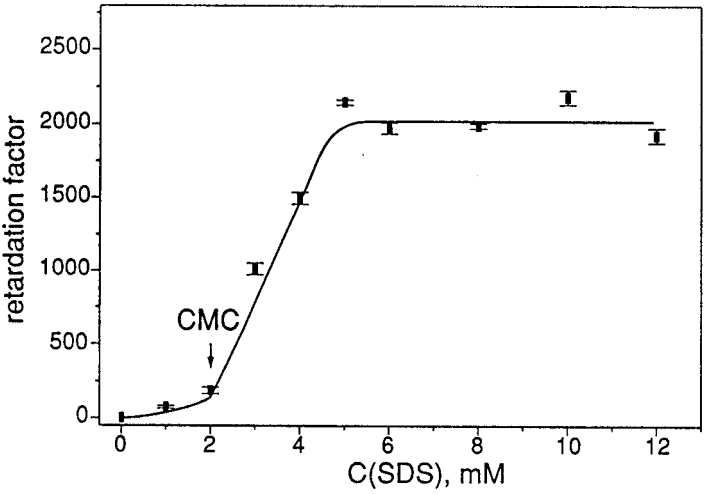

Fig. 2. The dependence of the retardation factor (RF = k_W/k_{SDS}) on the concentration of SDS for the reaction of NBA+ (6 μM) with hydrogen peroxide at 35 °C and pH 8.5.

Since the influence of SDS on the rate of NBA^+ oxidation with hydrogen peroxide is very pronounced, the kinetic measurements can be used for the precise detection of the surfactant concentration at which micelle formation occurs, which is generally considered to be the CMC of the surfactant. A typical dependence of the retardation factor on the concentration of SDS at pH 8.5 is shown in Fig. 2. The estimated CMC value (2 mM) is smaller than the reported CMC value at zero ionic strength.[21] The lower CMC value can be explained by the presence of the high

concentration (1 M) of hydrogen peroxide, which lowers the CMC of the surfactant. The CMC values, at different acidities in the presence of 1 M H_2O_2, were also determined by measuring the relative light scattering intensity as a function of the surfactant concentration. Agreement between the CMC values determined from light scattering and kinetic measurements was found.

И З В О Д

УТИЦАЈ НАТРИЈУМ-ДОДЕЦИЛСУЛФАТА НА РЕАКЦИЈУ *Nile Blue* А И ВОДОНИК-ПЕРОКСИДА

ИВАНА А. ЈАНКОВИЋ,[1*] МИРА М. ЧАКАР[2] и ЈОВАН М. НЕДЕЉКОВИЋ[1]

[1]*Институт за нуклеарне науке Винча, п.пр. 522, 11001 Београд и*
[2]*Фармацеутски факултет, Универзитет у Београду, Београд*

Испитиван је утицај анјонског сурфактанта натријум-додецилсулфата на брзину реакције катјонског облика Nile Blue A и водоник-пероксида у pH опсегу од 5 до 8,5. У поређењу са кинетичким резултатима добијеним у воденим растворима, у присуству анјонских мицела на pH 8,5 примећено је успорење оксидације Nile Blue A водоник пероксидом за три реда величине. У киселијим растворима ефекат успорења је мање изражен. Ови ефекти су објашњени електростатичком интеракцијом између негативно наелектрисане површине мицела и реагујућих врста, што води њиховом ефикасном раздвајању у близини површине мицеле.

(Примљено 25. новембра 1998, ревидирано 5. фебруара 1999)

REFERENCES

1. *Reaction Kinetics in Micelles*, E. H. Cordes, Ed., Plenum Press, New York, 1973
2. J. H. Fendler, E. J. Fendler, *Catalysis in Micellar and Micromolecular Systems*, Plenum Press, New York, 1975
3. I. V. Berezin, K. Martinek, A. K. Yatsimirski, *Rus. Chem. Rev.* **42** (1973) 787
4. A. D. James, B. H. Robinson, *J. Chem. Soc., Faraday Trans. 1* **74** (1978) 10
5. E. Pelizzetti, E. Pramauro, *Inorg. Chem.* **18** (1979) 882
6. E. Pelizzetti, E. Pramauro, *Inorg. Chem.* **19** (1980) 1407
7. E. Perez-Benito, E. Rodenas, *Langmuir* **7** (1991) 232
8. M. N. Khan, Z. Arifin, *J. Colloid Interface Sci.* **180** (1996) 9
9. V. M. Vasić, J. M. Nedeljković, *J. Serb. Chem. Soc.* **59** (1994) 157
10. V. M. Vasić, M. S. Tošić, J. M. Nedeljković, *J. Phys. Org. Chem.* **9** (1996) 398
11. M. S. Tošić, V. M. Vasić, J. M. Nedeljković, Lj. A. Ilić, *Polyhedron* **16** (1997) 1157
12. M. D. Graciani, A. Rodriguez, G. Fernandez, M. L. Moya, *Langmuir* **13** (1997) 4239
13. A. Rodriguez, M. D. Graciani, M. L. Moya, *J. Colloid Interface Sci.* **191** (1997) 58
14. A. Dominguez, E. Iglesias, *Langmuir* **14** (1998) 2677
15. A. Malpica, M. Calzadilla, H. Linares, *Int. J. Chem. Kin.* **30** (1998) 273
16. G. A. Milovanović, R. B. Petronijević, M. M. Čakar, *Mikrochim. Acta* **128** (1998) 43
17. G. M. Eisenberg, *Ind. Eng. Chem. Anal. Ed.* **15** (1943) 327
18. C. A. Bunton, K. Ohmenzetter, L. Sepulveda, *J. Phys. Chem.* **81** (1977) 2000
19. P. Mukerjee, K. Banerjee, *J. Phys. Chem.* **68** (1964) 3567
20. L. Sepulveda, *J. Colloid Interface Sci.* **46** (1974) 372
21. P. C. Shanks, E. I. Franses, *J. Phys. Chem.* **96** (1992) 1794
22. H. S. Harned, B. B. Owen, *The Physical Chemistry of Electrolytic Solutions*, Reinhold, New York, 1958.

J. Serb. Chem. Soc. 64(5– 6)365-374(1999)
JSCS-2677

UDC 546.41/.221:66.094.4:536.71
Original scientific paper

Thermodynamic analysis of copper(I) sulfide chlorination by calcium chloride in the presence of oxygen

RAJKO Ž. VRAČAR and KATARINA P. CEROVIĆ

*Faculty of Technology and Metallurgy, University of Belgrade, Karnegijeva 4, P.O.Box 494, YU-11000 Belgrade, Yugoslavia**

(Received 21 December 1998, revised 8 February 1999)

This paper presents a thermodynamic analysis of possible, but insufficiently studied, chemical reactions occurring during the chlorination of copper(I) sulfide by calcium chloride in the presence of oxygen. It formed the basis for assessing the probability and priority of their occurrence. Phase stability diagrams have been plotted for the Cu–S–O–Cl system in the coordinates log $p(S_2)$–log $p(O_2)$–log $p(Cl_2)$ in the temperature range from 473 to 773 K.

Key words: thermodynamic analysis, Cu–S–O–Cl system, chlorination, calcium chloride.

Many polymetallic ores and potential mineral raw materials containing non-ferrous metals are not exploited nowadays due to the fact that existing processing methods cannot solve the problems of their chemical, mineralogical and textural features in order to obtain the concentrates with high contents of base metals and low contents of impurities to enable their further metallurgical processing.[1,2]

From the technological viewpoint, new pyrometallurgical processing methods, used in the production of non-ferrous metals, are very complex and applied to relatively rich ores. However, for processing poor ores and other raw materials these processes are unacceptable either from the point of view of techniques or economics. For these reasons, there has been increased effort worldwide over the last few years, on the research and development of new processes that are more selective than the classical ones and that could enable a successful metallurgical processing of such raw materials. Chlorination is one of the processes being investigated worldwide.

The chlorination of metals in their ores and concentrates is based on the great activity chlorinating agents towards metals, sulfides, oxides and other composites, so that chlorination occurs at significantly lower temperatures than it is the case with other pyrometallurgical processes (oxidation and reduction). The chlorides are obtained with a high vapor pressure at relatively moderate temperatures, enabling either their easy separation from the waste, or they are easily dissolved, and can, thus be further treated hydrometallurgically.

* E-mail: cer@Eunet.yu

Chlorine, hydrochloric acid and metal chlorides, especially of alkaline-earth and alkaline metals, and, on the first place, calcium chloride are used as chlorinating agents.[2-11]

Calcium chloride can only be used as the chlorination agent in the presence of oxygen at sufficiently high temperatures to enable its decomposition. However, the decomposition of calcium chloride occurs at lower temperatures in the presence of SO_2 and SO_3, obtained during the oxidation of metal sulfides.[1,2,4-7,9-11]

The chlorination of metal sulfides by calcium chlroide in the presence of oxygen is particularly interesting from the aspect of using the energy obtained during the oxidation of sulfides and from the environmental point of view because of binding sulfur into dissoluble calcium sulfate. The calcium sulfate can be retreated by hydrometallurgical processes and converted into chloride again, enabling the simultaneous recycling of calcium chloride, which is another contribution to reducting the production cost.[1,2,7-10]

Bearing all this in mind, as well as that copper(I) sulfide is an important mineralogical component of copper in natural raw materials and a semiproduct of existing technologies, this paper aims at investigating the thermodynamics of the chlorination of copper(I) sulfide by calcium chloride in the presence of oxygen. The obtained information was used as the basis to assess the probability and priority of the occurrence of possible chemical reactions which have no been studied sufficiently.

EXPERIMENTAL

Copper(I) sulfide chlorination by calcium chloride was carried out as follows. Homogenized mixture of copper(I) sulfide (10 g) and 20% of calcium chloride (dried to its constant weight in a drying oven in order to remove humidity) more than stoichiometricaly required for the chlorination of copper(I) sulfide to copper(II) chloride was put on a silica vessel in an even layer. Then, it was put into a silica tube, which had been preheated in an electrical furnace to the investigation temperature. A constant flow of oxygen (20 dm^3/h) was introduced into the reaction area through a gas purification system and a rotameter. From that moment the reaction time was measured.

The X-ray diffraction of chlorinated samples was carried out on a Simens automatic powder diffractometer model D 5000 with CuK_α radiation λ=0.154051μm. Ni filter, the voltage of 40 kV and the current of 3 A were used for X-ray analysis. X-ray analysis was carried out in angle range from 10^o to 80^o with step of 0.02 and constant time of 0.25. Before X-ray analysis the chlorinated samples which had been sintered in the process were ground to the particle size 100% –100 mesh. The obtained X-ray recordings of chlorinated samples were analyzed by using "Diffract At" softer which has a data base for identifying phase composition of chlorinated samples.

RESULTS AND DISCUSSION

Thermodynamic analysis

Chemical reactions of the chlorination process. The chemical reactions of copper(I) sulfide chlorination by calcium chloride in the presence of gaseous oxygen have been little and insufficiently investigated without being uniformly determined. Therefore, in order to carry out a thermodynamic analysis, the possible chemical

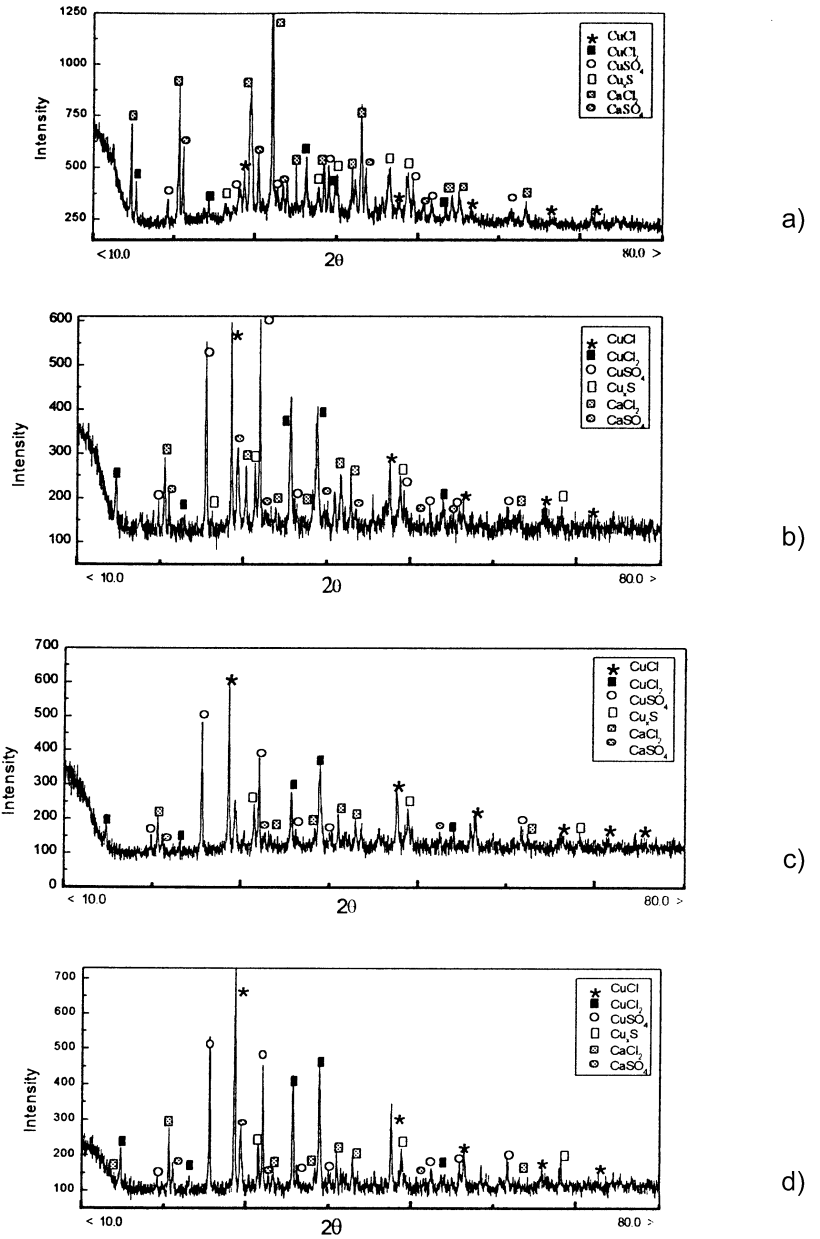

Fig. 1. X-ray diffractograms of the products of the chlorination of copper(I) sulphide by calcium chloride in the presence of oxygen for 30 min at for temperatures a) 473 K, b) 573 K, c) 673 K, d) 773 K.

reactions have been assumed whereas the conclusion of their probability has been drawn from the analysis itself.

The chemical reactions were assumed on the basis of literature data[1,2,4,7-15] as well as on X-ray analysis of the chlorination products obtained in the performed experiments (Fig. 1).

On the basis of the above and in accordance with the stability of copper sulfides, oxides and sulfates, *i.e.*, the chemical affinity of copper towards sulfur, oxygen and chlorine, it has been accepted that the chemical process starts with oxidation reactions of copper(I) sulfide to copper(I) oxide, copper(II) oxide and copper(II) sulfate and the oxidation of the copper oxides to copper(II) sulfate in the presence of the formed SO_2. Oxidation-reduction reactions of copper(I) sulfide with oxygen and copper(I) oxide to elementary copper have also been studied thermodynamically where the reaction of copper(I) sulfide with copper(I) oxide is known in copper metallurgy.

Therefore, oxidation reactions within the studied chlorination system investigated thermodynamically are as flows:

$$2/3\ Cu_2S(s)+O_2(g) = 2/3\ Cu_2O(s)+2/3\ SO_2(g) \quad (1)$$

$$1/2\ Cu_2S(s)+O_2(g) = CuO(s) + 1/2\ SO_2(g) \quad (2)$$

$$1/3\ Cu_2S(s)+O_2(g) + 1/3\ SO_2(g) = CuSO_4(s) \quad (3)$$

$$2/3\ Cu_2O(s) + O_2(g) + 4/3\ SO_2(g) = 4/3\ CuSO_4(s) \quad (4)$$

$$2\ CuO(s) + O_2(g) + 2\ SO_2(g) = CuSO_4(s) \quad (5)$$

$$Cu_2S + O_2 = 2Cu + SO_2 \quad (6)$$

$$Cu_2S + 2Cu_2O = 6\ Cu + SO_2 \quad (7)$$

$$SO_2(g) + O_2(g) = 2\ SO_3(g) \quad (8)$$

The oxidation products continue to take part in the chlorination, where the chlorine required for chlorination is either formed by decomposition of calcium chloride in the presence of SO_2 and SO_3, or in direct oxidation of calcium chloride by oxygen. In accordance with that Gibbs energies have been calculated for temperature range from 298 to 973 K for the following reactions:

$$CaCl_2(s) + 2\ SO_3(g) = CaSO_4(s) + Cl_2(g) + SO_2(g) \quad (9)$$

$$CaCl_2(s) + SO_2(g) + O_2(g) = CaSO_4(s) + Cl_2(g) \quad (10)$$

$$CaCl_2(s) + 1/2\ O_2(g) = CaO(s) + Cl_2(g) \quad (11)$$

The final results of copper chlorination within the investigated system are copper chlorides: copper(I) chloride and copper(II) chloride (identified on X-ray recordings), the first being insoluble in water and the later soluble. The probability

of stable copper(I) sulfide being chlorinated directly, as well as if less stable oxides, copper(I) oxide and copper(II) oxide, and the even more unstable copper(II) sulfate, *i.e.*, elementary copper, are chlorinated, has been shown by thermodynamic analysis of the following reactions:

$$Cu_2S(s) + Cl_2(g) = 2\ CuCl(s,g) + 1/2\ S_2(g) \quad (12)$$

$$1/2\ Cu_2S(s) + Cl_2(g) = CuCl_2(s) + 1/4\ S_2(g) \quad (13)$$

$$Cu_2O(s) + Cl_2(g) = 2\ CuCl(s,g) + 1/2\ O_2(g) \quad (14)$$

$$1/2\ Cu_2O(s) + Cl_2(g) = CuCl_2(s) + 1/4\ O_2(g) \quad (15)$$

$$2\ CuO(s) + Cl_2(g) = 2\ CuCl(s,g) + O_2(g) \quad (16)$$

$$CuO(s) + Cl_2(g) = CuCl_2(s) + 1/2\ O_2(g) \quad (17)$$

$$CuSO_4(s) + Cl_2(g) = 2\ CuCl(s,g) + 2\ SO_2(g) + 2\ O_2(g) \quad (18)$$

$$CuSO_4(s) + Cl_2(g) = CuCl_2(s) + SO_2(g) + O_2(g) \quad (19)$$

$$2\ Cu(s) + Cl_2(g) = 2\ CuCl(s,g) \quad (20)$$

$$Cu\ (s) + Cl_2(g) = CuCl_2(s) \quad (21)$$

The disssociation reaction of $CuCl_2$ to CuCl and Cl_2 was analyzed with particular interest as both products have been experimentally found:

$$CuCl_2(s) = 2\ CuCl(s,g) + Cl_2(g) \quad (22)$$

Reactions 12 and 13 show that the formation of elementary sulfur in the vapor state, can be expected in the utilized temperature range. Some authors[12] state that the sulfur vapors can react with gaseous O_2 and Cl_2 and for this reason the following reactions were included in the thermodynamic analysis:

$$1/2\ S_2(g) + O_2(g) = SO_2(g) \quad (23)$$

$$1/2\ S_2(g) + Cl_2(g) = SCl_2(g) \quad (24)$$

$$S_2(g) + Cl_2(g) = S_2Cl_2(g) \quad (25)$$

Gibbs energy of the investigated reactions

Thermodynamic analysis of given reactions in the studied system was made with the help of HSC Chemistry software and its data base of thermodynamic values required for the calculation of the change in the values of the Gibbs energy for the reactions in temperature range from 298 to 973 K.

The calculated values of the change of the Gibbs energy are given in Fig. 2,

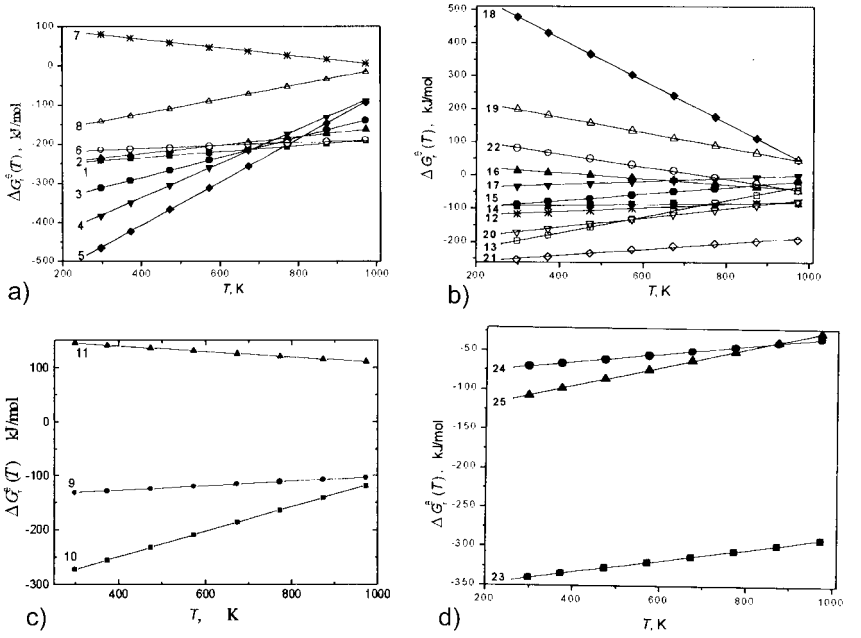

Fig. 2. ΔG_r° (T) Values as a function of temperature of the analyzed chlorination reactions of copper(I) sulfide by calcium chloride in the presence of oxygen: a) oxidation reaction; b) decomposition reaction of calcium chloride and formation of chlorine; c) reaction of copper chloride formation; d) reactions of sulfur reacting with oxygen and chlorine.

in accordance with an interpretation of certain reaction segments, their character and importance in the process.

The values of ΔG_r° (T) for the reactions from 1 to 8 (Fig. 2a) show that all, except No. 7, are thermodynamically possible and that their occurence can be expected in the process. The negative value of the change of the Gibbs energy of these reactions compared to the change in the value of all other reactions, prove the expectations that they have priority and that the overall sequence of chemical reactions starts with their occurrence. In the same way, the more negative values of reactions leading to the formation copper sulfate 3–5 at low temperatures than the values for the direct formation of Cu_2O and CuO oxides, as per reactions 1 and 2, comply to the industrial practice that copper sulfate is formed up to 923 K, whereas above 973 K the sulfate dissociates rapidly forming CuO. The positive values of the change of Gibbs energy for reaction 7 show that it is not thermodynamically possible within the given temperature range, as opposed to the occurrence of the same oxidation reaction of Cu_2S (white matte) in converters in the pyrometallurgical process of obtaining raw blister copper. However, the conversion is performed at higher temperatures (1673 K) and different conditions under which reaction 7 is intensive. This fact is also indicated by the decrease in the value of Gibbs energy with temperature (Fig. 2a).

The assumption that gaseous chlorine, formed by decomposition of calcium chloride, is a chlorinating agent is confirmed by the change in the Gibbs energy of reactions 9 and 10 (Fig. 2b). However, the formation of chlorine by the direct oxidation of calcium chloride by gasseous oxygen is not probable thermodynamically because the corresponding reaction 11 has a positive value of the change of the Gibbs energy. At the same time, reactions 9, 10 and 11 point to the fact that the presence of SO_2 and SO_3, formed in the oxidation of copper(I) sulfide, is necessary for chlorine to be formed. Thus, it proves again that the oxidation reactions of copper(I) sulfide are the initial chlorination reactions in the Cu_2S–$CaCl_2$–O_2 system. From the diagram (Fig. 2b) it can be clearly seen that reaction 10 has a more negative change of Gibbs energy than reaction 9 and, therefore, a greater probability of occurrence.

According to given chemical reactions, there arises the question of what is the thermodynamic probability and what is the chlorination priority of the oxidation products like Cu_2O, CuO, $CuSO_4$ and Cu, *i.e.*, of the initial copper(I) sulfide and of the formation of the final chlorination products, CuCl and $CuCl_2$. The answers to these questions are given in the changes of the Gibbs energies of the corresponding reactions, shown in Fig. 2c, from which it can be seen that the chlorination of Cu_2S (12 and 13), Cu_2O (14 and 15), CuO (16 and 17) and Cu (20 and 21), in temperature range from 293 to 973 K, are feasible. However, the positive values of the Gibbs energies for the chlorination reactions of $CuSO_4$ (18 and 19) show that these reactions do not occur. This is in accordance with literature data[12] and has been shown by our experiments.

Elementary copper and its oxides have not been found by X-ray analysis of the experimentally obtained chlorination products (Fig. 1), which proves that they are completely chlorinated according to reactions 14–17, 20 and 21. The small negative values of the Gibbs energies for the chlorination of copper oxides (CuO, Cu_2O), according to reactions 14–17, indicate the possibility of shifting the balance of their occurence to the left. However, the shifting of reactions 14–17 in the direction of oxide formation is prevented by the formation of S_2, according to reactions 12 and 13. On the one hand this is due to the fact S_2 can react with Cl_2, according to reactions 24 and 25, forming the thermally unstable chlorides S_2Cl_2 and SCl_2 which dissociate at temperature over 300 °C,[12] forming active chlorine atoms which take part in the chlorination. On the other hand, S_2 can react with oxygen according to reaction 23, whose values of the Gibbs energy change of which is significantly lower then the changes for reactions 24 and 25 (Fig. 2d). The formed SO_2 decreases the possibility of reactions 14–17 being shifted to the left, *i.e.*, in the direction of oxides formation. Basically, S_2 reacts here as a reducer and decreases the oxygen concentration in the reacting gas.

Even though the values of Gibbs energies within the investigated temperature range for the oxidation reactions of copper(I) sulfide, 1–3 and 6 (Fig. 2a), are more negative than the values for the chlorination of copper(I) sulfide by chlorine, reactions 12 and 13 (Fig. 2c), these reactions occur simultaneously. The simultane-

ous occurrence of the oxidation and chlorination of copper(I) sulfide results from chlorine ($t_b(Cl_2)$=−35 °C, $t_b(Cl_2)$ is boiling temperature of Cl_2) having higher adsorption properties than oxygen ($t_b(O_2)$=−185 °C, $t_b(O_2)$ is boiling temperature of O_2), as it is known that gases with low boiling temperatures adsorb on a solid surface with more difficulty than gases with high boiling temperatures.

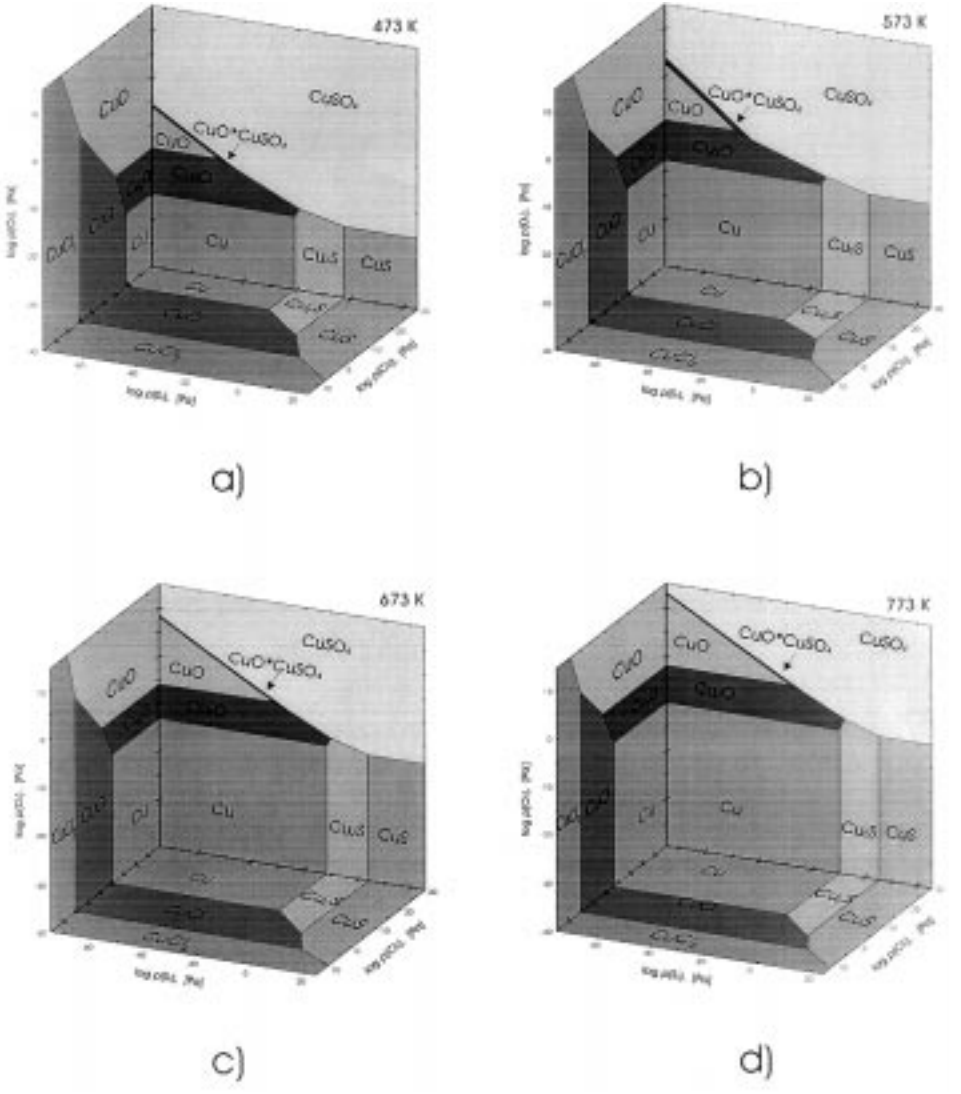

Fig. 3. Phase stability diagrams for the Cu–S–O–Cl system in the coordinates log $p(S_2)$–log $p(O_2)$–log $p(Cl_2)$, a) 473 K; b) 573 K; c) 673 K; d) 773 K.

Phase stability diagrams

The HSC-Chemistry thermodynamic analysis software and its data base of thermodynamic values required for the calculation of Gibbs energy changes were used for making the isothermal phase stability diagrams for the Cu–S–O–Cl system shown in Fig. 3 in the coordinates $\log p(S_2)$–$\log p(O_2)$–$\log p(Cl_2)$ for the temperature range from 473 to 773 K. The diagrams show that the presence of particular phases and the size of the phases area changes with temperature. To be more precise, the diagrams show that increasing the temperature has a positive influence on the chlorination, as the size of the phase stability area of $CuSO_4$, not taking part in the chlorination, decreases with temperature.

CONCLUSION

1. Thermodynamic analysis, based on the calculation of the Gibbs energy changes, of the chlorination reactions of copper(I) sulfide by calcium chloride in the presence of oxygen, the following most important thermodynamic possibilities, *i.e.*, probabilities have been determined:

- The initial starting reactions occurring in the investigated temperature range (298 – 973K) are oxidation reactions of copper(I) sulfide, whereby Cu_2O, CuO, $CuSO_4$, Cu and SO_2 are formed.

- Gaseous chlorine, formed by the decomposition of calcium chloride, is the chlorinating agent.

- The decomposition of calcium chloride with the release of chlorine occurs only in the presence of oxygen, as well as SO_2 or SO_3 formed during copper(I) sulfide oxidation.

- Copper chlorides, either the insoluble in water CuCl, or the soluble $CuCl_2$, are both, as final products of chlorination, formed in the chlorination of copper(I) sulfides, formed oxides (Cu_2O, CuO) and elementary copper, whereas copper sulfate is not chlorinated.

- Elementary $S_2(g)$, formed by sulfide chlorination, reacts on the one hand, with chlorine forming the thermally unstable compounds SCl_2 and S_2Cl_2, the decomposition of which forms active chlorine atoms, and is, on the other, bound in SO_2, reducing the possibility of oxidation of the formed oxides.

- Increasing temperature reduces the phase stability of $CuSO_4$ which has a positive effect on the chlorination process.

Acknowledgements. Particular thanks are due to Slavica Zec MSc and the staff of the Vinča Institute of Nuclear Sciences, for invaluable help in carrying out X-ray analysis.

И З В О Д

ТЕРМОДИНАМИЧКА АНАЛИЗА ХЛОРОВАЊА БАКРА(I)-СУЛФИДА КАЛЦИЈУМ-ХЛОРИДОМ У ПРИСУСТВУ КИСЕОНИКА

РАЈКО Ж. ВРАЧАР и КАТАРИНА П. ЦЕРОВИЋ

Технолошко-металуршки факултет, Карнегијева 4, 11000 Београд

У раду је дата термодинамичка анализа могућих, а недовољно изучених хемијских реакција које се одвијају у току процеса хлоровања бакар(I)-сулфида калцијум-хлоридом у присуству кисеоника и на тој основи изведена је оцена вероватноће и приоритета њиховог одигравања. Урађени су развијени дијаграми стабилности фаза за систем Cu–S–O–Cl у координатама log $p(S_2)$–log $p(O_2)$–log $p(Cl_2)$) за температурни интервал од 473 до 773 K.

(Примљено 21. децембра 1998, ревидирано 8. фебруара 1999)

REFERENCES

1. A. Holmstrom, *Scand. J. Metall.* **17** (1988) 248
2. G. Morizot, G. Barbery, *Extraction Metallurgy,* London Int. Min. Metall. (1980) 151
3. K.L. Luthra, H. S. Ray, D. Kumar, *J. Inst. Eng. India* **53** (1973) 58
4. E. M. L. Peek, *Ph. D. Thesis*, TU Delft, Nederland, (1996)
5. N. Rajmohan, K. T. Jacob, *Min. Metall.Process.* **8** (1992) 141
6. N. Rajmohan, K. T. Jacob, *Min. Eng.* **5** (1992) 235
7. A. Dashlsted, S. Seetharman, K. T. Jacob, *Scand. J. Metall.* **21** (1992) 242
8. T. K. Mukherjee, C. K. Gupta, *Min. Process. Tech. Rev.* **1** (1983) 111
9. R. Vračar, K. Cerović, *J. Serb. Chem. Soc.* **61** (1996) 903
10. I. Iwasaki, *AIME Annual Meeting,* New York (1971), p. 1
11. J. K. Gerlach, F. E. Pawlek, *Trans. Am. Inst. Min. Eng.* **239** (1967) 1557
12. F. Haupt, J. Korb, K. Hein, *Erzmetall* **36** (1983) 192
13. T. Rosenqvist, *Principles of Extractive Metallurgy,* McGraw-Hill International Editions, 2nd, Singapore, Sydney, London, 1988
14. V. V. N. S. Ramakrishna Rao, K. P. Abraham, *Metall. Trans.* **2** (1971) 2463
15. M. E. Wadsworth, K. L. Leiter, W. H. Porter, J. R. Lewis, *TMS-AIME*, **218** (1960) 519.

J. Serb. Chem. Soc. 64(5– 6)375-380(1999) UDC 539.16:546.718'811'':661.635.66
JSCS-2678 *Original scientific paper*

Influence of the radioactive concentration of the *in vitro* stability of Tc-99m(Sn)-pyrophosphate

JURIJ L. VUČINA

Laboratory for Radioisotopes, Vinča Institute of Nuclear Sciences, P.O.Box 522, YU-11001 Belgrade, Yugoslavia

(Received 18 December 1998)

The *in vitro* stability of ^{99m}Tc(Sn)-pyrophosphate solution was examined in dependence on the preparation conditions of the samples, the radioactive concentration of ^{99m}Tc in the kit and the time elapsed after labeling. The samples without any protection are highly unstable. The formation of ^{99m}Tc-pertechnetate does not depend on the radioactive concentration. Nitrogen purging provides protection in the case of low radioactive concentrations (37 MBq ^{99m}Tc/ml) but exhibits no effect at higher concentrations. The best stabilization was achieved by using ascorbic acid. A concentration of 60 μg/ml keeps the content of ^{99m}Tc-pertechnetate below 1% during six hours after labeling, even in solutions of high readioactive concentrations (740–814 MBq/ml). Gentisic acid is less effective. Concentrations about ten times higher than required using ascorbic acid are needed to keep the content of ^{99m}Tc-pertechnetate below 5% during six hours.

Key words: pyrophosphate, technetium-99m, ascorbic acid, gentisic acid, chemical stabilization.

The first step in the production of compounds labeled with ^{99m}Tc is its reduction, usually by stannous ions. Lower, less stable, positively charged states of technetium readily form complexes with different chelating agents. For the routine clinical practice, ligand, reductant and some additives (if needed) are prepared and delivered in the freeze-dried from under vacuum or in an inert atmosphere. The end user should only add ^{99m}Tc activity.

It is known that the radiochemical purity of tin-reduced ^{99m}Tc-labelled radiopharmaceuticals is time dependant. Therefore, their *in vitro* stability is a very important parameter. It should be sufficiently high to ensure their confident and economical use during a reasonable long time after preparation. This time span, denoted also as the shelf life, is usually up to six hours in most nuclear medical departments. During this time the radiochemical purity should preferably be $\geq 95\%$.

The decomposition of ^{99m}Tc-radiopharmaceuticals can be induced by the presence of some agents present in the ^{99m}Tc eluate[1] and/or in the inactive components of the kit. Enhanced investigations were devoted to the eximination of the

effects of the products of the radiolysis of water whereby different free radicals and molecular products, like hydrogen peroxide, are formed.

In a previous paper,[2] several methods aimed at maintaning a high radiochemical purity of ^{99m}Tc(Sn)-pyrophosphate (PyP) solutions were tested. Oxygen was partially excluded by nitrogen purging and the effect of some chemical stabilizers was also examined. These experiments were performed at low radioactive concentrations of ^{99m}Tc so that the decomposition of the complex was triggered by its exposure to air ("oxygen" conditions) or by the addition of hydrogen peroxide.

However, in routine practice, much higher technetium activities for labeling are needed. In this paper the applicability of these protection methods was examined over a broad region of radioactive concentrations of ^{99m}Tc. The effects of nitrogen purging or the addition of either ascorbic or gentisic acid into the PyP solution containing up to 814 MBq ^{99m}Tc (22 mCi) per ml of the kit were investigated. The aim was to show if these methods would still be effective enough and if the concentrations of the chemical stabilizers which were found sufficient at low radioactive concentrations would still be applicable when the labeling was performed under these experimental conditions.

EXPERIMENTAL

Tetrasodium pyrophosphate anhydrous (PyP, Fluka), L(+)-ascorbic acid (Merck), stannous chloride dihydrate (Merck) and 2,5-dihydroxybenzoic (gentisic) acid (Fluka) were commercial p.a. grade chemicals. For the experiments, fresh solutions of PyP dissolved in 0.154 mol dm^{-3} NaCl (self-made) and $SnCl_2$ dissolved in conc. HCl and diluted in bidistilled water were used. The other reagents were also prepared fresh. The ratio ligand/reductant was kept constant so that their concentrations in the kit were 4×10^{-2} mol dm^{-3} PyP and 9×10^{-4} mol dm^{-3} $SnCl_2$.

The formation of ^{99m}Tc-pertechnetate in the labeled PyP solution was followed in the samples prepared and treated under the following experimental conditions:

a) kit prepared directly from the reactant solutions and the experiment were performed without any protection ("oxygen" conditions);

b) kit prepared from solutions of PyP and $SnCl_2$ previously purged with nitrogen ("nitrogen" conditions); during the experiments the samples were kept in an air atmosphere;

c) to the kit solution prepared under "oxygen" conditions, small volumes ($\leq$ 1 ml) of an aqueous solution of either ascorbic or gentisic acid of known concentrations were added; during the experiments the samples were also kept in an air atmosphere.

Labeling was performed by the addition of ^{99m}Tc-eluate obtained by elution of the high activity ^{99}Mo/^{99m}Tc generators (Vinča Institute of Nuclear Sciences, Laboratory for Radioisotopes).

The elutions were performed in 24-hours intervals using self-made saline solution. The labelings were performed after not longer than 20 min after the elution of the generators.

The experiments were carried out in the following ranges of initial radioactive concentrations of ^{99m}Tc: 18.5–37 MBq (0.5–1 mCi), 370–444 MBq (10–12 mCi), 555–630 MBq (15–17 mCi) and 740–814 MBq (20–22 mCi) per ml of the kit sample.

The final pH of the samples was 7–7.5.

In definite time intervals after addition of ^{99m}Tc activity (15 min, 3 and 6 h) the content of ^{99m}Tc-pertechnetate was determined using ascending paper chromatography (Whatman No.1) with

acetone as the mobile phase. In this system ^{99m}Tc(Sn)-PyP and ^{99m}Tc-hydrolyzate remain at the start ($R_f = 0$), while ^{99m}Tc-pertechnetate migrates with the solvent front ($R_f = 1$). After developing, the paper strips were cut into 1-cm pieces and measured in a gamma scintillation counter (Gamma 3 33, ICN).

RESULTS AND DISCUSSION

It was supposed that among the products of water radiolysis, hydrogen peroxide is the species mainly responsable for the deterioration of the ^{99m}Tc(Sn)-PyP. It could cause the oxidation of the stannous ions, thus preventing the reduction of the heptavalent technetium, and/or the re-oxidation of the already reduced ^{99m}Tc. The extent of its formation depends on the decay time, the radioactive concentration of ^{99m}Tc and the pH of the kit solution.[3] It was found that at pH 6 and an initial radioactive concentration of about 7.4 GBq/ml, approximately 0.5μg H_2O_2/ml is formed when the eluate was allowed to stand for 1.5 h.[4] Thus, it could be expected that a significant quantity of hydrogen peroxide is generated, particularly when eluates of high radioactive concentrations are allowed to stand for many hours before use.

The yield of hydrogen peroxide also depends on the amount of oxygen dissolved in the water. Hence, the simplest method to protect the labeled preparation would be to suppress the peroxide formation by excluding oxygen. This can be done by purging the reactant solutions with nitrogen ("nitrogen" conditions). It is also important to ensure that no air is introduced into the kit vial.

Table I presents the data obtained with ^{99m}Tc(Sn)-PyP prepared under "nitrogen" conditions for the various ranges of radioactive concentrations of ^{99m}Tc in the kit solution. In practice it is difficult to prevent the introduction of air into the vial. So, in our experiments, this protection method was performed under the most unsuitable conditions. It was restricted to the preparation of the kit solution, *i.e.,* nitrogen purging of the reactant solutions only. After labeling the samples were kept in an air atmosphere.

TABLE I. Formation of ^{99m}Tc-pertechnetate in ^{99m}Tc(Sn)-PyP in dependance on the experimental conditions and the time elapsed after labeling. Concentrations: 4×10^{-2} mol dm^{-3} PyP and 9×10^{-4} mol dm^{-3} $SnCl_2$. (Oxygen: samples prepared directly from the reactant solutions; Nitrogen: reactant solutions previously purged with nitrogen). Initial ^{99m}Tc radioactive concentration ranges: 18.5–37 and 370-444 MBq/ml of the kit

Time after labeling, h	Initial radioactive concentration, MBq ^{99m}Tc/ml of the kit	Content of ^{99m}Tc-pertechnetate,%	
		"Oxygen" samples	"Nitrogen" samples
0.25	18.5–37	2.8±1.2	1.0±0.2
	370–444	4.4±1.4	3.8±1.12
3	18.5–37	10.1±0.8	2.4±0.9
	370–444	9.2±1.2	8.4±1.2
6	18.5–37	14.7±1.2	5.7±2.2
	370–444	14.2±2.5	–

For comparison, the content of hydrogen peroxide in the samples prepared without any protection ("oxygen" conditions) is shown. These samples were prepared simply by dissolving and dispensing of the corresponding chemicals.

As the measure of the efficiency of the applied stabilization procedure, an arbitrary upper limit of 5% of ^{99m}Tc-pertechnetate was taken. This means that a given procedure is considered satisfactory if not more than 5% of ^{99m}Tc-pertechnetate is formed in the kit solution during six hours.

From the results shown in Table I it can be concluded that the samples prepared under the "oxygen" conditions are highly unstable. The formation of ^{99m}Tc-pertechnetate does not depend on the radioactive concentration. Similar values were obtained for all the examined ranges of radioactive concentrations.

Nitrogen purging of the reactant solutions is efficient only at low ^{99m}Tc radioactive concentrations (up to 37 MBq/ml). Under these conditions the ^{99m}Tc(Sn)-PyP is stable for up to six hours after labeling. However, at higher radioactive concentrations of ^{99m}Tc this protection method is no longer efficient.

The second stabilization procedure was the addition of either ascorbic or gentisic acid into the PyP solution which was then labeled with ^{99m}Tc. The samples were prepared under "oxygen" conditions. The contents of these chemical stabilizators given in Table II and III represent the necessary concentration minimum of the given stabilizator to achieve the desired protecting effect.

TABLE II. Effect of ascorbic acid on the formation of ^{99m}Tc-pertechnetate in ^{99m}Tc(Sn)-PyP prepared under "oxygen" conditions, in dependence on the initial ^{99m}Tc radioactive concentration and the time elapsed after labeling. Concentrations: 4×10^{-2} mol dm^{-3} PyP and 9×10^{-4} mol dm^{-3} $SnCl_2$

Initial radioactive concentration, MBq ^{99m}Tc/ml of the kit	Content of ascorbic acid, μg/ml of the kit	Time after labeling, h		
		0.25	3	6
18.5–37	5	0.4±0.2	0.3±0.1	0.5±0.1
370–444	10	0.1±0.02	0.3±0.1	0.4±0.1
555–630	30	0.7±0.2	0.4±0.2	1.0±0.2
740–814	60	0.1±0.05	0.4±0.1	0.4±0.1

In Table II the influence of ascorbic acid on the stability of ^{99m}Tc(Sn)PyP is given. It can be seen that this chemical is a very efficient stabilizator already at low concentrations. Even in the highest range of the radioactive concentration of ^{99m}Tc (740–814 MBq/ml) only 60 μg of ascorbic acid per ml of the kit is sufficient to keep the content of ^{99m}Tc-pertechnetate below 1% during six hours.

The effect of gentisic acid is presented in Table III. The result show that, in comparison with ascorbic acid, the efficiency of gentisic acid is lower. Already at the lowest radioactive concentration range the content of pertechnetate in the presence of 50 μg of gentisic acid was 1–2%. In the highest examined range

(750–814 MBq ^{99m}Tc/ml) 500 μg/ml was needed to keep the content of ^{99m}Tc-pertechnetate below 5% during six hours.

TABLE III. Effect of gentisic acid on the formation of ^{99m}Tc-pertechnetate in ^{99m}Tc(Sn)-PyP prepared under "oxygen" conditions, in dependence on the initial ^{99m}Tc radioactive concentration and the time elapsed after labeling. Concentrations: 4×10^{-2} mol dm^{-3} PyP and 9×10^{-4} mol dm^{-3} $SnCl_2$

Initial radioactive concentration, MBq ^{99m}Tc/ml of the kit	Content of gentisic acid, μg/ml of the kit	Time after labelling, h		
		0.25	3	6
18.5–37	50	1.2±0.2	0.8±0.2	1.8±0.2
370–444	80	1.0±0.2	2.7±0.4	6.7±2.1
370–444	120	1.0±0.2	2.7±0.5	2.9±0.5
740–814	300	–	3.6±0.6	5.6±0.5
740–814	500	0.6±0.2	1.7±0.3	2.9±0.5

CONCLUSIONS

The results show that the unprotected ^{99m}Tc(Sn)-PyP kit solution (prepared under "oxygen" conditions) is unstable. Already in the first hour after labeling a considerable amount of ^{99m}Tc-pertechnetate is found. Its formation seems to be practically independent of the radioactive concentration.

The common protection procedure of nitrogen purging was effective only for kit solutions of low radioactive concentration. Taking arbitrarily the formation of 5% of free ^{99m}Tc-pertechnetate during six hours after labeling as a tolerable level, it can be seen that this method is reliable for at least 3 h. However, already in the next higher radioactive concentration range (370–444 MBq ^{99m}Tc/ml), this method of stabilization is not applicable.

The antioxidants ascorbic and gentisic acids can be successfully used for the stabilization of ^{99m}Tc(Sn)-PyP. However, already in the lowest radioactive concentration range ascorbic acid is more efficient. A similar conclusion can also be reached by comparing the results of the kit stability at higher concentrations of ^{99m}Tc radioactivity. By increasing the concentration of ascorbic acid up to 60 μg/ml, the content of ^{99m}Tc-pertechnetate is max. 1% even when the radioactive concentration was 814 MBq/ml.

Gentisic acid was found to be less efficient. In addition, the content of gentisic acid should be about ten times higher than that of ascorbic acid. When the radioactive concentration of ^{99m}Tc was raised up to 740–814 MBq/ml, it was necessary to add 500 μg of gentisic acid per ml of the kit solution to keep the content of ^{99m}Tc-pertechnetate below 5%. At these concentrations of gentisic acid a coloration of the kit solution appeared. It would be necessary to examine whether this content of stabilizator has eventually some side-effects, *e.g.*, a change in the biodistribution.

Generally, it was observed that with increasing radioactive concentration the content of both chemical stabilizers also has to be increased. This increase is much higher than expected taking into account only the supposed radiation-induced production of hydrogen peroxide. This indicates that the assumed reaction mechanism in the kit solution of high radioactive concentration is much more complex.

The difference in the efficiency of ascorbic and gentisic acid is probably due to their chemical structure. Ascorbic acid system is a combination of various components with different chemical properties. Some of them are very efficient radical scavengers. The reactions of gentisic acid, a derivative of salicilic acid, under the given experimental conditions need further investigation.

И З В О Д

УТИЦАЈ РАДИОАКТИВНЕ КОНЦЕНТРАЦИЈЕ НА *IN VITRO* СТАБИЛНОСТ Tc-99m(Sn)-ПИРОФОСФАТА

ЈУРИЈ Л. ВУЧИНА

Институт за нуклеарне науке "Винча", Лабораторија за радиоизотопе, п.пр. 522, 11001 Београд

Испитивана је *in vitro* стабилност раствора ^{99m}Tc(Sn)-пирофосфата (PyP) у зависности од услова припреме узорка, радиоактивне концентрације ^{99m}Tc и времена протеклог од обележавања. Узорци без заштите су нестабилни. Садржај ^{99m}Tc-пертехнетата у њима расте са временом практично независно од радиоактивне концентрације. Заштита барботирањем азотом раствора реактаната је ефикасна само код ниских радиоактивних концентрација (37 MBq/ml) док код виших нема више ефекта. Антиоксиданси аскорбинска и 2,5-дихидрокси бензоева киселина утичу на стабилност обележеног препарата. Аскорбинска киселина је ефикаснија. И код највећих испитиваних радиоактивних концентрација (740□814 MBq/ml) потребно је само око 60 μg/ml да садржај ^{99m}Tc пертехнетата не пређе 1% током целог испитиваног периода (6 h). 2,5-Дихидрокси бензоева киселина је мање ефикасна и потребне су знатно веће концентрације да садржај ^{99m}Tc-пертехнетата у препарату не пређе 5% током периода испитивања. Са повећањем радиоактивне концентрације повећава се и концентрација хемијских стабилизатора потребна да би се постигао тражени заштитни ефекат.

(Примљено 18. децембра 1998)

REFERENCES

1. J. Vučina, D. Vuga, N. Vanlić-Razumenić, *J. Radioanal. Nucl. Chem., Letters* **186** (1994) 333
2. J. L. Vučina, *J. Serb. Chem. Soc.* **62** (1997) 137
3. V. J. Molinski, *J. Int. Appl. Radiat. Isotopes* **33** (1982) 811
4. J. L. Vučina, Lj. M. Jaćimović, S. M. Milenković, *Radiol. Iugosl.* **17** (1983) 387.

J. Serb. Chem. Soc. 64(5– 6)381-388(1999) UDC 546.47'562''732''':541428.49:547.785,5
JSCS-2679 *Original scientific paper*

Complexes cobalt(II), zinc(II) and copper(II) with some newly synthesized benzimidazole derivatives and their antibacterial activity

S. O. PODUNAVAC-KUZMANOVIĆ,[a*] V. M. LEOVAC,[b] N. U. PERIŠIĆ-JANJIĆ,[b] J. ROGAN[c] and J. BALAŽ[d]

[a]*Faculty of Technology, Bul. Cara Lazara 1, YU-21000 Novi Sad,* [b]*Institute of Chemistry, Faculty of Science, Trg D. Obradovića 3, YU-21000 Novi Sad,* [c]*Department of General and Inorganic Chemistry, Faculty of Technology and Metallurgy, Karnegijeva 4, P.O.Box 494, YU-11001 Belgrade and* [d]*Faculty of Agriculture, Trg D. Obradovića 1, YU-21000 Novi Sad, Yugoslavia*

(Received 21 October 1998, revised 15 January 1999)

The preparation and properties of some complexes of cobalt(II), zinc(II) and copper(II) with several newly synthesized benzimidazole derivatives (L) are reported. The complexes, of the general formula $[MCl_2L_2]$ (M=Co(II), Zn(II)) and $[CuCl_2L(H_2O])$, have a tetrahedral structure. The complexes were characterized by elemental analysis, molar conductivity, magnetic susceptibility measurements, IR and absorption electronic spectra. The antibacterial activitiy of the benzimidazoles and their complexes was evaluated against *Erwinia carotovora* subsp. *carotovora* and *Erwinia amylovora*. The complexes were found to be more toxic than the ligands.

Key words: complexes, cobalt(II), zinc(II), copper(II), benzimidiazole derivatives, physico-chemical characterization, biological activity.

Benzimidazole and its derivatives are of considerable importance because of their biological properties.[1-6] Many different benzimidazoles have found commercial applications in the medical and agricultural fields where the derivatives have such activities as bacteriostats and bactericides, insecticides, fungicides, sedatives, anticarcinogens and phycopharmacological agents.[7-12] The complexes of transition metal salts with benzimidazole derivatives have been extensively studied as models of some important biological molecules.[13-17] The newly synthesized benzimidazole derivatives investigated in the present work possess good antibacterial and selective antifungal activities against different strains of bacteria and fung.[18]

In this paper we report the synthesis and some physico-chemical characteristics of complexes of three series of benzimidazoles (L) (Table I). The general formula of the complexes is $[MCl_2L_2]$ (M=Co(II), Zn(II)) and $[CuCl_2L(H_2O)]$. We also report the antibacterial activity of these complexes, the results of which are discussed in this communication.

* Author for correspondence

TABELA I. Structural formula of the ligands

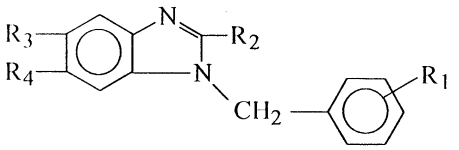

Series I	R_1	R_2	R_3	R_4
I-*p*-CH_3	*p*-CH_3	H	CH_3	CH_3
I-*m*-OCH_3	*m*-OCH_3	H	CH_3	CH_3
Series II				
II-*m*-F	*m*-F	NH_2	H	H
II-*m*-Cl	*m*-Cl	NH_2	H	H
Series III				
III-*m*-CH_3	*m*-CH_3	NH_2	CH_3	CH_3
III-*m*-F	*m*-F	NH_2	CH_3	CH_3
III-*m*-Cl	*m*-Cl	NH_2	CH_3	CH_3

EXPERIMENTAL

Reagents

Ligands were synthesized by Vlaović *et al.* according to a procedure described earlier.[18] All chemicals used for the preparation of the complexes were of analytical reagent grade, commercially available from different sources.

Synthesis of complexes

All the complexes are prepared following the same procedure. A solution of 1.25 mmol $CoCl_2 \cdot 6H_2O$, $ZnCl_2$ or $CuCl_2 \cdot 2H_2O$ in 5 cm^3 of EtOH was added to a solution of 2.5 mmol of the ligand in 5 cm^3 EtOH. The resulting mixture was boiled under reflux on a water bath for about 2 h and then cooled. The complexes were separated from the reaction mixture by filtration, washed with EtOH and dried *in vacuo* over $CaCl_2$.

Measurements methods

Elemental analysis was carried out by standard micromethods. Magnetic susceptibility measurements were made at room temperature using a MSB-MKI magnetic susceptibility balance (Sherwood Scientific Ltd., Cambridge, England). Molar conductivies of freshly prepared 10^{-3} mol dm^{-3} solutions (DMF) were measured on a Jenway 4010 conductivity meter. The infrared spectra (KBr pellets) were recorded on an Infrared 457 Perkin-Elmer spectrophotometer. The electronic absorption spectra (UV-VIS) were taken on a Cary 219 spectrophotometer.

Antibacterial investigations

For these investigations the filter paper disc method was applied. The investigated isolates of bacteria were seeded in tubes with nutrient broth (NB). The seeded NB(1 cm^3) were homogenized in the tubes with 9 cm^3 of melted (45 °C) nutrient agar (NA). The homogeneous suspensions were poured into Petri dishes.

The discs of filter paper (diameter 5 mm) were ranged on the cool medium. After cooling on the formed solid medium, 2×10^{-5} dm^3 of the investigated compounds were applied using a micropipette. After incubation for 24 h in a thermostat at 25–27 °C, the inhibition (sterile) zone diameters (including disc) were measured and expressed in mm. An inhibition zone diameter over 8 mm indicates that the tested compound is active against the bacteria under investigation. Every test was done in triplicate.

The antibacterial activities of the investigated compounds were tested against two strains of bacteria (*Erwinia carotovora* subsp. *carotovora* and *Erwinia amylovora*). Parallel with the antibacterial investigations of the Cu(II), Zn(II) and Co(II) complexes, all ligands were also tested, as well as the pure solvent. The concentration of each solution was 5×10^{-2} mol dm^{-3}. Commercial DMF was employed to dissolve the tested samples.

RESULTS AND DISCUSSION

The complexes were synthesized in the reaction of a warm ethanolic solution of the $MCl_2\cdot nH_2O$ (M = Co(II), Cu(II), Zn(II) with benzimidazole derivatives in a mole ratio 1:2. It should be noticed, that the reaction of $CuCl_2\cdot 2H_2O$ yielded mono (ligand) complexes, even when the ligand was presented in a double excess.

TABLE II. Some physical characteristics and analytical data of the complexes

Complex	Colour	$\mu_{eff}(\mu_B)$	λ_M*	Found (Calcd.)%		
				M	C	H
$[CoCl_2(L_{I\text{-}p\text{-}CH_3})_2]$	blue	4.41	2.1	9.30 (9.36)	67.14 (64.78)	6.37 (6.72)
$[CoCl_2(L_{II\text{-}m\text{-}Cl})_2]$	blue	4.58	11.2	9.28 (9.14)	51.56 (52.11)	3.12 (3.72)
$[CoCl_2(L_{III\text{-}m\text{-}F})_2]$	blue	4.69	7.7	8.95 (8.82)	56.59 (57.49)	4.47 (4.79)
$[CuCl_2(L_{I\text{-}p\text{-}CH_3})H_2O]$	yellow	2.00	34.5	16.49 (16.53)	53.97 (53.06)	5.56 (4.68)
$[CuCl_2(L_{II\text{-}m\text{-}F})H_2O]$	brown	1.95	30.2	16.64 (16.92)	42.55 (44.75)	4.22 (3.48)
$[CuCl_2(L_{III\text{-}m\text{-}CH_3})H_2O]$	grean	1.83	17.3	15.87 (15.91)	51.40 (51.07)	5,.32 5.14)
$[ZnCl_2(L_{I\text{-}m\text{-}OCH_3})_2]$	white	diam.	5.8	9.82 (9.78)	55.17 (61.05)	5.22 (5.39)
$[ZnCl_2(L_{II\text{-}m\text{-}Cl})_2]$	white	diam.	4.3	9.60 (10.04)	48.30 (51.59)	3.89 (3.68)
$[ZnCl_2(L_{III\text{-}m\text{-}Cl})_2]$	rose	diam.	3.6	8.63 (9.25)	50.91 (54.30)	4.05 (4.52)

*In DMF, 1 mmol dm^{-3} solution at 25 °C; in S cm^2 mol^{-1}

The results of the elemental analyses of the complexes, as well as the magnetic moment and molar conductance data are summarized in Table II. All the complexes

are insoluble in most common organic solvents. They are highly soluble in DMF, somewhat less soluble in MeOH and EtOH.

The molar conductances of the cobalt(II) and zinc(II) complexes in DMF solutions fall in the range 2.1–11.2 S cm^2 mol^{-1}. These values indicate that the complexes behave as non-electrolytes in DMF.[19] The molar conductance values of the copper(II) complexes, compared with the values of non-electrolytes, are higher (17.3–34.5 S cm^2 mol^{-1}). These values are considerably less than the molar conductances of 1:1 type electrolytes (λ_M = 65–90 S cm^2 mol^{-1}),[19] which indicates the partial substitution of coordinated chloride ions with solvent molecules.

Magnetic properties

An indication of the most probable geometric configuration of the synthesized Co(II) complexes is given by their colour and magnetic moments (Table II). Namely, blue cobalt(II) complexes usually have a tetrahedral configuration. The magnetic moment values (Table II) of the cobalt(II) complexes are in the expected range (4.2–4.7 μ_B) for tetrahedral stereochemistry.[20]

The room temperature effective magnetic moments of the copper(II) complexes are in the range of 1.73–2.20 μ_B, which corresponds to one unpaired electron typical for tetrahedral geometry.[21]

Electronic spectra

The electronic spectra of the investigated complexes and those of the corresponding ligands were recorded in DMF (Table III). The cobalt(II) complexes retained their blue colour in solution, the zinc(II) complexes are uncoloured, but all the different coloured copper(II)complexes are yellow in DMF solution.

TABLE III. Electronic spectral data of the complexes

Complex	Absorption maxima [kK]*	(ε_{max})[$dm^2mol^{-1}cm^{-1}$]
$[CoCl_2(L_{I\text{-}p\text{-}CH_3})_2]$	35.7*sh* (1110) 34.5 (1210) 16.4*sh* (280)	15.9 (320) 15.3*sh* (310)
$[CoCl_2(L_{II\text{-}m\text{-}Cl})_2]$	35.7*sh* (840) 33.9 (1040) 16.2*sh* (360)	15.9 (380) 15.4*sh* (360)
$[CoCl_2(L_{III\text{-}m\text{-}F})_2]$	35.7*sh* (920) 33.3 (1140) 17.1*sh* (260)	16.1 (470) 15.4*sh* (470)
$[CuCl_2(L_{I\text{-}p\text{-}CH_3})H_2O]$	35.7*sh* (385) 34.0 (475) 28.1 (240)	23.8*sh* (100)
$[CuCl_2(L_{III\text{-}m\text{-}F})H_2O]$	35.7*sh* (525) 33.6 (630) 28.2 (275)	23.5*sh* (130)
$[CuCl_2(L_{II\text{-}m\text{-}CH_3})H_2O]$	35.8*sh* (480) 33.8 (690) 28.6 (310)	26.7 *sh* (200)
$[ZnCl_2(L_{I\text{-}m\text{-}OCH_3})_2]$	35.7*sh* (375) 34.5 (430)	
$[ZnCl_2(L_{II\text{-}m\text{-}Cl})_2]$	35.7 *sh* (500) 34.0 (590)	
$[ZnCl_2(L_{III\text{-}m\text{-}Cl})_2]$	35.7 *sh* (455) 33.6 (560)	

**sh* = shoulder, kK = 1000 cm^{-1}

The spectra of the ligands show two intense bands in the UV region around 40 and 35 kK (splitted); the former may be assigned to the imidazole moiety and the latter to the benzene ring of the ligand.[22] The splitting of the second band may be due to a lowering of the symmetry of the benzene ring.

The complexes exhibit very intense bands in the UV region and weak broad bands in the visible region (except the Zn(II) complexes). The positions and features of the bands in the UV region are nearly the same as those of the ligand bands.

The electronic absorption spectra of the cobalt(II) complexes show a broad band in the 15.2–17.1 kK region. The visible spectrum is dominated by the highest energy $^4A_2 \rightarrow {}^4T_1(P)$ transition,[20,23] typical for tetrahedral cobalt(II) complexes. The high molar exctinction coefficients of the cobalt(II) complexes and their blue colour suggest the tetrahedral configuration is retained in solution.[23]

The electronic absorption spectra of the copper(II) complexes show a broad absorption band about 28 kK and a shoulder around 23–26 kK. The broad band at 28 kK overlaps with the intense band of the ligand at about 35 kK.[24]

The electronic spectra of the zinc(II) complexes exibit very intense bands in the UV region around 35 kK, the same as those of the ligand bands.

Infrared spectra

The infrared spectra of the ligands exhibit a band at 3450–3330 cm^{-1} and ca. 1650 cm^{-1}, assigned to ν (NH_2) and δ (NH_2) of the benzimidazole ring, respectively[25] (series II and III). The band appearing at about 1550 cm^{-1}, for all the ligands, may be assigned to ν (C=N) vibrations.[24,25] The substituted phenyl group shows ring vibrations at 1485 and 740 cm^{-1}. The infrared spectra of the complexes investigated are similar to those of the corresonding ligands.

An upward shift (5–15 cm^{-1}) of ν(C=N) band in the IR spectra of the complexes as compared to its value in the free ligand, suggests coordination through the pyridine nitrogen of the benzimidazoles.[24] The bands due to ν (NH_2) and δ (NH_2) in the complexes are shifted to lower frequency in all the complexes. These shifts may be indicative of the presence of hydrogen bonding.[26,27] In the case of $[CuCl_2L(H_2O)]$, hydrogen bonds may be formed between the NH_2 group of the ligands and the coordinated water molecule.

The other bands in the spectrum of each complex are similar to those in the corresponding ligand spectrum, except for slight shifts in their positions and changes in their intensities due to coordination.

The presented results (molar conductivities, magnetic moments, electronic and IR spectra) suggest that the Co(II) and Zn(II) complexes are tetrahedral, which is realized by participation of the pyridine nitrogen of two organic ligand molecules and two chloride anions, typical for these classes of organic ligands.[28,29] In the case of the Cu(II) complexes, two types of geometries of tetracoordinated copper(II) are possible: the tetrahedral and square-planar.[30] From the presented results, it was not

possible to determine the exact geometry. We concluded that the real structure is between the tetrahedral and square-planar geometries. This configuraiton is realized by the participation of the pyridine nitrogen of one organic ligand molecule, two chloride anions and one molecule of water.

Antibacterial activities

Some recent papers[18,31,32] dealing with the antibacterial, antiviral, antihistaminic and fungicidal activity of benzimidazoles encouraged us to investigate the biological activity of the complexes synthesized in the present work. The antibacterial activity of these complexes was tested against phytopathogenic strains of bacteria in order to obtain new potent formulations for plant protection. All the complexes were screened for their antibacterial activities against *Erwinia carotovora* subsp. *carotovora* and *Erwinia amylovora*. The relevant data are presented in Table IV.

TABLE IV. Antibacterial activity of the benzimidazole derivatives and their complexes

Compound	Inhibition zone diameter (mm)	
	Erwinia carotovora subsp. *carotovora*	*Erwinia amylovora*
Ligands		
I-*p*-CH_3	0	0
I-*m*-OCH_3	0	0
II-*m*-Cl	16	22
II-*m*-F	15	23
III-*m*-CH_3	13	17
III-*m*-Cl	10	9
III-*m*-F	8	11
Complexes		
$[CoCl_2(L_{I\text{-}p\text{-}CH_3})_2]$	0	0
$[CoCl_2(L_{II\text{-}m\text{-}Cl})_2]$	20	25
$[CoCl_2(L_{III\text{-}m\text{-}F})_2]$	12	15
$[CuCl_2(L_{I\text{-}p\text{-}CH_3})H_2O]$	0	0
$[CuCl_2(L_{II\text{-}m\text{-}F})H_2O]$	22	30
$[CuCl_2(L_{III\text{-}m\text{-}CH_3})H_2O]$	17	17
$[ZnCl_2(L_{I\text{-}m\text{-}OCH_3})_2]$	0	0
$[ZnCl_2(L_{II\text{-}m\text{-}Cl})_2]$	18	23
$[ZnCl_2(L_{III\text{-}m\text{-}Cl})_2]$	12	16

From the data, it is evident that ligands belonging to the series II and III and their complexes are active against both of the bacteria under investigations. In the case of the ligands, the most active compounds are from series II. Benzimidazoles from the series III come next in order of activity. It was found that compounds of series I are not effective against the investigated bacteria.

From the results, it can be concluded that the basic antibacterial activity of the benzimidazoles is due to the presence of an amino group at position 2 of the benzimidazole ring. At the same time, methyl groups at the 5 or 6 position decreases the general antibacterial activity of the relevant benzimidazoles.

On comparing the biological activity of the ligands and their complexes, it was found that the complexes are more effective against both of the bacteria.[26,33] The higher activity of the complexes, as compared to the free ligands, can be understood in terms of the chelation theory.[34] This theory explains that a decrease in the polarizability of the metal could enhance the lipophilicity of the complexes.

Of the complexes, the most active compounds are those containing copper(II). This may be attributed to the high biological activity of free copper(II) ions.

From the present investigations, it can be concluded that the newly synthesized benzimidazoles and their complexes could find application as various pharmaceuticals and for plant protection.

ИЗВОД

КОБАЛТ(II), ЦИНК(II) И БАКАР(II) КОМПЛЕКСИ СА НОВОСИНТЕТИСАНИМ ДЕРИВАТИМА БЕНЗИМИДАЗОЛА

С. О. ПОДУНАВАЦ-КУЗМАНОВИЋ[а], В М. ЛЕОВАЦ[б], Н. У. ПЕРИШИЋ-ЈАЊИЋ[б], Ј. РОГАН[ц] и Ј. БАЛАЖ[д]

[а]*Технолошки факултет, Булевар Цара Лазара 1, 21000 Нови Сад,* [б]*Институт за хемију, ПМФ. Трг Доситеја Обрадовића 3, 21000 Нови Сад,* [ц]*Технолошко-металуршки факултет, Карнегијева 4, 11001 Београд и* [д]*Пољопривредни факултет, Трг Доситеја Обрадовића 1, 21000 Нови Сад*

Описана је синтеза тетраедарских комплекса кобалта(II), цинка(II) и бакра(II) са новосинтетисаним дериватима бензимидазола опште формуле $[MCl_2L_2]$ (M=Co(II), Zn(II)) и $[CuCl_2L(H_2O)]$. Комплекси су окарактерисани елементарном анализом, магнетним и кондуктометријским мерењима, IR и електронским апсорпционим спектрима. Испитана је антибактеријска активност деривата бензимидазола и њихових комплекса на бактерије *Erwinia carotovora* subsp. *carotovora* и *Ervinia amylovora*. Нађено је да комплекси показују већу биолошку активност од самих лиганада.

(Примљено 21. октобра 1998, ревидирано 18. јануара 1999)

REFERENCES

1. K. H. Gibson, R. Wood, A. A. Oldham, J. S. Major, *Bioorg. Med. Chem. Let.* **3** (1993) 1019
2. I. Yalcin, E. Sener, *Int. J. Pharm.* **98** (1993) 1
3. D. L. Brandon, R. G. Binder, R. E. Wilson, W. C. Montague, *J. Agr. Food Chem.* **41** (1993) 996
4. R. R. Tidwell, S. K. Jones, N. A. Naimen, L. C. Berger, W. B. Brake, C. C. Dykstra, J. E. Hall, *Antimicrob. Agents Chemother.* **37** (1993) 1713
5. L. Mishra, V. K. Singh, N. K. Dubey, A. K. Mishra, *Biosci. Biotech. Biochem.* **57** (1993) 989
6. H. S. Gunes, G. Cosar, *Arzn. Forch. Drug. Res.* **42-2** (1992) 1045
7. M. Tuncbilek, H. Goker, R. Ertan, R. Eryigit, E. Kendi, N. Atlantar, *Arch. Pharm.* **330** (1997) 372
8. I. Oren, O. Temiz, I. Yalcin, E. Sener, A. Akin, N. Ucaturk, *Arzn. Forch. Drug. Res.* **47** (1997) 1393
9. A. Sparatore, F. Novelli, F. Sparatore, *Farmaco* **52** (1997) 509

10. H. Kucukbay, B. Durmaz, *Arzn. Forch. Drug. Res.* **47** (1997) 667
11. M. R. Cuberes, M. Contijoch, C. Calvet, J. Alegre, J. R. Quantana, J. Frigola, *Chem. Pharm. Bull.* **45** (1997) 1287
12. K. S. Gudmudsson, J. C. Drach, L. L. Wotring, L. B. Townsend, *J. Med. Chem.* **40**(1997) 785
13. L. Mishra, V. K. Singh, *Synth. React. Inorg. Met.- Org. Chem.* **24** (1994) 95
14. L. Mishra, V. K. Singh, *Indian J. Chem. Sect. A* **32** (1993) 446
15. V. Alexander, *Inorg. Chim. Acta* **204** (1993) 109
16. F. Kratz, B. Nuber, J. Weiss, B. K. Keoler, *Polyhedron* **11** (1992) 487
17. V. K. Revankar, V. B. Mahale, *Indian. J. Chem. Sect. A*. **28** (1989) 683
18. Đ. Vlaović, J. Čanadanović-Brunet, J. Balaž, I. Jurnaić, D. Đoković, K. Mackenzie, *Biosci.Biotech. Biochem.* **56** (1992) 199
19. W. J. Geary, *Coord. Chem. Rev.* **7** (1971) 81
20. M. Goodgame, F. A. Cotton, *J. Am. Chem. Soc.* **84** (1962) 1543
21. F. E. Mabbs, D. J. Machin, *Magnetism and Transition Metal Complexes*, Chapman Hall, London (1973)
22. C. N. Rao, *Ultra-violet and Visible Spectroscopy,* 3rd ed., Butterworth and Co. Ltd., (1975)
23. F. A. Cotton, G. Wilkinson, *Advanced Inorganic Chemistry*, Wiley, New York (1989)
24. V. H. Arali, V. K. Revankar, V. B. Mahale, P. J. Kulkarni, *Transition Met. Chem.* **19** (1994) 57
25. K. Nakamoto, *Infrared and Raman Spectra of Inorganic and Coordination Compounds*, Wiley, New York (1986)
26. S. B. Balaji, N. M. Nanje Gowda, *Indian J. Chem.* **31** (1992) 463
27. L. Mishra, Y. K. Singh, *Indian J. Chem.* **32 A** (1993) 446
28. F.Mani, G. Scapacci, *Inorg. Chim. Acta* **16** (1976) 163
29. J. B. Hodgson, G. C. Percy, D. A. Thornton, *J. Mol. Struct.* **66** (1980) 75
30. B. J. Hathaway, *"Copper", Comprehensive Coordination Chemistry*, G. Wilkinson, R. D. Gillard, J. Mc. Cleverty, Eds., Pergamon Press, Oxford (1987)
31. G. A. Mokrushina, S. K. Kotovskaya, G. N.Turienkova, V. I. Ilienko, V. G. Platonov, I. V. Kiselieva, *Khim. pharm. zh.* (1988) 195
32. N. Noyanalpan, E. Bercin, P. Cakar, V. Abbasoglu, *Gazi. Univ. Eczacilik Fak. Derg.* **4** (1987) 33
33. R. K. Parashar, R. C. Sharma, *Inorg .Chim. Acta* **151** (1988) 201
34. R. S. Srivastava, *Inorg. Chim. Acta* **56** (1981) 65.

J. Serb. Chem. Soc. 64(5– 6)389-392(1999) UDC 665.12:661.71:547.21
JSCS-2680 *Note*

NOTE

The fatty acids and alkanes of *Satureja adamovicii* Šilić and *Satureja fukarekii* Šilić

DUŠANKA KITIĆ,[1] RADOSAV PALIĆ,[2] NOVICA RISTIĆ[3] and GORDANA STOJANOVIĆ[2*]

[1]*Faculty of Occupational Safety, Čarnojevića 10a, YU-18000 Niš,*
[2]*Department of Chemistry, Faculty of Science, Ćirila i Metodija 2, YU-18000 Niš and*
[3]*Department of Chemistry, Faculty of Science, Vidovdanska b.b. YU-38000 Priština, Yugoslavia*

(Received 30 October 1998, revised 4 February 1999)

The content and composition of fatty acids and alkanes of *Satureja adamovicii* Šilić and *Satureja fukarekii* Šilić were analized by GC. It was found that unsaturated acids prevailed and that the major components were palmitic, oleic, linoleic and linolenic acids. The hydrocarbon fractions of pentane extracts were shown to consist of the alkane homologues (C_{17} to C_{34}) with nonacosane and hentriacontane being prevailing compounds.

Key words: *Satureja adamovicii* Šilić, *Satureja fukarekii* Šilić, fatty acids, hydrocarbons.

Satureja adamovicii Šilić and *Satureja fukarekii* Šilić are endemic species of the Balkan peninsula.[1]

Satureja adamovicii Šilić grows on the stony approaches to uncovered cliffs of small uneven spots of Macedonia. *Satureja fukarekii* Šilić, also known as *Satureja tenus* Formanec and *Satureja montana* L. var. *kitaiballi* (Weirzb.) Brig. subvar. *tenus* (Formanec),[2] usually grows on karst rocks and serpentine sides of some river gorges of Macedonia.

Chemical studies of these species concerned the qualitative nad quantitative determination of the essential oil content.[3] We could find only one paper dealing with hydrocarbon fractions of pentane extracts of some species of Satureja genus[4,5] and one about the content and composition of the fatty acids of the total nutlet lipids of 11 species of *Satureja*.[6] The aim of this study was to enrich the data of the above mentioned species to include those of the compositions of the acids and hydrocarbons, because of their insufficiency in the literature.

EXPERIMENTAL

Plant material. The plant material was collected in the blooming phase of vegetation. *S. adamovicii* Šilić specimens were collected from the valley of the Rajec river and *S. fukarekii* Šilić near

* Address for correspondence

Katlanovska banja in Macedonia. The specimens were deposited in the herbarium of Dr. Novica Randelović, at the Faculty of Technology in Leskovac. The leaves, flowers and the green parts of the stems were air-dried for ten days at room temperature. The fatty acids and hydrocarbons were determined by previously reported procdures.[7,8] The chloroform extraction of *S. adamovicii* Šilić gave 7.80% and of *S. fukarekii* Šilić 7.20% of residue. The pentane extraction of *S. adamovicii* Šilić gave 2.03% and of *S. fukarekii* Šilić 1.54% of residue.

The methyl esters of the fatty acids of *S. adamovicii* Šilić and *S. fukarekii* Šilić were analyzed with a Hewlett Packard series 2 Gas Chromatograph on a Carbowax 20 M capillary column 25 m × 0.32 mm with an FID. N_2 was the carrier gas (pressure 330 kPa). The column temperature was programmed, 40–50 °C (at 2 °C/min), 55–140 °C (at 10 °C/min), 140–200 °C (at 5 °C/min) and then held 12 min at 200 °C. The injector temperature was 200 °C and the detector temperature 300 °C. Identification of compounds was carried out by the co-injection of authentic compounds. The obtained results are shown in Table I.

The hydrocarbons fractions of *S. adamovicii* Šilić and *S. fukarekii* Šilić were analyzed on 4 m × 3mm fused silica DB-1 column, FID, carrier gas He (2 cm^3/min). The column temperature was programmed 50–250 °C at 15 °C/min. The injector and detector temperature were both 300 °C. Identification of compounds was carried out by the co-injection of authentic compounds.

RESULTS AND DISCUSSION

The chloroform extraction of aerial dry plant material gave a 7.80% residue for *S. adamovicii* Šilić and 7.20% for *S. fukarekii* Šilić.

The saponification of the chloroform extract with a 12% NaOH ethanolic solution afforded the free fatty acids, which were esterified by methanol and the obtained methyl esters GC analyzed.

Identification by the GC of the fatty acids gave the results shown in Table I. It is obvious that unsaturated fatty acids prevail in both examined species.

TABLE I. Methyl esters of the fatty acids of *S. adamovicii* Šilić and *S. fukarekii* Šilić

Components	*S. adamovicii* Yield,%	*S. fukarekii* Yield,%
Methyl laurate	0.17	0.15
Methyl myristate	1.99	1.43
Methyl palmitate	24.13	24.45
Methyl stearate	5.68	4.34
Methyl oleate	15.67	11.56
Methyl linoleate	8.39	14.53
Methyl linolenate	20.62	29.27
Methyl licanate	2.28	2.27

The U/S index (unsaturated/saturated acids) is 1.5 and the ratio linolenate/linoleate is 2.45 for *S. adamovicii* Šilić and 2.0 for *S. fukarekii*, while for the nutlet lipids of 11 species of *Satureja* genus the U/S index ranges from 10.0 to 22.8 and the average linolenate/linoleate value is 4.4 (ranging from 4.9 to 3.2).[6]

From our results, it may be supposed that the fatty acid composition, U/S and the linolenate/ linoleate index of the ground part of plant may serve as taxonomic markers, as well as for the nutlet lipids.

The pentane extracts of the dry aerial parts of *S. adamovicii* Šilić and *S. fukarekii* Šilić were found to contain 2.03% and 1.54% of residue, respectively (calculated per weight of dried plant material). The yield of the hydrocarbon fractions, calculated per weight of dry residue of pentane extracts, were 3.03% and 2.60%, respectively, for *S. adamovicii* Šilić and *S. fukarekii* Šilić.

The separated hydrocarbon fractions of the pentane extracts of *S. adamovicii* Šilić and *S. fukarekii* Šilić showed IR bands, ν_{max} cm^{-1}, at 1450 ($-CH_3$), 2853–2962 and 720–750 ($-CH_2-$) pointed to the presence of a large number of methylene groups. The ^{1}H-NMR data confirmed the presence of methyl (δ 0.9 ppm) and methylene (δ 1.25 ppm) protons. The melting interval was 63–66 °C. The results of GC analyses are summarized in Table II.

TABLE II. Percent composition of *n*-alkanes

Components	*S. adamovicii* Šilić	*S. fukarekii* Šilić
Heptadecane	0.58	0.92
Octadecane	1.59	0.88
Nonadecane	0.89	1.68
Icosane	0.56	1.02
Henicosane	0.56	1.34
Docosane	0.23	0.91
Tricosane	0.43	1.35
Tetracosane	0.20	1.12
Pentacosane	0.81	1.59
Hexacosane	0.49	1.41
Heptacosane	2.63	3.27
Octacosane	1.60	3.74
Nonacosane	32.55	25.59
Triacontane	2.87	2.82
Hentriacontane	26.43	14.65
Dotriacontane	2.93	2.39
Tritriacontane	10.30	5.73

The *n*-alkane distributions of *S. adamovicii* Šilić and *S. fukarekii* Šilić are odd carbon dominant, maximizing at C-29 (32.55% and 25.59%, respectively) with a Carbon Preference Index (CPI) of 7.2 and 3.7 and an Average Chain Length (ACL) of 25.44 and 19.78, respectively.

A survey of the literature reveals that there are some differences between our results and those published erlier.[5]

Acknowledgment. We thank the Ministry of Science and Technology of Serbia for financial support and NSF (OC6-9415568).

И З В О Д

МАСНЕ КИСЕЛИНЕ И АЛКАНИ ИЗ *Satureja adamovicii* ШИЛИЋ И *Satureja fukarekii* ШИЛИЋ

ДУШАНКА КИТИЋ,[1] РАДОСАВ ПАЛИЋ,[2] НОВИЦА РИСТИЋ[3] и ГОРДАНА СТОЈАНОВИЋ

[1]*Факултет заштите на раду, Чарнојевића 10а, 18000 Ниш*
[2]*Одсек за хемију, Филозофски факултет, Ћирила и Методија 2, 18000 Ниш и*
[3]*Одсек за хемију, Природно-математички факултет, Видовданска б.б., 38000 Приштина*

Испитиване су масне киселине и алкани врста *Satureja adamovicii* Шилић и *Satureja fukarekii* Шилић методом GC. Утврђено је да код обе врсте преовлађују незасићене масне киселине. Најзаступљеније масне киселине су: палмитинска, олеинска, линолна и линоленска. Такође је утврђено да су заступљени алкани од C_{17} до C_{34} са нонакозаном и хенетриаконтаном као најзаступљенијим компонентама.

(Примљено 30. октобра 1998, ревидирано 4. фебруара 1999)

REFERENCES

1. Č. Šilić, *A Monograph of genus Satureja L., Calamintha Miller, Micromeria Bentham, Acinos Miller and Clinopodium L. in Flora of Yugoslavia*, Svijetlost, Sarajevo 1979
2. J. D. Roberts, M. C. Caserio, *Basic Principles of Organic Chemistry*, California Institute of Technology, W. A. Benjamin, INC, New York-Amsterdam 1964
3. S. Pavlović, R. Ivanić, K. Savin, P. Živanović, R. Jančić, D. Milinković, S. Vujčić, *Arh. farm.* **33** (1982) 287
4. D. Savić, R. Palić, S. Anđelković, N. Simić, *XXXV Meeting of the Serbian Chemical Society*, Book of Abstracts (1993) 96
5. R. Palić, D. Savić, N. Simić, S. Anđelković, *Facta Universitatis* **1** (1994) 91
6. P. Marin, V. Sajdl, S. Kapor, B. Tatić, B. Petković, *Phytochemistry* **30** (1991) 979
7. N. Ristić, R. Palić, D. Kitić, G. Stojanović, *Facta Universitatis* **1** (1997) 53
8. R. Palić, N. Ristić, N. Simić, D. Kitić, R. Kapetanović, *J. Serb. Chem. Soc.* **62** (1997) 619.

J. Serb. Chem. Soc. 64(5– 6)391-394(1999)
JSCS-2681

UDC 547.92/.94:542.9
Note

NOTE

A novel route to 3-hydroxy-16,17-seco-estrone derivatives

SUZANA S. JOVANOVIĆ-ŠANTA,[1] VJERA M. PEJANOVIĆ[2] and JULIJANA A. PETROVIĆ[1*]

[1]*Faculty of Science, University of Novi Sad, Trg Dositeja Obradovića 3, YU-21000 Novi Sad, and* [2]*ICN Yugoslavia, Institute, 29. Novembra 111, YU-11000 Belgrade, Yugoslavia*

(Received 14 May 1998, revised 16 February 1999)

Starting from 3-benzyloxy-17-hydroxy-16,17-secoestra-1,3,5(10)-triene-16-nitrile (**1b**), 17-tosylate **2b** and also 17-chloro-, 17-bromo- and 17-iodo-derivatives **4b, 5**b, and **6b,** were obtained. The fluoro-derivative **3b** was obtained from **2b** in the reaction with tetrabutyl ammonium fluoride. The deprotection of the 3-hydroxyl group was achieved by action of hydrogen in presence of Pd/C as a catalyst, yielding six new 3-hydroxy-16,17-seco-estrone derivatives.

Key words: 3-hydroxy-16,17-seco-estrone derivatives, halogeno steroids, hydrogenolysis.

We previously synthesized a series of 3-methoxy-16,17-seco-estrone derivatives, which in biological tests performed on experimental animals showed a complete loss of estrogenic activity, with most of them demonstrating a pronounced antiestrogenic action.[1,2] However, the presence of the 3-methoxy funciton prevented us from investigating the mechanism of their biological action. Namely, it is known that antiestrogens (steroidal or nonsteroidal) act at the level of estrogen or progesterone receptors, whereby the presence of a free hydroxyl group at the aromatic moiety in the tested molecule is necessary.[3]

All attempts to deprotect the phenolic function in the synthesized derivatives led to the formation of various by-products, resulting, therefore, in low yields of derivatives bearing a free hydroxyl function at C-3.[4]

We presumed that this obstacle could be overcome by synthesizing 3-benzyloxy-16,17-seco-estrone derivatives, followed by hydrogenolysis of the benzyl ether function.

RESULTS AND DISCUSSION

As the starting compound we selected 3-benzyloxy-17-hydroxy-16,17-secoestra-1,3,5(10)-triene-16-nitrile (**1b**, Scheme 1), which was obtained from estrone

* Author for correspondence

in four steps, applying a known synthetic route.[5] Treating the secocyanoalcohol **1b** with *p*-toluenesulfonyl chloride afforded tosylate **2b**, which upon action of tetrabutyl ammonium fluoride in refluxing methyl ethyl ketone gave the 17-fluoro derivative **3b** in 70.4% yield. The chloro **4b** and bromo **5b** derivatives were obtained from **1b**, under the action of thiphenylphosphine in the presence of carbon tetrachloride, *i.e.*, tetrabromide.[6] On the other hand, the iodo derivative **6b** was formed in the reaction of **1b** with iodine, triphenylphosphine and imidazole in toluene at reflux temperature.[7]

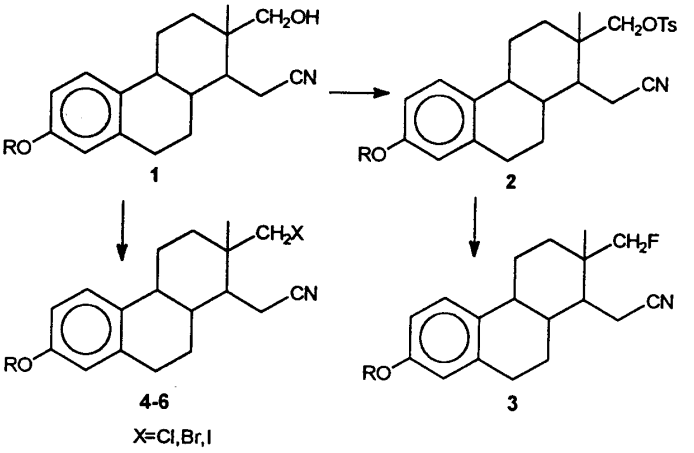

a) R=H
b) R=$CH_2C_6H_5$

Scheme 1.

Deprotection of the 3-hydroxyl function was performed by hydrogenolysis at room temperature and low hydrogen pressure, using Pd/C as catalyst. High yields of 3-hydroxy-16,17-seco-estrone derivatives were obtained, except in the case of the iodo derivative **6b**. Therefore, 3-hydroxy-17-iodo-16,17-secoestra-1,3,5(10)-triene-16-nitrile (**6a**) was prepared from 3-hydroxy-17-*p*-toluenesulfonyloxy-16,17-secoestra-1,3,5(10)-triene-16-nitrile (**2a**), by the action of tetrabutyl ammonium iodide.

EXPERIMENTAL

Compound **1a**. Yield 40.8%, m.p. 198–199 °C. IR-spectrum: 3600–3100, 2920, 2250, 1620, 1505, 1230, 1020. ^{1}H-NMR-spectrum (acetone-d_6): 0.92 (*s*,3H,CH_3); 3.28 (*dd*, 1H, H_a–C-17, J_{gem}=11.06Hz, $J_{Ha,OH}$ = 5.09Hz); 3.55 (*dd*, 1H, H_b–C-17, $J_{Hb,OH}$ = 5.12Hz); 6.62–7.12 (group of signals, 3H, arom.protons); 8.04 (*s*,1H, **HO**–C-3). ^{13}C-NMR-spectrum (acetone-d_6): 15.79 (C-15); 16.44 (C-18); 71.08 (C-17); 120.87 (C≡N); 156.06 (C-3). Mass spectrum: 343 (68; $(M+i\text{-Bu})^+$); 342 (100; $(M+i\text{-Bu}-1)^+$); 303 (17); 286 (87; $(M+1)^+$); 285 (38; M^+); 268 (17; $(M+1-H_2O)^+$).

Compound **2a**. Yield 93.94%, m.p.138–140 °C. IR-spectrum: 3500, 2920, 1600, 1500, 1450, 1375, 1310, 1180, 940, 670, 550. ^{1}H-NMR-spectrum (acetone-d_6): 0.95 (*s*, 3H, CH_3); 2.50 (*s*,3H,CH_3

from Ts); 2.65 (*dd*, 2H, C-15); 3.80 (*d*,1H, H_a–C-17); 4.07 (*d*,1H, H_b–C-17, J_{gem}=10.01Hz); 6.60–7.81(group of signals, 7H, arom. protons); 8.05 (*s*,1H, **H**O–C-3). ^{13}C-NMR-spectrum (acetone-d_6): 15.77 (C-15); 15.92 (C-18); 26.66 (CH_3 from Ts); 38.78 (C-17); 77.48 (**C**H_2–OTs); 120.13 (C≡N); 156.16(C-3). Mass spectrum: 497 (28; $(M+i\text{-Bu})^+$); 496 (88; $(M+i\text{-Bu}-1)^+$); 440 (7; $(M+1)^+$); 323 (100). Anal. Calcd. for $C_{25}H_{29}NO_4S$: C, 68.32; H, 6.65; N, 3.19, S, 7.28. Found: C, 67.87; H, 7.02; N, 3.10; S, 7.67.

Compound **3a**. Yield 47.22%, m.p. 182 ºC. IR-spectrum: 3600–3100, 2920–2880, 2250, 1620, 1505, 1450, 1215, 1000, 940, 620. ^{1}H-NMR-spectrum (acetone-d_6): 0.97 (*d*, 3H, CH_3, $J_{H,F}$=2.34Hz); 2.47(*dd*,1H, H_a–C-15); 2.68 (H_b–C-15); 4.19 (*dd*, 1H, H_a–C-17, J_{gem} = 9.53Hz, $J_{17a,F}$=47.37Hz); 4.41 (*dd*, 1H, H_b–C-17, $J_{17b,F}$=48.51Hz); 6.60–7.13 (group of signals, 3H, aromatic protons); 7.99 (*s*,1H, **H**O–C-3). ^{13}C-NMR-spectrum (acetone-d_6): 14.85 (*d*, C-18, $J_{C,F}$=6.29Hz); 17.76 (C-15); 91.18 (*d*,CH_2–F, $J_{C,F}$=173.60Hz); 120.41 (C≡N); 156.14 (C-3). Mass spectrum: 288 (100; $(M+1)^+$); 199 (72); 133 (52); 107 (48).

Compound **4a**. Yield 78.9%, m.p. 196–198 ºC. IR-spectrum: 3600–3100, 2930–2860, 2250, 1605, 1500, 1450, 1290, 1225, 740. ^{1}H-NMR-spectrum (acetone-d_6): 1.08 (*s*,3H, CH_3); 2.38 (*dd*,1H, H_a–C-15); 2.62 (*dd*, 1H, H_b–C-15); 3.42 (*d*,1H, H_a–C-17); 3.59 (*d*,1H, H_b–C-17, J_{gem}=10.95Hz); 6.60–7.18 (group of signals, 3H, arom. protons). ^{13}C-NMR-spectrum (acetone-d_6): 15.28 (C-15); 18.13 (C-18); 54.51 (**C**H_2–Cl); 118.97 (C≡N); 153.66 (C-3). Mass spectrum: 362 (64; $(M+i\text{-Bu})^+$); 361 (98; $(M+i\text{-Bu}-1)^+$); 360 (100; $(M+i\text{-Bu}-2)^+$); 346 (16); 304 (27; M^+). Anal. Calcd. for $C_{18}H_{22}ClNO$: C, 71.16; H, 7.30; N, 4.61. Found: C, 71.06; H, 7.20; N, 5.39.

Compound **5a**. Yield 88.3%, m.p. 212 ºC. IR-spectrum: 3400, 2920, 2250, 1605, 1500, 1240. ^{1}H-NMR-spectrum (acetone-d_6): 1.08 (*s*,3H, CH_3); 2.52 (*dd*, 1H H_a–C-15); 2.75 (*dd*, 1H, H_b–C-15, $J_{15a,15b}$=18Hz, $J_{15a,14}$=4.1Hz, $J_{15b,14}$=5.1Hz); 3.63 (*dd*, 2H, C**H**$_2$–Br, J_{gem}=10.7Hz); 6.55–7.13 (group of signals, 3H, arom. protons); 8.12 (*s*,1H,**H**O–C-3). ^{13}C-NMR-spectrum (acetone-d_6): 15.47 (C-15); 17.99 (C-18); 47.05 (**C**H_2–Br); 120.31 (C≡N); 156.07(C-3). Mass spectrum: 349 (97; $(M+1)^+$); 348 (27;M^+); 347 (100; $(M-1)^+$); 198 (70). Anal. Calcd. for $C_{18}H_{22}BrNO$: C, 62.08; H, 6.31; N, 4.02. Found: C, 61.97; H, 6.26; N, 3.93.

Compound **6a**. Yield 85.5%, m.p. 188 ºC. IR-spectrum: 3500, 2920, 1610, 1550, 1440, 1290, 930, 870, 610. ^{1}H-NMR-spectrum (acetone-d_6). 1.13 (*s*,3H, CH_3); 2.50 (*dd*, 2H, C-15); 3.50 (C**H**$_2$–I); 6.56–7.10 (group of signals, 3H, aromatic protons); 8.07 (*s*, 1H, **H**O–C-3). ^{13}C-NMR-spectrum (acetone-d_6): 15.51 (C-15); 17.99 (C-18); 25.48 (C-17); 120.21 (C≡N); 156.06 (C-3). Mass spectrum: 396 (62; M^++1); 395 (100; M^+); 268 (42; M^+–1I); 133 (49).

Aknowledgement: The authors are grateful to the Ministry of Science and Technology of the Republic of Serbia for financial support.

ИЗВОД

НОВИ ПОСТУПАК ЗА ДОБИЈАЊЕ 3-ХИДРОКСИ-16,17-СЕКО-ЕСТРОНСКИХ ДЕРИВАТА

СУЗАНА С. ЈОВАНОВИЋ-ШАНТА,[1] ВЈЕРА М. ПЕЈАНОВИЋ[2] и ЈУЛИЈАНА А. ПЕТРОВИЋ[1]

[1]*Природно-математички факултет, Универзитет у Новом Саду, Трг Доситеја Обрадоавића 3, 21000 Нови Сад и* [2] *ICN Југославија, Институт, 29. Новембра 111, 11000 Београд*

Полазећи од 3-бензилокси-17-хидрокси-1,3,5(10)-триен-16-нитрила (**1b**), добијени су 17-тозилокси дериват **2b**, односно 17-хлоро, 17-бромо и 17-јодо деривати **4b, 5b** и **6b**, док је 17-флуоро дериват **3b** добијен у реакцији **2b** са тетрабутил амонијум флуоридом. Уклањање заштитне групе са C-3 изведено је дејством водоника у присуству Pd/C, при чему је добијено шест нових 3-хидрокси-16,17-секо-естронских деривата.

(Примљено 14. маја 1998, ревидирано 16. фебруара 1999)

REFERENCES AND NOTES

1. J. A. Petrović, V. M. Pejanović, D. A. Miljković, J. T. Hranisavljević, *Steroids* **55** (1990) 276
2. V. Pejanović, *Ph. D. Thesis*, University of Novi Sad, 1991
3. P. Van de Velde, F. Nique, F. Bouchoux, J. Bremaud, M. C. Hameau, D. Lucas, C. Moratille, S. Viet, D. Philibert, G. Teutsch, *J. Steroid Biochem. Molec. Biol.* **48** (1994) 187
4. V. Pejanović, Lj. Medić-Mijačević, J. Petrović, D. Miljković, *Proceed. Nat. Sci., Matica Srpska* **88** (1995) 81
5. D. Miljković, J. Petrović, *J. Org. Chem.* **42** (1977) 2101
6. A. Kashem, M. Anisuzzaman, R. L. Whisler, *Carbohydrate Research* **61** (1978) 511
7. P. J. Garegg, B. Samuelson, *J. Chem. Soc., Perkin I* (1980) 2866
8. IR spectra (wave nombers in cm^{-1}) were recorded using a Perkin-Elmer 457 spectrometer in KBr pellets. The ^{1}H and ^{13}C-NMR spectra were recorded with a Brucker AC 250E instrument with tetramethylsilane as internal standard. The chemical shifts are given in ppm (δ-scale). The mass spectra were measured using a Finnigan-MAT 8230 (the first number denotes the m/z value, and the ion abundances are given in parentheses). The melting points were determined with a Büchi SMP-20 apparatus and are uncorrected.

.